



POLITECNICO
MILANO 1863

SCUOLA DI INGEGNERIA INDUSTRIALE
E DELL'INFORMAZIONE

mpsd



Max-Planck-Institut für
Struktur und Dynamik der Materie

QED Solver for ab-initio cavity materials engineering

TESI DI LAUREA MAGISTRALE IN
PHYSICS ENGINEERING - INGEGNERIA FISICA

Author: **Francesco Troisi**

Student ID: 962700

Advisor: Prof. Dr. Giacomo Claudio Ghiringhelli

Co-advisors: Prof. Dr. Angel Rubio, Dr. Simone Latini, Dr. Hannes Hübener,
Dr. Umberto De Giovannini

Academic Year: 2021-22

Abstract

In this work an *ab-initio* approach for studying materials in the framework of cavity QED is presented. In a cavity, the coupling between light and matter can reach the strong regime, which means that the system is described by a mix of the electronic states describing the matter and the Fock states describing the electromagnetic field. Such states are called dressed or polaritonic states. Indeed, polaritons are quasi-particles associated with the propagation of light in matter and are described as a mix of electronic and photonic states.

While molecules and finite systems have been deeply studied in the strong light-matter coupling regime, much less has been done for crystals/solids. Such systems are characterized by a greater physical and computational complexity compared to finite ones. The software proposed in this work attempts to tackle these complexities, on one hand by having at its core a programming language highly optimized for numeric computation and by being specifically designed to run on high performance computers, and on the other hand by the fact that it is tailored to polaritonic properties of periodic cavity-matter systems and it is designed on top of Density Functional Theory which is the workhorse approach for the *ab-initio* description of condensed matter systems. After describing the theoretical model and the implementation, we use the code to study both finite and period systems. In particular, we show the emergence of polaritons in the strong coupling regime and how the linear optical response of prototype crystals is modified by the photons confined in the cavity. Finally, we show that it is possible to modify the fundamental properties of materials, for instance by opening a gap in Graphene using chiral light.

The software is released under the TDDFT code Octopus, with the name of *QED Solver*. This thesis work was carried out at the Max Planck Institute for the Structure and Dynamics of Matter (Hamburg, Germany), in particular in the Theory Department directed by Prof. Dr. Angel Rubio.

Keywords: Cavity QED, Strong light-matter coupling, Polaritons, HPC, Parallel Programming

Abstract in lingua italiana

In questo lavoro di tesi è presentato un metodo *ab-initio* per studiare i materiali in cavità ottiche, nell'ambito dell'elettrodinamica quantistica. In una cavità, l'accoppiamento tra la luce e la materia è intenso, ciò implica che il sistema è descritto da un'unione degli stati elettronici (descriventi il materiale) e degli stati di Fock (descriventi il campo elettromagnetico). Questi sono definiti come stati vestiti, o polaritonici. I polaritoni sono quasi particelle associate alla propagazione della radiazione nella materia, e sono descritti parzialmente dagli stati elettronici e parzialmente da quelli fotonici.

Se da un lato le molecole (e in generale i sistemi non periodici) sono stati a lungo studiati nell'ambito dell'accoppiamento forte tra luce e materia, dall'altro non molto è stato fatto per i solidi e i cristalli. Questi ultimi sono caratterizzati da una grande complessità, sia per la fisica che avviene al loro interno sia per la complessità computazionale richiesta per simularli. Il software sviluppato in questo lavoro di tesi si propone di affrontare queste complessità, da un lato utilizzando un linguaggio di programmazione ottimizzato per problemi numerici, oltre che un design specifico per computer ad alte prestazioni, dall'altro descrivendo le proprietà polaritoniche dei sistemi periodici partendo dalla *density functional theory*, cavallo di battaglia per la descrizione *ab-initio* dei sistemi di fisica dello stato solido. In questo elaborato, dopo aver descritto il modello teorico e l'implementazione del codice, il software viene applicato per studiare sia sistemi periodici che non periodici (molecole). In particolare, si evidenzia la formazione dei polaritoni nel regime di accoppiamento forte e in che misura la cavità modifica la risposta del materiale agli impulsi ottici. Mostriamo infine che è possibile modificare le proprietà del materiale, aprendo per esempio un gap nel Grafene mediante l'uso di luce polarizzata circolarmente.

Il presente software è rilasciato come parte del codice TDDFT Octopus, sotto il nome di *QED Solver*.

Il presente lavoro di tesi è stato svolto presso il *Max Planck Institute for the Structure and Dynamics of Matter* (Amburgo, Germania), in particolare nel dipartimento di teoria diretto da Prof. Dr. Angel Rubio.

Parole chiave: QED in cavità ottiche, forte accoppiamento luce-materia, polaritoni, HPC, programmazione in parallelo

Contents

Abstract	i
Abstract in lingua italiana	iii
Contents	v
Introduction	1
1 Light-Matter Coupling	3
1.1 Quantization of the EM field	3
1.2 Electrons in solids	7
1.2.1 Mean-field approach for the electronic problem	7
1.2.2 Kohn-Sham equations and Density Functional Theory	11
1.2.3 Slater determinants	13
1.2.4 Second quantization and Slater determinant excitation	15
1.3 QED Hamiltonian	16
1.3.1 Optical Cavities	18
1.3.2 Weak regime	19
1.3.3 Strong regime	21
1.4 Polaritons	22
2 Methods	25
2.1 Approximations and Working Assumptions	25
2.1.1 Assumptions of the matter part	26
2.1.2 Assumptions of the radiation part	27
2.2 Structure of the QED Hamiltonian matrix	28
2.2.1 Basis for the QED Hamiltonian	28
2.2.2 Structure of the blocks	28
2.2.3 Ab-Initio Polaritons: Simple case of H atom	31

3	QED Matrix Solver and Response Functions Ab-initio Implementation	35
3.1	Octopus Code	35
3.2	Features of the QED Solver	36
3.2.1	Density Of States	41
3.2.2	Linear Optical Response	42
3.3	Parallelization of the code	43
3.3.1	Limitations of the serial approach	44
3.3.2	High Performance Computing	46
3.3.3	Serial vs Parallel code performance	47
3.4	Parallel code examples	49
4	Results & Discussion	53
4.1	Benzene molecule	53
4.2	LiH 1D chain	58
4.3	Graphene	61
5	Conclusions and future developments	67
	Bibliography	69
	A Derivation of QED matrix elements	73
	List of Figures	79
	List of Tables	83
	List of Symbols	85
	Acknowledgements	87

Introduction

Since the very beginning of mankind, being able to create tools and engineer new materials has been a central theme in societies. As an example, the first known evidence of metal smelting date back to 8000 years ago and the first production of superior metals (like Bronze, which is an alloy made of Copper and Tin) started years later [1]. From those early attempts to control the mixing of atoms, as scientific discoveries were made and technology progressed, we have always improved the ability to control how elements combine. However, it is not until the last century that this quest for control over the ordering of nature improved exponentially. Thanks to the development of Quantum Theories (starting from the Schrodinger equation in 1925) and of technology, we became able to engineer materials at the nanoscale level. Arguably, the most advanced manipulations of the nanoscale structures are reached in the semiconductors used in electronics (where recently it was possible to fabricate transistors with a 2nm channel [2]) and optics for the generation of laser light [3]. Usually it is possible to reach those results by means of varying doping concentration or mechanical stress or strain. These latter modify the bonds between atoms (in terms of length and orientation), which lead to a variation in the electronic structure due to symmetry breaking. However, that is not the only way in which one can modify the microscopic properties of materials, but one could also use light [4]. Light-matter interaction phenomena have been studied for a long time, but as will be discussed in this work, to be able to modify the properties of materials one has to reach a strong coupling between light and matter. This only became possible in the last century thanks to the invention and description of the laser [5], and to its improvements. However, focusing high-intensity laser light on a material to reach strong coupling is potentially destructive, as the optical power in a small spot would be so high that the matter would begin to melt. To overcome this limitation, one can place the material inside an optical cavity to reach the strong coupling. This allows a photon to be trapped in the cavity for a long time, which allows it to interact multiple times with material [6]. Being able to achieve strong coupling with a low-intensity field or just exploiting the quantum fluctuations of light, opens many possibilities for controlling materials even at equilibrium [6]. This allows for instance to generate and control excitonic states [7, 8], to enhance ex-

isting properties like ferroelectricity or electron-phonon coupling [9, 10] or to induce new properties and phases in the material [6]. Moreover, one could also dynamically break the symmetries to change the band structure, allowing to open gaps [4, 11] and change the topology of the material (Floquet engineering [12]). One final phenomenon that is worth mentioning is the induction or the enhancement of the superconductivity [13, 14]. All these exciting possibilities are made possible by the strong coupling light-matter interaction, which mixes the electronic and photonic states, to generate the so-called polaritons [15, 16]. As it will be explored later, they are quasi-particles associated with the propagation of light in matter. In some applications it is also possible to mix the phonon states, thus generating the phonoriton states [17]. The latter will not be discussed in this work. As it was mentioned, polaritons arise from the mixing of the electronic and photonic states, which means they have to be combined at the level of the Hamiltonian of the system. This means that one has to start from the known states of the matter and of the radiation field, and then couple them through the QED Hamiltonian.

In this work, a tool for computing the polaritonic states arising from materials in optical cavities is presented. We use a quantum description of both the matter (using Slater determinants built from the single-particle states calculated using Density Functional Theory) and of the radiation field (using Fock states). After defining and solving the QED Hamiltonian on that basis, we use the obtained polaritonic states to compute response functions in the framework of linear response theory. This allows studying how the states are modified and also to see interesting features such as the opening of a gap in the band structure of Graphene. The significance of this work lies in the fact that while finite systems coupled to cavity light have been studied in detail, not much has been done for periodic systems. This is due to the big computation cost that comes from building and diagonalizing the matrix representation of the QED Hamiltonian for those systems. The software presented in this work is designed to deal with such complexity, thanks to the fact that it was written in a programming language highly optimized for numeric computation (Fortran 90) and to the fact that parallelization techniques were used to allow the software to run on supercomputers.

The present work is organized as follows, first the theoretical framework is presented, starting from the quantization of the electromagnetic field and the description of the electronic states, then QED and finally the concept of polaritons is discussed. Subsequently, the approximations and assumptions are introduced, and a first formulation of the QED matrix is given. Then, the implementation and the characteristics of the code are described. Finally, the software is applied to three different systems and the obtained results are discussed.

1 | Light-Matter Coupling

Since physicists started studying radiation fields, the theme of their interaction with matter has always been a central problem, starting from the first laws on the static description of the electric and magnetic field, then through Maxwell's equations, the semi-classical and finally the modern full quantum light-matter interaction theories.

In this chapter we give an introduction to the coupling between light and matter in the framework of second quantization. We start by describing the quantization of the electromagnetic field. This step is necessary to move on from the semi-classical theories (where the electromagnetic field was treated classically) to the theory of Quantum Electrodynamics (QED). Subsequently, we describe the behavior of electrons in solids, firstly by deriving the mean-field equations and then by introducing Density Functional Theory (DFT). As the last step, Slater determinants are explored as well as the formalism of second quantization, which will be used in the following sections. Then we introduce QED by deriving the Hamiltonian for light-atoms coupling and by describing the different operation regimes. Finally, we introduce the concept of polariton as a quasi-particle arising from the propagation of light in matter.

1.1. Quantization of the EM field

The electromagnetic field is fully described by the well-known Maxwell's equations. If we formulate them in free space, they have the following form:

$$\nabla \cdot \mathbf{E} = 0 \tag{1.1}$$

$$\nabla \times \mathbf{E} = -\frac{\partial \mathbf{B}}{\partial t}, \tag{1.2}$$

$$\nabla \cdot \mathbf{B} = 0, \tag{1.3}$$

$$\nabla \times \mathbf{B} = \mu_0 \epsilon_0 \frac{\partial \mathbf{E}}{\partial t} \tag{1.4}$$

and their solution is a linear combination of plane waves. Despite the classical formulation of Maxwell's equation can describe most of the phenomena we observe, others require a

quantum description [18]. Among them we can acknowledge the spontaneous emission, and in general every phenomenon that involves a beam of light with a strongly reduced number of photons (up to a single photon) requires the quantization of the electromagnetic field. To quantize the field we will follow the steps of Dirac's Canonical Quantization Protocol [19], which states that one should first write the Hamiltonian of the field in terms of classical conjugated variables, then substitute them with the quantum operator and finally impose the commutation relations. The classical Hamiltonian of the electromagnetic field is

$$\mathcal{H} = \frac{1}{2} \int \left[\epsilon_0 \mathbf{E}(\mathbf{r}, t) \cdot \mathbf{E}(\mathbf{r}, t) + \frac{1}{\mu_0} \mathbf{B}(\mathbf{r}, t) \cdot \mathbf{B}(\mathbf{r}, t) \right] dV \quad (1.5)$$

To deal with it, it is more convenient to reformulate Maxwell's equations in terms of the vector potential \mathbf{A} and the scalar potential ϕ , and then to use the expressions for \mathbf{E} and \mathbf{B} in (1.5). We have that

$$\mathbf{B} = \nabla \times \mathbf{A} \quad (1.6)$$

$$\mathbf{E} = -\nabla\phi - \frac{\partial\mathbf{A}}{\partial t} \quad (1.7)$$

If we substitute (1.6), (1.7) into Maxwell's equations, we get the field equations that describe the vector potential. Before showing them, one should note that the solution to these equations do not change if we substitute \mathbf{A} and ϕ with \mathbf{A}' and ϕ' , such that $\mathbf{A} = \mathbf{A}' - \nabla\Xi$ and $\phi = \phi' + \frac{\partial\Xi}{\partial t}$. This is known as Gauge transformation, and the scalar function Ξ is known as the gauge function. Since the gauge function is arbitrary, we can choose it so that we have $\nabla \cdot \mathbf{A} = 0$ and $\phi = 0$ that is the Coulomb gauge. Under these assumptions, the field equation for the vector potential becomes:

$$\nabla^2 \mathbf{A} - \frac{1}{c^2} \frac{\partial^2 \mathbf{A}}{\partial t^2} = 0 \quad (1.8)$$

where $c = \frac{1}{\sqrt{\epsilon_0 \mu_0}}$ is the speed of light.

Equation 1.8 is solved by a superposition of plane waves, however since we considered Maxwell's equations in free space their normalization is not straightforward. To overcome the problem, we solve the equation in a large cubic box of size L , and we impose periodic boundary conditions: $\mathbf{A}(x, y, z) = \mathbf{A}(x+L, y+L, z+L)$. Since we are using a superposition of plane waves as solution, the boundary conditions imply that only the wave vectors that satisfy the above relation should be included, so that the solutions are now discretized. In particular, one has that $\exp(i\mathbf{k} \cdot \mathbf{r}) = \exp(i\mathbf{k} \cdot (\mathbf{r} + \mathbf{L})) \rightarrow k_{x,y,z} = \frac{2\pi}{L} n_{x,y,z}$. The solution for the vector potential then becomes [20]:

$$\mathbf{A}(\mathbf{r}, t) = \sum_{\mathbf{k}} \sum_{\lambda=1,2} \mathbf{e}_{\mathbf{k},\lambda} A_{\mathbf{k},\lambda}(\mathbf{r}, t) = \sum_{\mathbf{k}} \sum_{\lambda=1,2} \mathbf{e}_{\mathbf{k},\lambda} \left[A_{\mathbf{k},\lambda} e^{i(\mathbf{k} \cdot \mathbf{r} - \omega_{\mathbf{k}} t)} + A_{\mathbf{k},\lambda}^* e^{-i(\mathbf{k} \cdot \mathbf{r} - \omega_{\mathbf{k}} t)} \right] \quad (1.9)$$

where $\mathbf{e}_{\mathbf{k},\lambda}$ represents the polarization vector and λ represent the polarization (left or right). If we substitute (1.9) in (1.6) and in (1.7), we obtain an expression for \mathbf{E} and \mathbf{B} :

$$\mathbf{B}(\mathbf{r}, t) = \sum_{\mathbf{k}} \sum_{\lambda=1,2} i\mathbf{k} \times \mathbf{e}_{\mathbf{k},\lambda} A_{\mathbf{k},\lambda}(\mathbf{r}, t) \quad (1.10)$$

$$\mathbf{E}(\mathbf{r}, t) = \sum_{\mathbf{k}} \sum_{\lambda=1,2} i\omega_{\mathbf{k}} \mathbf{e}_{\mathbf{k},\lambda} A_{\mathbf{k},\lambda}(\mathbf{r}, t) \quad (1.11)$$

where $A_{\mathbf{k},\lambda}(\mathbf{r}, t)$ is the one defined in equation (1.9). From these equations, remembering that $k = \frac{2\pi}{\lambda} = \frac{\omega}{c}$, where c is the speed of light, one can see that the contribution of the electric field to the electromagnetic field energy is much bigger than the one of the magnetic field. These last equations can be then used in (1.5) to get an expression for the total energy of the electromagnetic field:

$$\mathcal{H} = \sum_{\mathbf{k}} \sum_{\lambda=1,2} \epsilon_0 V \omega_{\mathbf{k}}^2 (A_{\mathbf{k},\lambda} A_{\mathbf{k},\lambda}^* + A_{\mathbf{k},\lambda}^* A_{\mathbf{k},\lambda}) \quad (1.12)$$

It should be noted that equation (1.12) is not time dependent because the exponentials canceled out. This is in agreement with the principle of conservation of the total energy of the system. Once obtained the expression for the classical energy of the electromagnetic field, it should be expressed in terms of the conjugated variables. Before doing that, it is worth considering the Hamiltonian of an harmonic oscillator with unitary mass, $\hat{H}_{OSC} = \frac{\hat{p}^2}{2} + \frac{1}{2}\omega^2 \hat{q}^2$ where $\hat{p} = -i\nabla$ is the momentum operator and \hat{q} is the position operator. It is useful to define new dimensionless operators starting from \hat{p} and \hat{q} . This leads to the definition of the creation and annihilation operators [20]:

$$\hat{a}^\dagger = \frac{1}{\sqrt{2\omega}} (\omega\hat{q} - i\hat{p}) \quad (1.13)$$

$$\hat{a} = \frac{1}{\sqrt{2\omega}} (\omega\hat{q} + i\hat{p}) \quad (1.14)$$

Since $[\hat{q}, \hat{p}] = i$, it follows that $[\hat{a}, \hat{a}^\dagger] = 1$ and $\hat{a}\hat{a}^\dagger = \frac{1}{\omega} \left(\hat{H}_{OSC} + \frac{1}{2}\omega \right)$, so that

$$\hat{H}_{OSC} = \omega \left(\hat{a}\hat{a}^\dagger + \frac{1}{2} \right) \quad (1.15)$$

If we consider only a single mode, equation (1.15) and (1.12) are formally equivalent, as long as we perform the substitutions

$$A_{\mathbf{k},\lambda} \rightarrow \frac{1}{2\epsilon_0 V \omega_{\mathbf{k}}} \hat{a}_{\mathbf{k},\lambda}, \quad A_{\mathbf{k},\lambda}^* \rightarrow \frac{1}{2\epsilon_0 V \omega_{\mathbf{k}}} \hat{a}_{\mathbf{k},\lambda}^\dagger$$

Substituting the above relations in (1.12), and applying the commutation relations for the creation and annihilation operators, the full quantum Hamiltonian for the electromagnetic field can be written as

$$\hat{H} = \sum_{\mathbf{k}} \sum_{\lambda=1,2} \omega_{\mathbf{k}} \left(\hat{a}_{\mathbf{k},\lambda}^\dagger \hat{a}_{\mathbf{k},\lambda} + \frac{1}{2} \right) \quad (1.16)$$

It should be noted that since we defined the creation and annihilation operators from the momentum and position operator, and since $[\hat{q}, \hat{p}] = i$ we implicitly satisfied the last step of the Canonical Quantization Protocol. In particular, the commutation relation for the creation and annihilation operators is $[\hat{a}_{\mathbf{k},\lambda}, \hat{a}_{\mathbf{k}',\lambda'}^\dagger] = \delta_{\mathbf{k},\mathbf{k}'} \delta_{\lambda,\lambda'}$.

The quantized electromagnetic field can be interpreted as a sum of harmonic oscillators, each of which corresponds to a certain mode. The eigenstates $|n_{\mathbf{k},\lambda}^{(i)}\rangle$ of the Hamiltonian (1.16) are called photon number states (or Fock states), and they constitute a complete and orthonormal basis. The action of the creation and annihilation operators is to add a photon or remove a photon to/from a certain mode and it can be written as:

$$\hat{a}_{\mathbf{k},\lambda}^\dagger |n_{\mathbf{k},\lambda}\rangle = \sqrt{n_{\mathbf{k},\lambda} + 1} |n_{\mathbf{k},\lambda} + 1\rangle \quad (1.17)$$

$$\hat{a}_{\mathbf{k},\lambda} |n_{\mathbf{k},\lambda}\rangle = \sqrt{n_{\mathbf{k},\lambda}} |n_{\mathbf{k},\lambda} - 1\rangle, \hat{a}_{\mathbf{k},\lambda} |0\rangle = 0 \quad (1.18)$$

The number of photons in each mode can be computed by applying the photon number operator $\hat{n}_{\mathbf{k},\lambda} = \hat{a}_{\mathbf{k},\lambda}^\dagger \hat{a}_{\mathbf{k},\lambda}$. Using the formalism of quantum mechanics, we can represent the state of the total field as the tensor product of the state of each mode, that is

$$|n_{\mathbf{k},\lambda}^{(1)}, n_{\mathbf{k},\lambda}^{(2)}, \dots\rangle = |n_{\mathbf{k},\lambda}^{(1)}\rangle \otimes |n_{\mathbf{k},\lambda}^{(2)}\rangle \otimes \dots = |\{n_{\mathbf{k},\lambda}\}\rangle \quad (1.19)$$

An interesting feature of equation (1.16) is that even if there are zero photons in a certain mode, there would still be a contribution to the total energy of the system due to the term $\frac{\omega_{\mathbf{k}}}{2}$. This is the so-called zero point energy, and it can be observed in several phenomena such as the spontaneous emission, the Casimir forces [21] and the Lamb shift [22]. If we consider the vacuum states $|\{0\}\rangle$, it is immediate to see that the energy of the electromagnetic field diverges to infinity. Usually, this problem is disregarded because in a numerical approach one cannot consider an infinite number of modes, and also usually it is interesting to study variations of energy. Finally, assuming linear polarization, the expression for the quantized vector potential reads

$$\mathbf{A}(\mathbf{r}, t) = \sum_{\mathbf{k}} \sum_{\lambda=1,2} \mathbf{e}_{\mathbf{k},\lambda} A_{\mathbf{k}} \left[\hat{a}_{\mathbf{k},\lambda} e^{i(\mathbf{k}\cdot\mathbf{r} - \omega_{\mathbf{k}}t)} + \hat{a}_{\mathbf{k},\lambda}^\dagger e^{-i(\mathbf{k}\cdot\mathbf{r} - \omega_{\mathbf{k}}t)} \right] \quad (1.20)$$

where $A_{\mathbf{k}} = \frac{1}{2\epsilon_0 V \omega_{\mathbf{k}}}$.

1.2. Electrons in solids

All the matter that surrounds us is made up of atoms, which in turn are made of nuclei (protons and neutrons) and electrons. When we deal with isolated atoms, electrons are in the electronic cloud which surrounds the nucleus. Since protons and electrons are charged particles, the system is mainly described by the Coulomb interaction $V_{q_1, q_2} = \frac{q_1 q_2}{4\pi\epsilon_0 d_{q_1, q_2}}$, where q_i is the charge of the i -th particle and can be both positive or negative, and $d_{q_1, q_2} = |\mathbf{r}_1 - \mathbf{r}_2|$ is the distance between the particles. When atoms come together to form more complex systems such as molecules or crystals, each atom contributes to the electronic cloud with some electrons, depending on its outermost shell. Consequently, in principle one could describe condensed matter systems by using Coulomb interaction for every couple of particles in the system. As for the momentum operator, one should sum over the momentum of all particles (both electrons and nuclei). Therefore, one obtains (using atomic units):

$$\hat{H} = \left[-\sum_i \frac{\nabla_i^2}{2} - \sum_I \frac{\nabla_I^2}{2M_I} - \sum_{i,I} \frac{Z_I}{|\mathbf{r}_i - \mathbf{R}_I|} + \frac{1}{2} \sum_{i \neq j} \frac{1}{|\mathbf{r}_i - \mathbf{r}_j|} + \frac{1}{2} \sum_{I \neq J} \frac{Z_I Z_J}{|\mathbf{R}_I - \mathbf{R}_J|} \right] \quad (1.21)$$

$$\hat{H}\Psi(\{\mathbf{r}_i\}, \{\mathbf{R}_I\}) = E_{tot}\Psi(\{\mathbf{r}_i\}, \{\mathbf{R}_I\})$$

where Z_I, M_I are the charge and mass of the I -th nucleus and $\Psi(\{\mathbf{r}_i\}, \{\mathbf{R}_I\})$ is the many-body wave function, which depends on the position of all electrons and all nuclei. As it is known in quantum mechanics, taking the square modulus of the wave functions represents the probability of finding the electron 1 in position \mathbf{r}_1 , the electron 2 in position \mathbf{r}_2 and so on. Instead, taking the integral over all spatial coordinates $\{\mathbf{r}_i\}$ but one leads to the electronic density.

However, due to the terms that mix the coordinates of electrons and ions, equation (1.21) is too complex to be solved. In fact, we cannot solve the Schroedinger equation for the Helium atom, and equation (1.21) is prohibitive also for numerical approaches. Therefore, we have to introduce approximations to be able to solve the system.

1.2.1. Mean-field approach for the electronic problem

To derive the mean-field equations to model materials, one should start by applying approximations to equation (1.21). Later, these approximations will be corrected with the introduction of functionals, thanks to which it is possible to compute exact quantities out of Kohn-Sham equations (see section 1.2.2). It should be underlined that all approximations must be justified with strong physical arguments, otherwise this approach would

lead to inconsistent results.

Solids are a particular class of condensed matter systems, for which the position of the nuclei is almost fixed (within the limit of Heisenberg's uncertainty principle). Therefore, if one considers the nuclei as fixed, then the positions $\{\mathbf{R}_I\}$ of the nuclei are not variables anymore, but rather parameters of the system. Moreover, also the kinetic energy of the nuclei will be negligible with respect to the one of electrons. This becomes clear if one consider that $m_n \approx m_p \approx 1836m_e \gg m_e$, consequently $M_I \gg m_e$. This approximation allows one to separate the electronic problem from the nuclear one, so that one can solve them separately thus simplifying equation (1.21). Defining

$$E = E_{tot} - \frac{1}{2} \sum_{I \neq J} \frac{Z_I Z_J}{|\mathbf{R}_I - \mathbf{R}_J|} \quad (1.22)$$

$$V_n(\mathbf{r}) = - \sum_I \frac{Z_I}{|\mathbf{r} - \mathbf{R}_I|} \quad (1.23)$$

one has that

$$\left[- \sum_i \frac{\nabla_i^2}{2} + \sum_i V_n(\mathbf{r}_i) + \sum_{i \neq j} \frac{1}{|\mathbf{r}_i - \mathbf{r}_j|} \right] \Psi(\{\mathbf{r}_i\}) = E \Psi(\{\mathbf{r}_i\}) \quad (1.24)$$

where the term $V_n(\mathbf{r}_i)$ is called Coulomb potential, and it corresponds to the potential generated by the nuclei that is felt by each electron. The Hamiltonian in equation (1.24) is almost a sum of single-particle Hamiltonians, except for the Coulomb repulsion between electrons, which mixes the coordinates. In fact, the wave function $\Psi(\{\mathbf{r}_i\})$ still depends on the coordinates of all electrons. As a consequence, although equation (1.24) is simpler than equation (1.21), it still cannot be solved.

A further approximation is to disregard the electron-electron interaction and then re-introduce it using a mean-field approach. Within this framework, one can reformulate the many-body problem into a set of single-particle equations for independent particles (*independent particles approximation*). In this approach electrons only know about each other thanks to the mean field that they feel (which is the same for all of them). In this framework, the total Hamiltonian is simply the sum of n single-particle Hamiltonians, the total energy is the sum of the energies of the single-particle problems and the total wave function of the solid can be written as the product of many single-particle wave functions $\Psi(\{\mathbf{r}_i\}) = \phi(\mathbf{r}_1) \phi(\mathbf{r}_2) \dots \phi(\mathbf{r}_n)$. This approximation is very strong because it completely disregards the fermionic nature of the electrons and because the Coulomb interaction terms have the same order of magnitude as the other two in equation (1.24). The first problem is a direct consequence of Pauli's exclusion principle and can be partially

addressed by building the final solution using the Slater determinant formalism. This will allow to recover an anti-symmetric global wave function. Therefore, after solving the single-particle Schroedinger equations, one can build the total wave function as

$$\Psi(\{\mathbf{r}_n\}) = \frac{1}{\sqrt{N!}} \begin{bmatrix} \phi_1(\{\mathbf{r}_1\}) & \phi_1(\{\mathbf{r}_2\}) & \dots & \phi_1(\{\mathbf{r}_N\}) \\ \phi_2(\{\mathbf{r}_1\}) & \phi_2(\{\mathbf{r}_2\}) & \dots & \phi_2(\{\mathbf{r}_N\}) \\ \dots & \dots & \dots & \dots \\ \phi_N(\{\mathbf{r}_1\}) & \phi_N(\{\mathbf{r}_2\}) & \dots & \phi_N(\{\mathbf{r}_N\}) \end{bmatrix} \quad (1.25)$$

It can be shown that if in equation (1.25) the positions of two electrons are swapped, then the wave function changes sign, therefore being anti-symmetric with respect to inversion. This is the expected behavior for fermions. Slater determinants will be discussed more in-depth in section 1.2.3.

The problem of the missing Coulomb potential can be addressed using the Hartree mean field potential. In the previous discussion, we pictured a material as a collection of fixed nuclei surrounded by electrons, which form the electronic cloud. These latter are delocalized in all the volume of the material, with density $n(\mathbf{r}) = \sum_i |\phi_i(\mathbf{r})|^2$, where $\phi_i(\mathbf{r})$ are the single-particle wave functions. From classical electrostatic, it is known that a distribution of charges produces a potential thanks to the Poisson equation [23]. Calling V_H such a potential, and remembering that electrons have a negative charge, one has that

$$\nabla^2 V_H(\mathbf{r}) = -4\pi n(\mathbf{r}) \quad (1.26)$$

$$V_H(\mathbf{r}) = \int \frac{n(\mathbf{r}')}{|\mathbf{r} - \mathbf{r}'|} d\mathbf{r}' \quad (1.27)$$

The new single-particle Hamiltonian can now be written as

$$\left[-\frac{\nabla^2}{2} + V_n(\mathbf{r}) + V_H(\mathbf{r}) \right] \phi_i(\mathbf{r}) = \epsilon_i \phi_i(\mathbf{r}) \quad (1.28)$$

Equation (1.28) is conceptually different from what we wrote before because it intrinsically requires an iterative approach. In fact, it depends on the electronic density $n(\mathbf{r})$, which is calculated from the single-particle wave functions calculated from equation (1.28) itself. We will write the full procedure in section 1.2.2, but the underlying concept is that one chooses an initial electronic density and computes the Hartree potential, then solves the N three-dimensional Schroedinger equation (1.28) and finally uses the obtained wave functions to compute the new density. If the variation within a convergence parameter, then the algorithm stops, and we can compute the many-particle wave function using Slater determinants. The two corrections discussed, allow us to justify the use of the

independent particle approximation and still capture the right physics in the solid. The last step to derive the Hartree-Fock equations is to refine the accounting for the fermionic quantum nature of electrons in (1.28) by introducing the exchange and the correlation potentials. When we introduced the independent particle approximation, we said that one could introduce the fermionic nature by using the single particle wave function to build the Slater determinant Ψ . However, Ψ is only computed at the end of the self-consistent cycle, meaning that when we evaluate the electronic density at each step, the single-particle wave functions ϕ do not account for the Pauli exclusion principle. Since we want to keep using a single-particle Schroedinger equation, we can try to prevent two electrons from occupying the same quantum state by introducing another potential in (1.28). This is called exchange potential V_X and it was first introduced by Fock. Since its derivation is rather complicated and can be found in books [23], we will simply state the main results. We can start by noticing that the *exact* solution of the many-body problem is a linear combination of Slater determinants Ψ_i , built from the *exact* single-particle wave functions ϕ . However, due to the approximations introduced, the ϕ we get after solving equation (1.28) are not exact. From the variation principle [24], we know that the energy calculated

$$E = \langle \Psi | \hat{H} | \Psi \rangle$$

will be minimum if Ψ are the eigenstates of \hat{H} , while it will be higher if, as in our case, the Ψ are only an approximated solution. We can exploit this property by minimizing the energy calculated from equation (1.28) with respect to the single-particle wave functions ϕ , and then imposing the ortho-normality of such states. Therefore we can write:

$$\frac{\delta E}{\delta \phi^*} = 0 \tag{1.29}$$

$$\langle \phi_i | \phi_j \rangle = \delta_{i,j} \tag{1.30}$$

Then, the exact form of the exchange potential is

$$V_X(\mathbf{r}, \mathbf{r}') = - \sum_j \frac{\phi_j^*(\mathbf{r}') \phi_j(\mathbf{r})}{|\mathbf{r} - \mathbf{r}'|} \tag{1.31}$$

The potential (1.31) allows considering the Pauli principle using a single-particle approach. The correlation potential, on the contrary, arises from the fact that in a many-body picture electrons interact via the repulsive Coulomb potential. Therefore the probability of finding two electrons next to each other is lower for the Slater determinant than for the single-particles wave function that we use in each iteration. In formulas, $|\Psi(\{\mathbf{r}_i\})|^2 < |\prod_i \phi_i(\mathbf{r}_i)|^2$. As for the exchange potential, we can account for this effect by introducing

the potential $V_c(\mathbf{r})$.

These final two potentials are computationally expensive as they require the evaluation of the wave functions in different spatial coordination, and are therefore non-local. To reduce the cost, usually one defines the local potential V_{xc} , which accounts for both effects. Finally, one can rewrite equation (1.28) as

$$\left[-\frac{\nabla^2}{2} + V_n(\mathbf{r}) + V_H(\mathbf{r}) + V_{xc}(\mathbf{r}) \right] \phi_i(\mathbf{r}) = \epsilon_i \phi_i(\mathbf{r}) \quad (1.32)$$

The set of equations (1.32) (one for each particle) is called *Kohn-Sham equations*, and it will be discussed more in-depth in the next section. It should be noted that V_H, V_{xc} arise from the fact that after equation (1.24) we neglected the Coulomb interaction.

1.2.2. Kohn-Sham equations and Density Functional Theory

Density functional theory is an exact ground state theory that allows describing the properties of materials from a microscopic point of view. It is based on the Hohenberg-Kohn theorems (1964) [25], and since then its implementations (which have approximations) have evolved to include more corrections and features. A partial timeline of DFT may be found in chapter 1.3 of [23]. In this chapter the main ideas of DFT starting from the aforementioned theorems are briefly described. Subsequently, the implementation of this theory is discussed, with a focus on the self-consistent algorithm for the Kohn-Sham (KS) equations.

In the previous section, before introducing the independent particles approximation, we derived equation (1.24) which still depends on the many-body wave function $\Psi(\{\mathbf{r}_i\})$. We should note that the material dependence of the Hamiltonian is in the position of the nuclei, which were assumed to be fixed, and in the number of electrons, which is assumed to be constant (isolated system). Therefore, a change in the energy of the system can only be caused by a variation of the wave function (apart from changes in the phase). This concept can be formulated by saying that the energy is a functional of Ψ : $E = \mathcal{F}[\Psi(\{\mathbf{r}_i\})]$. This is generally true for all states, both the excited and the ground state. However Hohenberg-Kohn noticed that for the ground state, one can say that the energy is a function of the electronic density which has a one-to-one correspondence with the external potential. This becomes clear if one considers the proof of the Hohenberg-Kohn theorem, but for the sake of conciseness, it will not be discussed here. Quoting directly the original paper [25], this can be expressed as *the external potential $V_{ext}(\mathbf{r})$ is (to within a constant) a unique functional of $n(\mathbf{r})$; since, in turn $V_{ext}(\mathbf{r})$ fixes \hat{H} we see that the full many particle ground state is a unique functional of $n(\mathbf{r})$* . The

procedure that arises from the Hohenberg-Kohn theorem is that the electronic density uniquely defines an external potential. This uniquely defines the Hamiltonian of the system which in turn uniquely defines the many-body wave function of the ground state: $n \leftrightarrow V_{ext,n} \leftrightarrow [\hat{T} + \hat{V}_{ext,n}] \Psi = E\Psi \leftrightarrow E$.

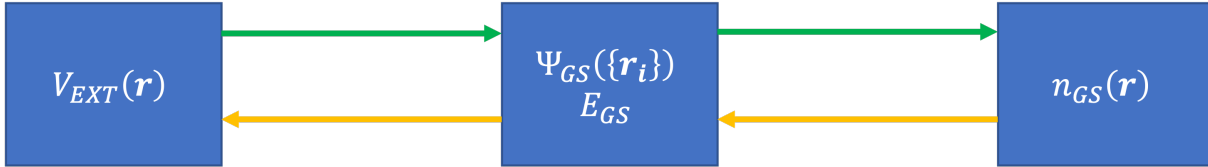


Figure 1.1: Representation of the Hohenberg-Kohn theorem. The green arrows representing the mapping from the external potential to the density are straightforward from the previous discussion. The Hohenberg-Kohn theorem proves the mapping from the density to the external potential.

Therefore, one can write

$$E = F[n(\mathbf{r})] \quad (1.33)$$

Equation (1.33) is immensely simpler than the general formulation $E = \mathcal{F}[\Psi(\{\mathbf{r}_i\})]$ because it only depends on the three spatial variables rather than on the coordinates of all the particles in the many-body problem. It should be stressed that equation (1.33) is valid only if we are interested in the ground state of the material. The functional $F[n(\mathbf{r})]$ then takes the form

$$F[n(\mathbf{r})] = \int n(\mathbf{r}) V_n(\mathbf{r}) d\mathbf{r} + \langle \Psi[n] | \hat{T} + \hat{W} | \Psi[n] \rangle \quad (1.34)$$

where \hat{T} is the kinetic energy operator and \hat{W} is the Coulomb energy operator. To recover the form of the Kohn-Sham equations (1.32) one should then make the density dependency explicit in all terms. The idea is to build a system of independent particles whose ground state density is the same as the one of the interacting many-body system. Then, since the ground state energy is a universal functional of the density, having the density of the system of independent particles allows computing the ground state energy. This expressed this, one defines the total potential V_{tot} that is the sum of the Coulomb potential V_n , of the Hartree potential V_H and of the exchange-correlation potential V_{xc} . The density of the ground is then the one for which

$$\left. \frac{\delta F[n]}{\delta n} \right|_{n_0} = 0$$

from which follows that

$$V_{xc}(\mathbf{r}) = \left. \frac{\delta E_{xc}[n]}{\delta n} \right|_{n(\mathbf{r})} \quad (1.35)$$

Despite having a formulation for the exchange-correlation potential, to this day the exact analytical form is not known. Therefore, we can think that V_{xc} is a collector for everything that is not included in the Hartree potential. Nevertheless, the presence of such a potential is vital for DFT as its effectiveness depends on the approximation that one chooses for $E_{xc}[n]$. From this perspective, it is easy to understand why after the original formulation of the Kohn-Sham equation a lot of effort has been put into constructing an approximation that was both simple (computationally) and accurate for describing the system.

Finally, we can state the full algorithm to solve the Kohn-Sham equations self consistently.

Algorithm 1.1 Self consistent solution of the Kohn-Sham equations

- 1: Given the coordinates of the nuclei, compute $V_n(\mathbf{r}) = -\sum_I \frac{Z_I}{|\mathbf{r}-\mathbf{R}_I|}$
 - 2: Choose a suitable approximation for the exchange-correlation potential $E_{xc}[n]$
 - 3: Make an initial guess of the electronic density $n(\mathbf{r})$ and choose a tolerance δ
 - 4: **while** $n_i(\mathbf{r}) - n_{i+1}(\mathbf{r}) > \delta$ **do**
 - 5: Compute the Hartree potential $\nabla^2 V_H(\mathbf{r}) = -4\pi n(\mathbf{r})$
 - 6: Compute the exchange-correlation potential $V_{xc}(\mathbf{r}) = \left. \frac{\delta E_{xc}[n]}{\delta n} \right|_{n(\mathbf{r})}$
 - 7: Compute the total potential $V_{tot}(\mathbf{r}) = V_n(\mathbf{r}) + V_H(\mathbf{r}) + V_{xc}(\mathbf{r})$
 - 8: Solve the single particle Hamiltonian $\left[-\frac{\nabla^2}{2} + V_{tot}(\mathbf{r}) \right] \phi_i(\mathbf{r}) = \epsilon_i \phi_i(\mathbf{r})$
 - 9: Compute the new ground state density $n_{i+1}(\mathbf{r}) = \sum_i |\phi_i(\mathbf{r})|^2$
 - 10: **end while**
-

1.2.3. Slater determinants

In the previous section we described how we can calculate the electronic states in a solid. We followed a single-particle approach that led us to the definition of the Kohn-Sham equation. We also mentioned that once we have the wave function ϕ we can combine them with the formalism of the Slater determinant to build the many-body wave function Ψ . We shall now explore this formalism.

When we introduced the independent particles approximation, we supposed that we could describe the global wave function as $\Psi(\{\mathbf{r}_i\}) = \phi(\mathbf{r}_1)\phi(\mathbf{r}_2)\dots\phi(\mathbf{r}_n)$. We may rewrite this relation using the bra/ket formalism, thus obtaining

$$|\Psi\rangle = |\mathbf{x}_1\rangle |\mathbf{x}_2\rangle \dots |\mathbf{x}_n\rangle \quad (1.36)$$

where $\mathbf{x} = (\mathbf{r}, \sigma)$ is the position-spin operator. These kets form an orthonormal basis, so that $\langle \mathbf{x}'_i | \mathbf{x}_i \rangle = \delta(\mathbf{x}'_i - \mathbf{x}_i)$, and if one takes the integral of the square modulus of $|\Psi(\{\mathbf{x}_i\})|^2 d\mathbf{r}_1 d\mathbf{r}_2 \dots d\mathbf{r}_{i-1} d\mathbf{r}_{i+1} \dots d\mathbf{r}_n$ one gets the probability of finding an electron with spin σ_i in a volume element $d\mathbf{r}_i$. However, describing the electrons in solids means dealing with a many-body problem of identical particles which means that in equation (1.36) we should not put labels on electrons, thus obtaining

$$|\Psi\rangle = |\mathbf{x}_1, \mathbf{x}_2, \dots, \mathbf{x}_N\rangle \quad (1.37)$$

The object Ψ belongs to the Hilbert space \mathcal{H}_N , where N is the number of particles in the system. This notation is very general and applies to both bosons and fermions. Since we want to deal with electrons, we can state that Ψ should be anti-symmetric with respect to the inversion of two coordinates, such that $|\mathbf{x}_{P(1)} \mathbf{x}_{P(2)} \dots \mathbf{x}_{P(N)}\rangle = (\pm)^P |\mathbf{x}_1 \mathbf{x}_2 \dots \mathbf{x}_N\rangle$. In the latter, P is the permutation applied to a particle, therefore applying $P(1)$ to a generic electron would swap its position with the one the electron in position 1. Therefore, many configurations represent the same physical state. This is understandable if we think that the wave function has no direct physical meaning, whereas its square modulus (which represents a probability) does not change if we change the sign. We may still write an orthonormality relation as

$$\langle \mathbf{x}'_1 \dots \mathbf{x}'_N | \mathbf{x}_1 \dots \mathbf{x}_N \rangle = \sum_P (\pm)^P \prod_{j=1}^N \delta(\mathbf{x}'_j - \mathbf{x}_{P(j)}) = N! \delta(0)^N \quad (1.38)$$

where $N!$ is the total number of possible configurations for the system. This formalism may seem heavy, but it simplifies many problems because we can perform the calculation in the most suitable base for the problem, and then project the wave function onto the base of the position-spin. Thus, if we consider a generic state $|n\rangle$, then its projection onto the position-spin base is given by $\langle \mathbf{x} | n \rangle = \phi_n(\mathbf{x})$. If we define

$$\Psi = |n_1, n_2, \dots, n_N\rangle = \int \phi_{n_1}^* \dots \phi_{n_N}^* |\mathbf{x}_1 \dots \mathbf{x}_N\rangle d\mathbf{x}_1 \dots d\mathbf{x}_n \quad (1.39)$$

and we use equation (1.38) to perform the projection onto the base of the position-spin, then we obtain

$$\Psi_{n_1 \dots n_N}(\mathbf{x}_1 \dots \mathbf{x}_n) = \sum_P (\pm)^P \phi_{n_1}(\mathbf{x}_{P(1)}) \dots \phi_{n_N}(\mathbf{x}_{P(N)}) = \begin{bmatrix} \phi_{n_1}(\{\mathbf{x}_1\}) & \phi_{n_1}(\{\mathbf{x}_2\}) & \dots & \phi_{n_1}(\{\mathbf{x}_N\}) \\ \phi_{n_2}(\{\mathbf{x}_1\}) & \phi_{n_2}(\{\mathbf{x}_2\}) & \dots & \phi_{n_2}(\{\mathbf{x}_N\}) \\ \dots & \dots & \dots & \dots \\ \phi_{n_N}(\{\mathbf{x}_1\}) & \phi_{n_N}(\{\mathbf{x}_2\}) & \dots & \phi_{n_N}(\{\mathbf{x}_N\}) \end{bmatrix} \quad (1.40)$$

which is equivalent to the Slater determinant (1.25). Since we did not make any assumption of the general state (1.39), and yet we obtained the expression of the Slater determinant only following general algebraic rules, it is easy to guess that this method is very powerful and it can be done for any property of our system.

1.2.4. Second quantization and Slater determinant excitation

After having obtained the expression for the Slater determinant in a general form, we should now explore what it means to excite such a state. This is particularly important because in chapter 2 we will use Slater determinants as a basis for the Cavity QED Hamiltonian.

Before starting to explore such excitation, it is useful to introduce the language of the second quantization. Let us consider the state (1.37), which lives in the Hilbert space \mathcal{H}_N . If we want to build such a state, we can start from the vacuum state $\Psi = |\{0\}\rangle$, which lives in the Hilbert space \mathcal{H}_0 and define a *field operator* $\widehat{\psi}^\dagger(\mathbf{x}_i)$ such that

$$|0, 0, \dots, \mathbf{x}_i, \dots, 0\rangle = \widehat{\psi}^\dagger(\mathbf{x}_i) |0\rangle \quad (1.41)$$

$$|\mathbf{x}_1, \mathbf{x}_2, \dots, \mathbf{x}_N\rangle = \prod_{i=1}^N \widehat{\psi}^\dagger(\mathbf{x}_i) |0\rangle \quad (1.42)$$

The commutation relation between two creation operators applied at different coordinates can easily be obtained by considering the change in the sign of the state if we swap two coordinates, and then rewrite it in terms of the products of creation operators. If we do so we obtain $\left[\widehat{\psi}^\dagger(\mathbf{x}_1), \widehat{\psi}^\dagger(\mathbf{x}_2) \right]_{\pm} = 0$, where the $+$ refers to the fermions, the $-$ to bosons. Analogously, we can define an annihilation operator $\widehat{\psi}(\mathbf{x}_i)$ which removes a particle from a state. It follows the same commutation rules as the creation operator, but it has a significant difference in that if we apply the annihilation operator to the vacuum state, then we get zero (the Hilbert space \mathcal{H}_{-1} is not defined, and physically it would not make

sense to have a negative number of particles in a state). The action of the annihilation operator on a generic Slater determinant is less trivial due to the conservation of the symmetry of the wave function after the application of the operator. It can be shown [26] that

$$\hat{\psi}(\mathbf{x}_i) |\mathbf{y}_1, \mathbf{y}_2, \dots, \mathbf{y}_N\rangle = \sum_{k=1}^N (\pm)^{N+k} \delta(\mathbf{x} - \mathbf{y}_k) |\mathbf{y}_1, \dots, \mathbf{y}_{k-1}, \mathbf{y}_{k+1}, \dots, \mathbf{y}_N\rangle \quad (1.43)$$

which means that the annihilation operator produces a state which is the sum of many states belonging to the Hilbert space \mathcal{H}_{N-1} . Finally, we state the commutation relation between the field creation and annihilation operators

$$\left[\hat{\psi}(\mathbf{x}_1), \hat{\psi}^\dagger(\mathbf{x}_2) \right]_{\pm} = \delta(\mathbf{x}_1 - \mathbf{x}_2) \quad (1.44)$$

Note that equation (1.44) is a generalization of the commutation relation between the creation and annihilation operators defined in (1.13) and (1.14).

Now that we introduced the second quantization, we can deal with understanding what it means to excite a Slater determinant. In this work, by exciting a state it is meant removing a particle from an occupied state and adding it to a non-occupied state. This can be expressed by using the transition operator $\hat{t} = \hat{\psi}_I^\dagger \hat{\psi}_J$, where I, J are the set of indices that describe the particular state in our system. For an atom or a molecule they might simply be the index of the state, while in a solid one should also include the k-point index. It may happen that one finds a many transitions operators applied in sequence $\hat{t}_1 \hat{t}_2 \dots$. In that case it is possible to use repeatedly equation (1.44) to reorganize the operators in such a way that is easy to exploit the application of the annihilation operator of a vacuum state, thus simplifying the expression. For examples of the application of such operators, refer to Appendix A.

1.3. QED Hamiltonian

In the previous sections we dealt with the quantization of the electromagnetic field and with the description of electrons in solid. We shall now combine the two to study their interaction. We will study their interaction in the framework of Quantum Electrodynamics (QED). Firstly we will derive the QED Hamiltonian for a single mode, then we will briefly introduce optical cavities and finally we will study the two limits for the QED Hamiltonian (weak and strong).

To write the Hamiltonian of the QED problem, let us first consider the Hamiltonian for

a single particle in a generic system.

$$\hat{H} = \frac{\hat{\mathbf{p}}^2}{2} + \hat{V}_{tot}(\mathbf{r}) \quad (1.45)$$

where \mathbf{p} represents the momentum of the particle and V_{tot} is the potential to which the particle is subjected. When a charged particle moves in an electromagnetic field (in our case we refer to electrons), its momentum $\mathbf{p} = m\mathbf{v}$ is not a conserved quantity anymore, therefore it cannot be used to write the Hamiltonian of the system. Instead, one should use the generalized momentum $\mathbf{p} = m\mathbf{v} - q\mathbf{A}(\mathbf{r}, t)$, where $\mathbf{A}(\mathbf{r}, t)$ is the vector potential describing the field and q is the charge of the particle. Since in the present work we operate with atomic units, we set both q and m to 1. Thus, the new Hamiltonian for a single particle becomes:

$$\hat{H} = \frac{(\hat{\mathbf{p}} - \hat{\mathbf{A}})^2}{2} + \hat{V}_{tot}(\mathbf{r}) \quad (1.46)$$

Before continuing with the calculation, it is important to set a Gauge for the vector potential. A common choice in the field of QED is the velocity Gauge (see Appendix A), thanks to which the momentum p of the particle and the vector potential commute ($[\mathbf{p}, \mathbf{A}] = 0$). Since the system we want to describe has both electrons and photons, we shall also introduce the Hamiltonian of the electromagnetic field in the case of a single mode. Therefore one can write:

$$\begin{aligned} \hat{H}_{QED} &= \frac{(\hat{\mathbf{p}} - \hat{\mathbf{A}})^2}{2} + \hat{V}_{tot}(\mathbf{r}) + \omega \left(\frac{1}{2} + \hat{a}^\dagger \hat{a} \right) \\ &= \frac{\hat{\mathbf{p}}^2}{2} + \hat{V}_{tot}(\mathbf{r}) + \frac{\hat{\mathbf{A}}^2}{2} + \omega \left(\frac{1}{2} + \hat{a}^\dagger \hat{a} \right) - \hat{\mathbf{p}} \cdot \hat{\mathbf{A}} \end{aligned} \quad (1.47)$$

In equation (1.47) one can easily recognize three terms, an Hamiltonian for the electron part, one for the photon part and an interaction Hamiltonian: $\hat{H}_{QED} = \hat{H}_{el} + \hat{H}_{ph} + \hat{H}_{el-ph}$

- $\hat{H}_{el} = \frac{\hat{\mathbf{p}}^2}{2} + \hat{V}_{tot}(\mathbf{r})$
- $\hat{H}_{ph} = \omega \left(\frac{1}{2} + \hat{a}^\dagger \hat{a} \right)$
- $\hat{H}_{el-ph} = \frac{\hat{\mathbf{A}}^2}{2} - \hat{\mathbf{p}} \cdot \hat{\mathbf{A}}$

The latter term, which arises uniquely from the canonical momentum substitution, is the one that couples the electrons with the electromagnetic field. In the matrix representation of this Hamiltonian, all the non-diagonal elements are generated by \hat{H}_{el-ph} (which contains the bi-linear coupling term and the diamagnetic term $\hat{\mathbf{A}}^2$), so if that term was not present we would simply have a material (electronic system) in the same region of space of an electromagnetic field, which would lead to a simple absorption problem.

Finally, since our system of interest is made of many electrons equation (1.45) should be generalized to

$$\sum_{i=1}^{N_{el}} \frac{\hat{\mathbf{p}}_i^2}{2} + \hat{V}_{tot}(\mathbf{r}_i)$$

Since all electrons in the systems move in the same electromagnetic field, we have to perform the canonical momentum substitution $\hat{\mathbf{p}} \rightarrow \hat{\mathbf{p}} - \hat{\mathbf{A}}$ for every electron. After some algebra, one obtains:

$$\hat{H}_{QED} = \sum_{i=1}^{N_{el}} \left(\frac{\hat{\mathbf{p}}_i^2}{2} + \hat{V}_{tot}(\mathbf{r}_i) \right) + \omega \left(\frac{1}{2} + \hat{a}^\dagger \hat{a} \right) + \frac{N_{el} \hat{\mathbf{A}}^2}{2} - \sum_{i=1}^{N_{el}} \hat{\mathbf{p}}_i \cdot \hat{\mathbf{A}} \quad (1.48)$$

where N_{el} represents the total number of electrons in each unit cell. It is easy to see that the first term corresponds to a sum of single particles Hamiltonians. The second term corresponds to the Hamiltonian of the radiation field and the last terms are the ones that effectively couple different matrix elements.

1.3.1. Optical Cavities

Optical cavities are regions of space confined by two mirrors, that can trap photons inside them. The simplest layout is given by a Fabry-Perot interferometer, which is simply made of two plane mirrors with reflectivity R_1, R_2 separated by a distance L_{cav} . Due to the presence of the mirrors only specific modes which satisfy the appropriate boundary conditions can be confined by the cavity. Their frequency can be expressed as

$$\omega_n = m \frac{\pi c}{n L_{cav}}$$

where m is the order of the FP window. Each mode is then characterized by a spectral width

$$\Delta\omega = \frac{\pi c}{n \mathcal{F} L_{cav}}$$

where \mathcal{F} is the finesse, a parameter of the FP interferometer which depends only on the reflectivity of the mirrors, and controls the losses of the cavity [27].

Controlling the losses is a central topic for optical cavities. If one wants to realize a laser, then the losses control firstly whether a specific mode can be supported by the cavity and also the optical power emitted. On the contrary, if we want to have a cavity for studying QED phenomena we want to reduce the losses as much as possible. Optical losses are mainly caused by non-resonant decay (whose rate is called rate γ) and photon decay (whose rate is called κ). For atoms in cavities, the former can be modeled as

$\gamma = \frac{A_{21}}{2} \left(1 - \frac{\Delta\Omega}{4\pi}\right)$, where A_{21} is the Einstein coefficient for spontaneous emission (from an excited state 2 to the ground state 1) and $\Delta\Omega$ is the solid angle subtended by the cavity mode. For solids it should include also other phenomena such as phonon scattering, whose importance increases with temperature. The photon decay rate can be modeled as $\kappa = \frac{\omega}{Q}$, where $Q = \frac{\omega}{\Delta\omega}$, is the quality factor of the cavity.

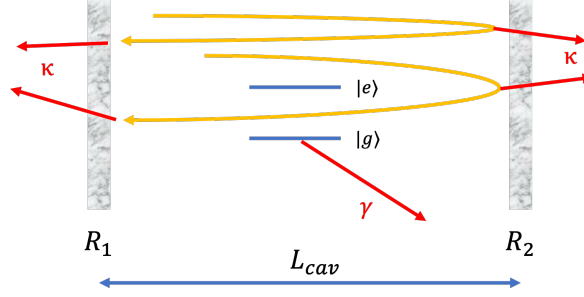


Figure 1.2: FP cavity with a single atom (two-level system) inside. The yellow lines represent the round-trip of the light, while the red lines represent the losses κ and γ

Although FP interferometers constitute a good model, they cannot be used as cavities in real QED applications, as they can only confine photons whose k vector is exactly perpendicular to the mirrors. Instead, the mirrors should be curved so that the light can be confined. Then, the interaction between the confined light and the cavity is described by (1.48), and the solution depends on the coupling strength g_0 . For atoms in optical cavities it can be shown that

$$g_0 = \frac{\mu_{12}^2 \omega}{2\epsilon_0 \hbar V_0}$$

where μ_{12} is the electric dipole moment. In particular, if we are in the weak regime then we can diagonalize the \hat{H}_{el} and \hat{H}_{ph} separately and treat \hat{H}_{el-ph} with perturbation theory, whereas if the coupling is strong one has to diagonalize the full \hat{H}_{QED} . The condition to distinguish the two is $\sqrt{N}g_0 \gg \max(\kappa, \gamma)$ [27], where N is the number of atoms in the cavity.

1.3.2. Weak regime

As we discussed in the previous section, the weak regime corresponds to the case when $\sqrt{N}g_0 < \max(\kappa, \gamma)$. Physically it corresponds to having a low-intensity laser or being in a low-Q cavity. To study the weak regime, let us consider a two-level system describing the ground $|g\rangle$ and the excited state $|e\rangle$. Since we want to study an excitation or a relaxation phenomenon, we should write the operators that correspond to the transition between

those states. We will have that

$$\hat{\sigma}_+ = \hat{c}_e^\dagger \hat{c}_g, \quad \hat{\sigma}_+ |e\rangle = 0 \quad (1.49)$$

$$\hat{\sigma}_- = \hat{c}_g^\dagger \hat{c}_e, \quad \hat{\sigma}_- |g\rangle = 0 \quad (1.50)$$

where \hat{c}, \hat{c}^\dagger are the creation and annihilation operators for the electronic states. To keep the model as simple as possible, we can then choose our base to be $\{|g\rangle, |e\rangle\} \otimes \{|n\rangle, |n+1\rangle\}$ with obvious meaning of the symbols. Since we are in the weak regime, we can describe the system using perturbation theory, in particular with the Fermi Golden Rule. With that, one can compute the transition probability per unit of time W between two states as

$$W = \frac{2\pi}{\hbar^2} |M_{if}|^2 g(\omega) \delta(\hbar\omega - E_{if}) \quad (1.51)$$

where $g(\omega)$ is the density of states and M_{if} is the transition matrix element between the initial state $|i\rangle$ and the final state $|f\rangle$. In the following, it will be assumed that the interaction Hamiltonian is given by the electric dipole. To do this we basically have to substitute \hat{A} with \hat{E} in equation (1.48). This assumption is reasonable in most setups, as it fails when the wavelength of the photon is comparable with the characteristic dimension of the system or when the electrons are very energetic. If we further assume that the system is centered at $\mathbf{r} = 0$ and that the transition is perfectly resonant, then from equation (1.48), we have:

$$\hat{H}_{int} = i\hbar g \sum_{i=+,-} \hat{\sigma}_i (\hat{a} - \hat{a}^\dagger) = i\hbar g (\hat{\sigma}_+ \hat{a} - \hat{\sigma}_- \hat{a}^\dagger) \quad (1.52)$$

where g is the coupling strength and in the last step we already excluded the non-physical transitions $\hat{\sigma}_+ \hat{a}^\dagger$ and $\hat{\sigma}_- \hat{a}$. Finally, by specifying the initial and final states as $|g, n+1\rangle, |e, n\rangle$, if we compute the transition matrix elements between them we get:

$$\text{absorption} : \langle g, n+1 | \hat{H}_{int} | e, n \rangle = i\hbar g \sqrt{n} \quad (1.53)$$

$$\text{emission} : \langle e, n | \hat{H}_{int} | g, n+1 \rangle = i\hbar g \sqrt{n+1} \quad (1.54)$$

When these are substituted into equation (1.51) we get the absorption and emission rates between those two states. It should be noted that for emission we have $\sqrt{n+1}$, and therefore we get two terms for the emission coefficient. The one corresponding to the +1 is the spontaneous emission, which in the semi-classical theory has to be introduced manually, whereas in QED is directly described because we are accounting for the quantized nature of the electromagnetic field.

1.3.3. Strong regime

In the strong coupling regime it holds that $\sqrt{N_{el}}g_0 \gg \max(\kappa, \gamma)$. This regime could be reached either by using a high-Q cavity (so we allow a photon to interact multiple times with the atom because it stays in the cavity for a long time before being lost) or by using a high-intensity beam. In the following it former case will be discussed, as with the latter one should use a laser intensity that is so high that the material starts to melt.

Since the coupling between light and matter is strong, we cannot use perturbation theory as in the previous section. Besides not being able to use the Fermi Golden Rule and therefore having to diagonalize the QED Hamiltonian, it has a deeper physical meaning. The states of the atom and of the electromagnetic field are now mixed, which means that alone they do not provide a good description of the system. We will refer to these atomic and photonic states as the *bare* states. The eigenstates of the system are therefore a mix of *bare* states, $|\Psi\rangle = |\psi, n\rangle$, and they will be referred to as *dressed* states.

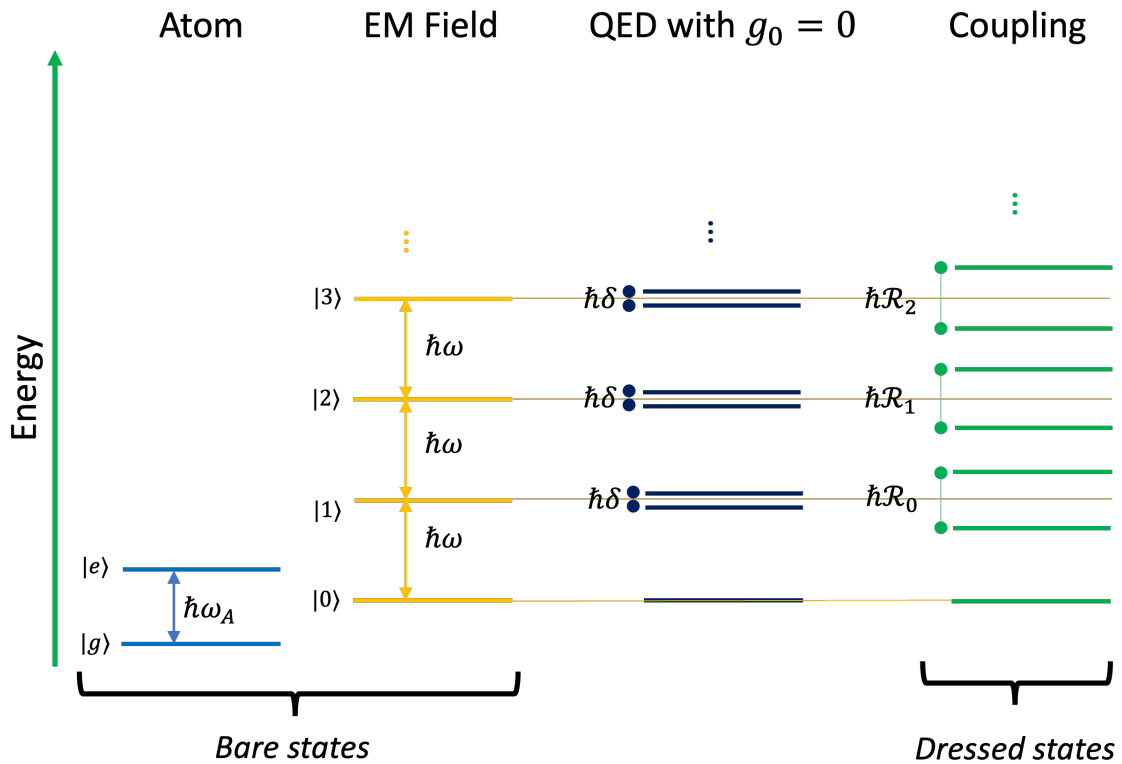


Figure 1.3: Energy diagram for a single atom (represented by a two level system) in a QED Cavity in strong regime. The first two columns represent the bare states, which constitute the base for our interaction Hamiltonian. Their coupling generates a pairs of degenerate levels, which constitute the sub-spaces of our problem. The degeneracy is broken when $g_0 > 0$, and then we have the dressed states

To build the QED Hamiltonian we will start from a base that is the tensor product of the atomic and photonic bare states. In this picture, the ground state of the system corresponds to the dressed state $|\Psi\rangle = |g, 0\rangle$ and it is the only non-degenerate state. If we are at resonance, all the other states are double degenerate as their energy can be obtained both by using the atomic ground state and the photonic state with an extra photon or vice-versa. If we are not at resonance, this degeneracy is broken by a small amount. This allows separating the space of our dressed states into many sub-spaces, each of which is composed of two quasi-degenerate (or degenerate) dressed states. The strong coupling does not allow to have transitions between different sub-spaces (for that we need the ultra-strong coupling), but only within a subspace.

This means that we can describe each sub-space with a 2x2 matrix. Using equation (1.48), we get:

$$\hat{H}_{QED} = \begin{bmatrix} H_{g,n+1;g,n+1} & H_{g,n+1;e,n} \\ H_{e,n;g,n+1} & H_{e,n;e,n} \end{bmatrix} = \begin{bmatrix} (n + \frac{1}{2}) \hbar\omega + \frac{\hbar}{2}\delta & \hbar g\sqrt{n+1} \\ \hbar g\sqrt{n+1} & (n + \frac{1}{2}) \hbar\omega - \frac{\hbar}{2}\delta \end{bmatrix} \quad (1.55)$$

where $\delta = \omega_A - \omega$ is the detuning parameter, and it is a measure of the resonance. ω_A is the energy separation of the atomic levels. By diagonalizing equation (1.55) we get

$$\lambda_n^\pm = \hbar\omega \left(n + \frac{1}{2} \right) \pm \frac{\hbar}{2} \mathcal{R}_n \quad (1.56)$$

$$\Psi_n^\pm = \frac{1}{\sqrt{2}} (|g; n\rangle \mp |e; n-1\rangle) \quad (1.57)$$

where $\mathcal{R}_n = \sqrt{4g^2(n+1) + \delta^2}$ is the Rabi splitting. It is interesting to note that even if there are no photons in the cavity ($n = 0$), the Rabi splitting is non zero. This is a consequence of the zero point energy that comes from the quantization of the electromagnetic field.

Strong coupling has been observed both in single atoms [28] and in solid state physics whenever the local structure can be described with discrete level (e.g. quantum dots [29] or quantum wells).

1.4. Polaritons

In the previous section we described the strong coupling regime between atoms and photons, introducing the concepts of dressed states and Rabi splitting. In more recent times it has been shown possible to reach strong coupling for solid-state in cavities, leading to the discovery of new interesting physics [15, 30].

When light propagates through a medium, it couples with the latter through the polarization vector $\mathbf{P} = \epsilon_0 (\epsilon(\omega) - 1) \mathbf{E}$. This relation can be derived directly from Maxwell's equation. In classical terms, the propagation of electromagnetic waves in a material generates the oscillation of the electronic cloud (described in terms of Hertzian dipoles). The latter then emits new radiation, which contributes to the evolution of the radiation wave. Using the formalism of section 1.3.3, if the coupling between light and matter is strong we may say that the states of matter and light are mixed and we may call them dressed states. The quasi-particles associated with these new states are called polaritons (a mixture of polarization and photons). In quantum mechanical terms, they are a superposition between the particle representing the matter (more than 70 types of polaritons exist [16]) and the photons [30].

Like every quasi-particle, polaritons are characterized by a dispersion relation $E(\mathbf{k}) = \hbar\omega(\mathbf{k})$ [31]. To obtain such a relation, we can start by considering the \mathbf{k} vector of photons propagating in matter, that is

$$\mathbf{k}^2 = k^2 = \tilde{n}^2(\omega) k_v^2 \quad (1.58)$$

where $k_v = \frac{2\pi}{\lambda}$ is the k vector in vacuum and $\tilde{n}(\omega)$ is the complex refractive index. By calling $\tilde{n}^2(\omega) = \epsilon(\omega)$ and using the relation for the complex refractive index in materials we get

$$\frac{c^2 k^2}{\omega^2} = \epsilon_b + \frac{f}{\omega_0^2 - \omega^2 + i\omega\gamma} \quad (1.59)$$

where γ is a damping parameter [31].

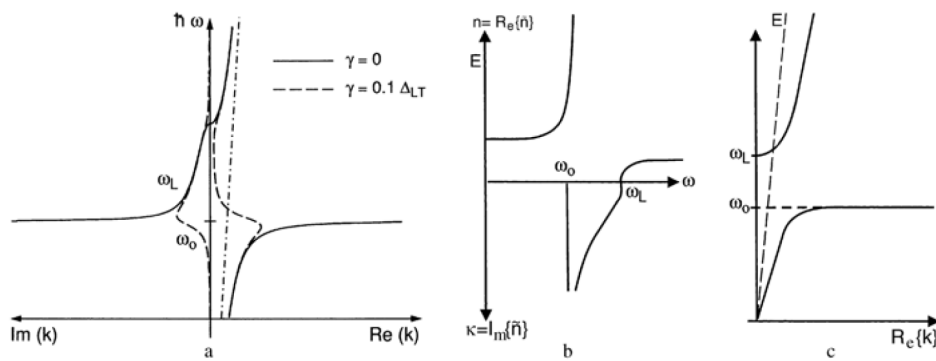


Figure 1.4: The polariton dispersion in the vicinity of a single resonance for vanishing damping (solid lines) and finite damping (dashed lines) for $\epsilon_b = 1$. The dashed-dotted line gives the dispersion of photons in vacuum (a); real and imaginary parts of $\tilde{n}(\omega)$ for vanishing damping (b) and the creation of the polariton dispersion (solid lines) from those of excitons and photons (dashed lines) and the non-crossing rule: $\epsilon_b = 1$ (c). This figure is taken from [31]

Apart from the dispersion relation, it is interesting to consider what the polaritonic spectrum looks like. In section 1.3.3 we said that when the states of light and matter are coupled, then the system is divided into many sub-spaces, each of which has two states. If the light is perfectly resonant the two are degenerate, otherwise they are slightly split. When the light-matter interaction is turned on, then the degeneracy is removed thanks to the Rabi splitting. The two levels are now separated, but they still interact thanks to the polaritons. The dispersion relation of a polariton then follows the one of the photons in vacuum as long as we are far from the resonance (Rabi frequency) of the two dressed states. As it can be seen in Fig 1.4 a polaritonic dispersion relation, this feature is observed. In fact, as it can be seen in Figure 2 of [7], by plotting the linear optical response for different coupling parameters, one can see that when there is no coupling the absorption spectrum has all the lines of the material. When the coupling is turned on, those lines begin to separate in the upper and lower branch, called indeed upper and lower polariton.

2 | Methods

In chapter 1 we described the theoretical framework of the present work, starting from the quantization of the electromagnetic field and the behavior of electrons in solid, and then combining the two. We will now describe the specific problem of this work, discussing the relevant assumption to simplify the QED Hamiltonian introduced in the previous chapter to make it approachable with computational techniques. We also provide a simple example of a single Hydrogen atom in the cavity.

2.1. Approximations and Working Assumptions

The goal of the software developed in this work is to diagonalize the QED Hamiltonian (1.48) when we put any material in an optical cavity. We can mainly distinguish between two types of systems, non-periodic (like atoms and molecules) and periodic ones (solids). Both of them are described using the many-body version of equation (1.48). In fact, in section 1.3 we derived the QED Hamiltonian starting from a single particle for the matter part, and then we simply increased the number of particles without considering their interaction. However, in section 1.2 we said that the quantum state of electrons in solids (and more in general in many-body systems) is described by a linear combination of Slater determinants, each of which can be built using the single particle wave functions. Therefore, in equation (1.48) the single-particles momentum operator $\sum_i \hat{\mathbf{p}}_i$ should be substituted with the momentum operator between Slater determinants $\hat{\mathbf{P}}$. Therefore, equation (1.48) becomes:

$$\hat{H}_{QED} = \hat{H}_{el} + \frac{N_{el} A_0^2}{2} \left(\hat{a}^{\dagger 2} + \hat{a}^2 + 2\hat{a}^{\dagger} \hat{a} + 1 \right) + \omega \left(\frac{1}{2} + \hat{a}^{\dagger} \hat{a} \right) - \hat{\mathbf{P}} \cdot \hat{\mathbf{A}} \quad (2.1)$$

Let us now further explore the specific approximations for the light part and the matter part.

2.1.1. Assumptions of the matter part

In this section we will deal with the terms \hat{H}_{el} and $\hat{H}_{int} = -\hat{\mathbf{P}} \cdot \hat{\mathbf{A}}$. Before doing that, we should introduce the concept of *k point*, which has a different meaning in solid state theory and electronic-structure theory [32]. In the former, it refers to a generic element of the Brillouin zone. Among all possible k points, some of them are high-symmetry points and represent specific points in the Brillouin zone. For instance, taking Graphene as a reference, one can acknowledge the Γ point, which has coordinates $\Gamma = (0, 0, 0)$ or the point in the middle of an edge joining two hexagonal faces, called *K point* and has coordinates $K = (\frac{1}{3}, \frac{1}{3}, 0)$. Conversely, in electronic-structure theory they are sampling points of the Brillouin zone, and we will refer to them as *k points*. In those, the states are calculated, so that the more k points one uses, the more the result will be accurate.

As we discussed in the previous sections, the matter part is described by Slater determinants, which are built on top of the single-particle Kohn-Sham states. In section 3 we will discuss more in-depth what the software developed in the present work does, but we can already say that the starting point is represented by the single-particle Kohn-Sham states. Those are read from Octopus, a real-time real-space TDDFT code upon which the present work is based (see section 3.1). We will have a set of states (one for each band) for each k point of our simulation which can be described by the Hamiltonian:

$$\hat{H}_{el} = \sum_{i,k} \epsilon_{i,k}^{KS} \hat{c}_{i,k}^\dagger \hat{c}_{i,k} \quad (2.2)$$

where $\hat{c}_{i,k}^\dagger, \hat{c}_{i,k}$ are the electronic creation and annihilation operators for the state i at a certain k point. Applying those two operators in this order means that firstly we remove an electron from that state, and then we re-add it; in other words we measure the occupation of that state. $\epsilon_{i,k}^{KS}$ is the energy of the single-particle state i at k point k , which comes from the solution of (1.32).

Let us now focus on the interaction Hamiltonian. We also assume that the excited states will be singly-excited [7], which means that we are only allowed to remove one electron from the ground state. Therefore, the momentum operator between Slater determinants can be written as

$$\hat{\mathbf{P}} = \sum_{i \neq j, k, k'} \langle \phi_{i,k} | \hat{\mathbf{p}} | \phi_{j,k'} \rangle \hat{c}_{i,k}^\dagger \hat{c}_{j,k'} \quad (2.3)$$

where ϕ are the single-particle Kohn-Sham states and $\hat{\mathbf{p}} = -i\nabla$ is the single-particle momentum operator. The single excitation of the Slater determinant is given by the fact that we are removing a single particle from the state j, k' and adding it to the state i, k . Here we assumed that $i \neq j$ because we are interested in studying transitions, otherwise

in general we could also have $i = j$. Finally, in this work only semi-conductors or semi-metallic systems are considered so that one has not to deal with fractional occupation of the states (which is the case for metals).

2.1.2. Assumptions of the radiation part

In this section we will deal with the terms \widehat{H}_{ph} and \widehat{H}_{int} . In section 1.1 we derived the expression for a multi-mode vector potential, while in section 1.3 we derived the QED Hamiltonian in the case of single-mode electromagnetic field. In the following discussion we will always consider a single-mode radiation field for two reasons. The first one is that including more modes strongly increases the dimension of the Hamiltonian, making it virtually impossible to diagonalize (except for small systems). The second is that as long as we consider only low energy polaritons (i.e. with energy smaller than the second photon mode), including more modes has little effect and does not change the qualitative results [7]. Therefore, equation (2.1) already contains the correct \widehat{H}_{ph} , while for \widehat{H}_{int} we simply have to use the expression for the vector potential, that it $\widehat{\mathbf{A}} = A_0 \mathbf{e} (\widehat{a}^\dagger + \widehat{a})$, where \mathbf{e} is the polarization vector and A_0 groups all the constants.

Finally, we also assume that the optical transitions can only be vertical in the reciprocal space. This is very common in the field of solid-state physics, and it is motivated by the fact that the wave vector of the radiation field is much smaller than the wave vector of the Bloch waves. This holds as long as we do not consider X-rays. Moreover, in this work this approximation is also justified by taking only the mode with $\mathbf{k} = 0$. Therefore, equation (2.3) can be further simplified by imposing that $k = k'$. Therefore, the final form of equation (2.1) is:

$$\begin{aligned} \widehat{H}_{QED} = & \sum_{i,k} \epsilon_{i,k}^{KS} \widehat{c}_{i,k}^\dagger \widehat{c}_{i,k} + \\ & \frac{N_{el} A_0^2}{2} \left(\widehat{a}^{\dagger 2} + \widehat{a}^2 + 2\widehat{a}^\dagger \widehat{a} + 1 \right) + \omega \left(\frac{1}{2} + \widehat{a}^\dagger \widehat{a} \right) \\ & - A_0 \sum_{i \neq j, k} \langle \phi_{i,k} | \widehat{\mathbf{p}} \cdot \mathbf{e} | \phi_{j,k} \rangle \widehat{c}_{i,k}^\dagger \widehat{c}_{j,k} (\widehat{a}^\dagger + \widehat{a}) \end{aligned} \quad (2.4)$$

Finally, at the beginning of section 2.1 we stated that we can study both periodic and non-periodic systems. The difference between the two is that for non-periodic isolated systems k is not a good quantum number so we should simply sum directly over the molecular state. From a technical point of view, this implies that for molecules we have just one k point, so equation (2.4) does not have the sum over the index k .

2.2. Structure of the QED Hamiltonian matrix

In this section we will explore the QED Hamiltonian in detail, starting from defining the basis, then analysing the blocks and finally providing a simple example.

2.2.1. Basis for the QED Hamiltonian

After defining the Hamiltonian of the system we have to choose a basis onto which to project it, so that we can give a representation of the problem. In principle it is possible to represent the problem on any basis as long as it is complete, but by choosing a suitable one it is possible (using physical intuition) to reduce the number of basis states to include, which makes the calculations will be more efficient. In this problem we have a system where the electrons in the solid interact with the photons of the radiation field. If we look at equation (2.4), we see that these two problems would be perfectly separable if the interaction Hamiltonian was zero. We also know from section 1.4 that the effect of this latter is to mix the electronic and photonic states, to obtain the polaritonic states.

Therefore, a reasonable choice is to consider a basis that diagonalizes the electronic part, a basis that diagonalizes the photonic part, and then take their tensor product. As we discussed, electrons in solids can be described by Slater determinants $|\Psi\rangle$ so a suitable basis is to consider the Slater determinant for the ground state plus one Slater determinant for each excitation. Thus we have: $\{el\} : \{|\Psi_{GS}\rangle, |\Psi_{ex,1}\rangle \dots |\Psi_{ex,n}\rangle\}$. The photon part is diagonalized by the photon number states $\{|n\rangle\} = \{|0\rangle, |1\rangle, \dots, |n\rangle\}$, where $|0\rangle$ means that there are zero photons in the cavity.

Therefore, the final base for our Hamiltonian will be

$$\{|\Psi_{GS}\rangle, \{|\Psi_{ex}\rangle\}\} \otimes \{|n\rangle\} \quad (2.5)$$

and the generic matrix element of the Hamiltonian will be

$$\langle n | \langle \Psi_i | \hat{H}_{QED} | \Psi_j \rangle | m \rangle \quad (2.6)$$

For the expression of the specific matrix element, please refer to Appendix A.

2.2.2. Structure of the blocks

In the chosen basis, the matrix representing the QED Hamiltonian is penta-block-diagonal. This means that if we put the photon number states of the rows and columns, the matrix can be divided into blocks and all non-zero elements will be on the blocks of the main

diagonal and the two diagonals above and below. The dimension of each block is given by the expression

$$DIM_{QED} = (1 + VB_{states} * CB_{states} * k_{points}) * (N_{ph} + 1) \quad (2.7)$$

where VB_{states} , CB_{states} are the number of states in valence band and conduction band, k_{points} the number of k points used in the calculation and N_{ph} the number of Fock states included. The product $VB_{states} * CB_{states} * k_{points}$ represents the fact that we can have excitations from each state in the valence band to each state in the conduction band for each k point. From this expression it is evident the tensor product in equation (2.5). The 1+ in the matter part represents the Slater determinant of the ground state, while the one in the photonic part represents the photonic vacuum state $|0\rangle$.

A visual representation is given in Figure 2.1.

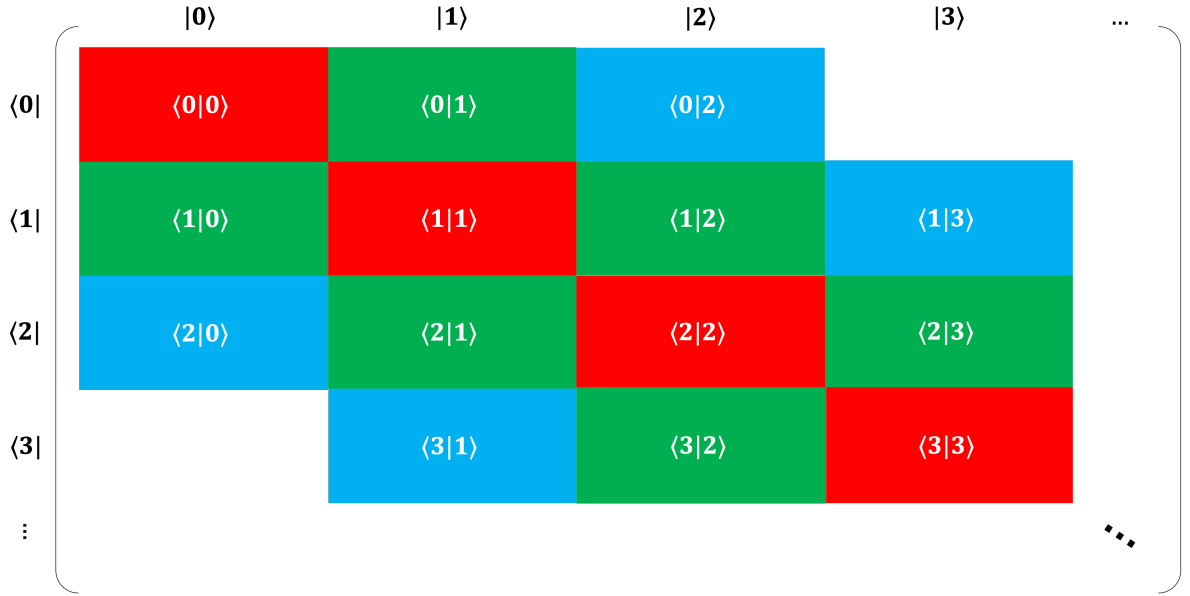


Figure 2.1: Structure of the QED matrix as implemented in the code. If we put the photon number states on the rows/columns, then the matrix is penta-block-diagonal. The red block is diagonal and only terms from \hat{H}_{el} and \hat{H}_{ph} contribute to it. The green block is the bi-linear coupling block, whose elements are defined by \hat{H}_{int} . Finally, the blue blocks are again diagonal, and only the terms that contains $\hat{a}^{\dagger 2}, \hat{a}^2$ contribute to it

From equation (2.7) it is evident that the dimension of each block is

$$DIM_{Block} = 1 + VB_{states} * CB_{states} * k_{points} \quad (2.8)$$

On the rows (and the columns) of each block we shall put the Slater determinant of the ground state followed by all the Slater determinants representing an excitation from the valence state v to the conduction state c at a given k point k .

$$\begin{array}{c}
 \langle GS | \\
 \langle c_1 v_1, k_1 | \\
 \langle c_1 v_2, k_1 | \\
 \dots \\
 \langle c_2 v_1, k_1 | \\
 \dots \\
 \langle c_1 v_1, k_2 | \\
 \langle c_1 v_2, k_2 | \\
 \dots \\
 \langle c_2 v_1, k_2 | \\
 \dots
 \end{array}
 \begin{pmatrix}
 |GS\rangle & |c_1 v_1 k_1\rangle & |c_1 v_2 k_1\rangle & \dots & |c_2 v_1 k_1\rangle & \dots & |c_1 v_1 k_2\rangle & |c_1 v_2 k_2\rangle & \dots & |c_2 v_1 k_2\rangle & \dots \\
 GS & c_1 v_1 k_1 & c_1 v_2 k_1 & \dots & c_2 v_1 k_1 & \dots & c_1 v_1 k_2 & c_1 v_2 k_2 & \dots & c_2 v_1 k_2 & \dots \\
 v_1 c_1 k_1 & c_{11} v_{11} k_{11} & c_{11} v_{12} k_{11} & \dots & c_{12} v_{11} k_{11} & \dots & c_{11} v_{11} k_{12} & c_{11} v_{12} k_{12} & \dots & c_{12} v_{11} k_{12} & \dots \\
 v_1 c_1 k_1 & c_{11} v_{21} k_{11} & c_{11} v_{22} k_{11} & \dots & c_{12} v_{21} k_{11} & \dots & c_{11} v_{21} k_{12} & c_{11} v_{22} k_{12} & \dots & c_{12} v_{21} k_{12} & \dots \\
 \dots & \dots & \dots & \dots & \dots & \dots & \dots & \dots & \dots & \dots & \dots \\
 v_1 c_2 k_1 & c_{21} v_{11} k_{11} & c_{21} v_{12} k_{11} & \dots & c_{22} v_{11} k_{11} & \dots & c_{21} v_{11} k_{12} & c_{21} v_{12} k_{12} & \dots & c_{22} v_{11} k_{12} & \dots \\
 \dots & \dots & \dots & \dots & \dots & \dots & \dots & \dots & \dots & \dots & \dots \\
 v_1 c_1 k_2 & c_{11} v_{11} k_{21} & c_{11} v_{12} k_{21} & \dots & c_{12} v_{11} k_{21} & \dots & c_{11} v_{11} k_{22} & c_{11} v_{12} k_{22} & \dots & c_{12} v_{11} k_{22} & \dots \\
 v_2 c_1 k_2 & c_{11} v_{21} k_{21} & c_{11} v_{22} k_{21} & \dots & c_{12} v_{21} k_{21} & \dots & c_{11} v_{21} k_{22} & c_{11} v_{22} k_{22} & \dots & c_{12} v_{21} k_{22} & \dots \\
 \dots & \dots & \dots & \dots & \dots & \dots & \dots & \dots & \dots & \dots & \dots \\
 v_1 c_2 k_2 & c_{21} v_{11} k_{21} & c_{21} v_{12} k_{21} & \dots & c_{22} v_{11} k_{21} & \dots & c_{21} v_{11} k_{22} & c_{21} v_{12} k_{22} & \dots & c_{22} v_{11} k_{22} & \dots \\
 \dots & \dots & \dots & \dots & \dots & \dots & \dots & \dots & \dots & \dots & \dots
 \end{pmatrix}$$

where $|c_i v_j k_k\rangle = \hat{c}_{c_i, k_k}^\dagger \hat{c}_{v_j, k_k} |\Psi_{GS}\rangle$ and H is the generic matrix element. As it can be seen from the matrix above, the Slater determinant of the ground state is followed by a series of Slater determinants for excitations in the first k point. Within those, firstly we find all the possible excitation from all possible valence band states to the first conduction band state, then the same for the second conduction band state. After all states combination at k point = 1 are completed, the ones for k point = 2 start and the structure is repeated. Let us now examine each block more in-depth. For doing that, we should consider equation (2.4). Due to the action of the creation and annihilation operators, each term of equation (2.4) will be non-zero only in some of the blocks in Fig 2.1. In particular, for the red block we must have that the photon number on the rows is equal to the photon number of the columns, which implies that only the Hamiltonian inside the red block will be

$$\hat{H}_{QED} = \sum_{i,k} \epsilon_{i,k}^{KS} \hat{c}_{i,k}^\dagger \hat{c}_{i,k} + \frac{N_{el} A_0^2}{2} (2\hat{a}^\dagger \hat{a} + 1) + \omega \left(\frac{1}{2} + \hat{a}^\dagger \hat{a} \right) \quad (2.9)$$

It is evident then that the red block will be diagonal.

In the blue block we should have that $ph_{rows} = ph_{cols} \pm 2$, so the Hamiltonian will contain only terms that shift the number of photons by two. The blue block is also purely diagonal.

Therefore:

$$\hat{H}_{QED} = \frac{N_{el} A_0^2}{2} (\hat{a}^{\dagger 2} + \hat{a}^2) \quad (2.10)$$

Finally the green block, also known as bi-linear coupling block, is characterized by $ph_{rows} = ph_{cols} \pm 1$. Therefore its Hamiltonian will be:

$$\hat{H}_{QED} = -A_0 \sum_{i \neq j, k} \langle \phi_{i,k} | \hat{\mathbf{p}} \cdot \mathbf{e} | \phi_{j,k} \rangle \hat{c}_{i,k}^\dagger \hat{c}_{j,k} (\hat{a}^\dagger + \hat{a}) \quad (2.11)$$

The bi-linear coupling block is the only non-diagonal block, as can be seen from the fact that in the sum we have $i \neq j$. Its action is to mix different electronic states through photons. Its structure will look like this:

$$\begin{array}{c} \langle GS | \\ \langle c_1, v_1, k_1 | \\ \langle c_1, v_2, k_1 | \\ \dots \\ \langle c_2, v_1, k_1 | \\ \dots \\ \langle c_1, v_1, k_2 | \\ \langle c_1, v_2, k_2 | \\ \dots \\ \langle c_2, v_1, k_2 | \\ \dots \end{array} \begin{pmatrix} |GS\rangle & |c_1, v_1, k_1\rangle & |c_1, v_2, k_1\rangle & \dots & |c_2, v_1, k_1\rangle & \dots & |c_1, v_1, k_2\rangle & |c_1, v_2, k_2\rangle & \dots & |c_2, v_1, k_2\rangle & \dots \\ \left(\begin{array}{cccccccccccc} 0 & H_{c_1, v_1, k_1} & H_{c_1, v_2, k_1} & \dots & H_{c_2, v_1, k_1} & \dots & H_{c_1, v_1, k_2} & H_{c_1, v_2, k_2} & \dots & H_{c_2, v_1, k_2} & \dots \\ H_{v_1, c_1, k_1} & 0 & 0 & \dots & H_{c_1, c_2, k_1} & \dots & 0 & 0 & \dots & 0 & \dots \\ H_{v_2, c_1, k_1} & 0 & 0 & \dots & 0 & \dots & 0 & 0 & \dots & 0 & \dots \\ \dots & \dots & \dots & \dots & \dots & \dots & \dots & \dots & \dots & \dots & \dots \\ H_{v_1, c_2, k_1} & H_{c_2, c_1, k_1} & 0 & \dots & 0 & \dots & 0 & 0 & \dots & 0 & \dots \\ \dots & \dots & \dots & \dots & \dots & \dots & \dots & \dots & \dots & \dots & \dots \\ H_{v_1, c_1, k_2} & 0 & 0 & \dots & 0 & \dots & 0 & 0 & \dots & H_{c_1, c_2, k_2} & \dots \\ H_{v_2, c_1, k_2} & 0 & 0 & \dots & 0 & \dots & 0 & 0 & \dots & 0 & \dots \\ \dots & \dots & \dots & \dots & \dots & \dots & \dots & \dots & \dots & \dots & \dots \\ H_{v_1, c_2, k_2} & 0 & 0 & \dots & 0 & \dots & H_{c_2, c_1, k_2} & 0 & \dots & 0 & \dots \\ \dots & \dots & \dots & \dots & \dots & \dots & \dots & \dots & \dots & \dots & \dots \end{array} \right) \end{pmatrix}$$

One can see that apart from the element in the top left corner, the first line and the first column only have non-zero elements corresponding to the ground state coupling to all possible excitations. Physically this corresponds to transitions from the valence band to the conduction band. However there are also other non-zero elements, which correspond to transition between two conduction bands, which are allowed only if $v_i = v_f, k_i = k_f, c_i \neq c_f$. The first two conditions are due to the orthogonality of Slater determinants and the vertical transitions.

2.2.3. Ab-Initio Polaritons: Simple case of H atom

In this section we will provide an example of the problem described so far by building the Hamiltonian of a very simple system. We will consider the case of a single Hydrogen atom in a FP cavity at resonance energy ω coupled to three For states $\{|0\rangle, |1\rangle, |2\rangle\}$. The Hydrogen atom will be described as a three-level system, therefore having the occupied state $1s$ and the two first unoccupied states $2s, 2p$. Following from equation (2.5), the

basis for the Hamiltonian will be

$$\{|\Psi_{v_1}\rangle, |\Psi_{c_1}\rangle, |\Psi_{c_2}\rangle\} \otimes \{|0\rangle, |1\rangle, |2\rangle\} \quad (2.12)$$

where Ψ_{v_1} is the state $1s$ written using the valence/conduction states notation. Analogously for Ψ_{c_1}, Ψ_{c_2} . According to the second quantization formalism introduced in section 1.2.4, it will hold that

$$|\Psi_{v_1}\rangle = \hat{c}_{v_1}^\dagger |0\rangle \quad (2.13)$$

$$|\Psi_{c_1}\rangle = \hat{c}_{c_1}^\dagger \hat{c}_{v_1} |\Psi_{v_1}\rangle \quad (2.14)$$

$$|\Psi_{c_2}\rangle = \hat{c}_{c_2}^\dagger \hat{c}_{v_1} |\Psi_{v_1}\rangle \quad (2.15)$$

Subsequently we can compute the matrix dimension using (2.7). Remembering that since we are describing a single atom we only have one k point, we obtain:

$$DIM_{H,QED} = (1 + 1 * 2 * 1) * (2 + 1) = 9 \quad (2.16)$$

Once we have the basis and the dimensions, we can start considering the matrix elements, $\langle m | \langle \Psi_i | \hat{H}_{QED} | \Psi_j \rangle | n \rangle$, where \hat{H}_{QED} is the one defined in equation (2.4), m, n represent the photon number states and Ψ_i, Ψ_j represent the electronic states. These latter are taken from (2.12).

The actual expression for the matrix element depends on the indexes of the states and in general it is quite complicated. Its derivation is treated in Appendix A, and for the sake of clarity the result is split among many equations. In particular, for the matrix element coming from the electronic part, the reader should refer to equation (A.8), for the photonic part to equation (A.9), for the one from the bi-linear coupling to equations (A.10), (A.11), (A.13).

Therefore, the matrix representation of the QED Hamiltonian takes the form:

$$\begin{array}{c}
 \langle \Psi_{v_1, 0} | \\
 \langle \Psi_{c_1, 0} | \\
 \langle \Psi_{c_2, 0} | \\
 \langle \Psi_{v_1, 1} | \\
 \langle \Psi_{c_1, 1} | \\
 \langle \Psi_{c_2, 1} | \\
 \langle \Psi_{v_1, 2} | \\
 \langle \Psi_{c_1, 2} | \\
 \langle \Psi_{c_2, 2} |
 \end{array}
 \begin{pmatrix}
 |\Psi_{v_1, 0}\rangle & |\Psi_{c_1, 0}\rangle & |\Psi_{c_2, 0}\rangle & |\Psi_{v_1, 1}\rangle & |\Psi_{c_1, 1}\rangle & |\Psi_{c_2, 1}\rangle & |\Psi_{v_1, 2}\rangle & |\Psi_{c_1, 2}\rangle & |\Psi_{c_2, 2}\rangle \\
 \epsilon_{v_1} + \frac{\Omega_1}{2} & 0 & 0 & 0 & A_0 P_{v_1, c_1} & P_{v_1, c_2} & \frac{\sqrt{2}}{2} A_0^2 & 0 & 0 \\
 0 & \epsilon_{c_1} + \frac{\Omega_1}{2} & 0 & P_{c_1, v_1} & 0 & P_{c_1, c_2} & 0 & \frac{\sqrt{2}}{2} A_0^2 & 0 \\
 0 & 0 & \epsilon_{c_2} + \frac{\Omega_1}{2} & P_{c_2, v_1} & P_{c_2, c_1} & 0 & 0 & 0 & \frac{\sqrt{2}}{2} A_0^2 \\
 0 & P_{v_1, c_1} & P_{v_1, c_2} & \epsilon_{v_1} + \frac{\Omega_3}{2} & 0 & 0 & 0 & \sqrt{2} P_{v_1, c_1} & \sqrt{2} P_{v_1, c_2} \\
 P_{c_1, v_1} & 0 & P_{c_1, c_2} & 0 & \epsilon_{c_1} + \frac{\Omega_3}{2} & 0 & \sqrt{2} P_{c_1, v_1} & 0 & \sqrt{2} P_{c_1, c_2} \\
 P_{c_2, v_1} & P_{c_2, c_1} & 0 & 0 & 0 & \epsilon_{c_2} + \frac{\Omega_3}{2} & \sqrt{2} P_{c_2, v_1} & \sqrt{2} P_{c_2, c_1} & 0 \\
 \frac{\sqrt{2}}{2} A_0^2 & 0 & 0 & 0 & \sqrt{2} P_{v_1, c_1} & \sqrt{2} P_{v_1, c_2} & \epsilon_{v_1} + \frac{\Omega_5}{2} & 0 & 0 \\
 0 & \frac{\sqrt{2}}{2} A_0^2 & 0 & \sqrt{2} P_{c_1, v_1} & 0 & \sqrt{2} P_{c_1, c_2} & 0 & \epsilon_{c_1} + \frac{\Omega_5}{2} & 0 \\
 0 & 0 & \frac{\sqrt{2}}{2} A_0^2 & \sqrt{2} P_{c_2, v_1} & \sqrt{2} P_{c_2, c_1} & 0 & 0 & 0 & \epsilon_{c_2} + \frac{\Omega_5}{2}
 \end{pmatrix}$$

Where $P_{i,j} = A_0 \langle \phi_i | \hat{p} | \phi_j \rangle$, $P_{i,j} = P_{j,i}^*$ and $\Omega_n = n\omega + A_0^2$. We can therefore see that the Hamiltonian written above is Hermitian, as we would expect since it represents the energy of the system. As we discussed in previous sections, by diagonalizing this matrix we obtain the polaritonic eigenvalues and eigenvectors, which can be then used to compute the new properties of the material, as shown in sections 3.2.1 and 3.2.2. We stress that not having included more photon number states or more electron states is not a limiting factor for this section. In fact, for the former by looking at figure 2.1 and considering the first row, any other block to the right would contain only zeros, and the same applies if we consider the first column and for the latter we would simply have enabled more optical transition, but the structure of the matrix would remain unchanged.

3 | QED Matrix Solver and Response Functions Ab-initio Implementation

After discussing the theory and the approximations used in the present work, we shall now discuss the software implementation. We will refer to it as *QED Solver*. For doing that we will start by discussing the main code upon which this work is based, Octopus. Afterward, we will discuss the code structure of the *QED Solver* and the quantities it can calculate in the current implementation (namely the linear optical response and the density of states). Finally we will discuss the parallelization of the code, firstly saying why it is important to overcome the serial implementation, then describing the main concepts of the parallel approach and in the end comparing the performances of the two.

3.1. Octopus Code

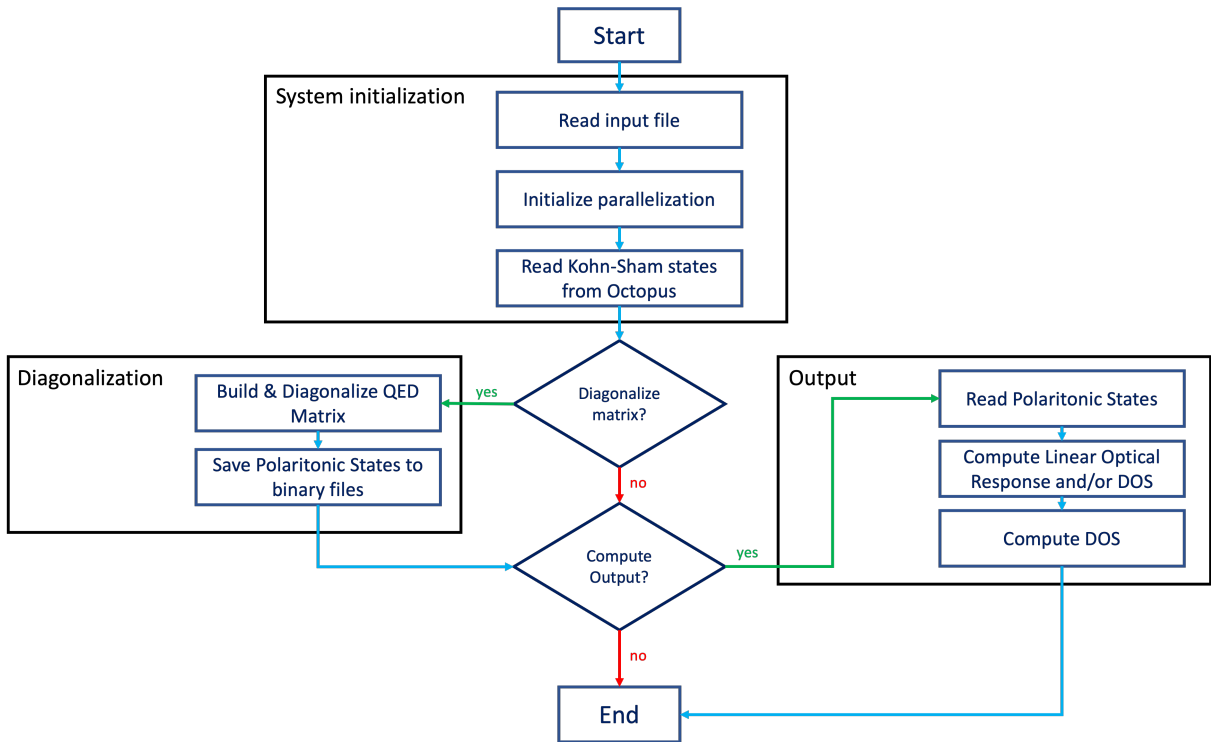
As we already mentioned in section 2.1.1, the *QED Solver* is based on an existing software, which is Octopus. As the reader might have understood from previous sections, the *QED Solver* reads the single-particle Kohn-Sham states calculated by Octopus and then computes the QED matrix. For such a reason it is worth briefly describing the main code. Octopus is a real-grid real-time based scientific program aimed at the *ab initio* virtual experimentation [33], firstly released in 2003 [34] and mainly written in Fortran 90. It allows to study the equilibrium and non-equilibrium properties of materials (both finite and periodic systems) using mostly DFT (see section 1.2.2 for details) and its variations (Time-Dependent Density Functional Theory -TDDFT- for time propagation, TDDFT+U for studying Hubbard-like systems and others [33]). In its most recent version Octopus is also able to solve Maxwell's equations together with the matter part, to study the feedback between the two during time evolution. In particular, the software solves the Kohn-Sham equations 1.1 in real time using finite differences as derivatives and it discretizes all quantities using a real grid approach. This means that a simulation box is defined

(typically a sphere, a cylinder or a parallelepiped), and then the software builds the grid onto which all the quantities are calculated. The points of this grid are separated by user-definable spacing and the materials are defined by the real-space position of the ions (either with real positions or reduced coordinates if one wants to study periodic systems). Since the code uses DFT, it will calculate a set of single-particle Kohn-Sham states computed on the aforementioned grid. The interaction between electrons and ions is described by pseudopotentials (to reduce the computational cost) [35] and in each point of the grid the Hamiltonian is defined and diagonalized (until the solution is self-consistent). This implies that each electronic state will have a value for each point of the grid, which allows having a precise description of the system (if the chosen spacing is small). The real space approach has a good scaling to big systems, as well as other advantages. In particular, it can capture the free particle states (vacuum) better than codes based on localized basis sets, it equally applies to finite and periodic systems and it implements routines to calculate physical observables more conveniently [36]. Finally, one can deal with the increasing computational cost introduced by big systems by distributing the resources over many processors, therefore using a parallel approach (see sections 3.3, 3.4 for more details). In fact, Octopus has many parallelization techniques that allow it to run on both CPUs (Message Passing Interface -MPI-, OpenMPI) and GPUs (Compute Unified Device Architecture -CUDA- and Open Computing Language -OpenCL-).

3.2. Features of the QED Solver

In this section we will explore the main features of the code *QED Solver*. As we already mentioned in the previous discussion, the goal of the software is to build the QED matrix from equation (2.4) and from the basis (2.5), then diagonalize it to obtain the dressed states (i.e. the polaritonic states). Subsequently, the software computes the linear optical response function and the density of states. *QED Solver* is developed as a utility of Octopus, which means that it is an independent software that relies on Octopus for doing some calculations (i.e. the Kohn-Sham states) and it uses many subroutines of Octopus. In practice, this implies that the user should firstly run Octopus to compute the Kohn-Sham states, and then execute the utility *QED Solver* (which goes under the name of *oct-qed_matrix*).

The structure of the code is briefly summarized in fig 3.1. After the program starts, the first thing that has to be done is to read the input file to understand what the user wishes to compute. Coherently with the main Octopus code [34], the input is provided via a file called "inp" located in the execution folder and it is composed of blocks and single variables.

Figure 3.1: Flow chart of the software *QED Solver*

A single variable is a line of type $variable = value$, while a block is a more complicated structure which is delimited by the character `%` (example are provided in the following discussions). The variables introduced by the this utility are:

QED Solver: Input variables

Variable Name	Type	Optional	Values	Default Value
<code>QEDMatrixDiagonalizeMatrix</code>	logical	yes	yes/no	yes
<code>QEDMatrixDistributedMatrix</code>	logical	yes	yes/no	no
<code>QEDMatrixParallelEigensolver</code>	integer	yes	1/2	1
<code>QEDMatrixOpticalResponse</code>	logical	yes	yes/no	yes
<code>QEDMatrixDOS</code>	logical	yes	yes/no	yes

Table 3.1: Input variables that define the calculation mode of the utility.

In table 3.1 the list of variables related to the general setup of the software is reported. The first three allow the user to choose whether to diagonalize the matrix or not, and how to do it. It is possible to do this because the user might want to run the code only to compute

one of the outputs. This is possible only if the polaritonic states are available. The input variables *QEDMatrixDistributedMatrix* and *QEDMatrixParallelEigensolver* control the parallelization of the code and the eigensolver (1 corresponds to ELPA -Eigenvalue solvers for Petaflop Applications- [37], 2 corresponds to ScaLAPACK -Scalable Linear Algebra PACKage- [38]), respectively. The parallelization will be discussed more in-depth in section 3.3. The last two variables allow the user to choose what output to compute (the linear optical response and/or the DOS). They will be discussed more in-depth in section 3.2.2 and 3.2.1. It should be noted that if the user wants to compute only one of the outputs, but the *QED Solver* is not able to find the polaritonic states, then the execution fails.

Variable Name	Type	Optional	Values	Default Value
QEDMatrixA0	float	no	≥ 0.0	0.0
QEDMatrixCavityEnergy	block	no	/	/
QEDMatrixNumberOfPhotons	integer	yes	≥ 0	0
QEDMatrixCavityPolarization	block	yes	/	linear x dir

Table 3.2: Input variables that define the parameters of the optical cavity.

In table 3.2 the list of variables related to the specifications of the cavity is reported. In particular, *QEDMatrixA0* is the same that appears in equation (2.4) (and all ones that derive from it) and it describes the light-matter coupling parameter. *QEDMatrixNumberOfPhotons* defines how many photon number states are used in the QED basis (2.5). *QEDMatrixCavityEnergy* and *QEDMatrixCavityPolarization* are two variables of block type. The former defines how many cavity energies the calculation should be repeated. For cavity energy we mean the energy of the photon mode in the cavity, as in section 1.3.1.

Algorithm 3.1 Cavity Energy Block and Cavity Polarization Block

```

1: CAVITY ENERGY:
2: %QEDMatrixCavityEnergy
3: 0.001 | 1 | 0.005
4: %
5: CAVITY POLARIZATION:
6: %QEDMatrixCavityPolarization
7: 'circular' | 1 | 1.0 | 1.0 | 0.0
8: %

```

The latter defines the polarization of the photon mode. The two blocks have the shape in algorithm 3.1.

In the cavity mode energy block the user should input three floats, the first one corresponding to the starting value for the cavity mode energy, the second one corresponding to the last value and the last one representing the energy step. All values should be in Hartree. In the reported example, the calculations will be repeated for

$$\frac{1 - 0.001}{0.005} = 199.8 \rightarrow 200$$

cavity energies. This means that the QED matrix will be diagonalized 200 times, so this block has a great impact on the computational cost. Conversely, in the cavity polarization block the user should first choose whether the polarization should be circular or linear. Then if the polarization is circular the user should indicate in which direction the $\frac{\pi}{2}$ shift should be added. Finally, three floats follow, each defining the value of the polarization in a certain direction (x, y, z) . The software automatically takes care of the normalization, so that the norm of the polarization vector is one. In the reported example, the polarization vector would look like:

$$\mathbf{e} = \frac{1}{\sqrt{2}} (\mathbf{e}_x + i\mathbf{e}_y)$$

Variable Name	Type	Optional	Values	Default Value
<code>QEDMatrixValenceBandStates</code>	integer	yes	$\geq 1, \leq CB_{states}$	CB_{states}
<code>QEDMatrixConductionBandStates</code>	integer	yes	$\geq 1, \leq VB_{states}$	VB_{states}

Table 3.3: Input variables that define band of the material used in the calculation.

In table 3.3 the list of parameters related to the matter degree of freedom is reported. Before analyzing them, it should be noted that since the *QED Solver* reads the data from Octopus, some parameters such as the geometry, the number of states, the occupation of states and the k point are already defined. The two variables in the table allow the user to deselect some of the available bands to reduce the complexity of the problem, both from a computational point of view (the matrix dimension is reduced according to equation (2.7)) and a physical point of view (one might want to focus only on the first bands to understand local features). The user should select at least one band for the valence and conduction band. The former should not exceed the number the occupied states from the ground state calculation performed by Octopus, while the latter should not exceed the number

of unoccupied states computed by Octopus. For the sake of clarity, we shall provide an example. Let us consider Graphene, with three unoccupied bands. the number of occupied bands is four. Let the variables in table 3.3 be: $QEDMatrixValenceBandStates = 3$, $QEDMatrixConductionBandStates = 2$, then the lowest state in energy in the valence band and the highest state in energy in the conduction band would be excluded. A schematic representation is provided in figure 3.2.

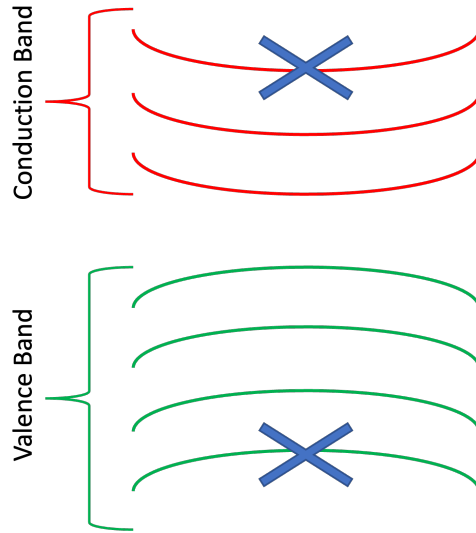


Figure 3.2: Schematic representation of the bands of Graphene for a DFT calculation with three unoccupied states. Since $QEDMatrixValenceBandStates = 3$ and $QEDMatrixConductionBandStates = 2$ the first and last states are excluded.

Variable Name	Type	Optional	Values	Default Value
QEDMatrixEta	float	yes	≥ 0.0	0.001837466 <i>Ha</i>
QEDMatrixOpticalSpectrum	block	no	/	/
QEDMatrixProbePolarization	block	yes	/	linear x dir
QEDMatrixGamma	float	yes	≥ 0.0	0.001837466 <i>Ha</i>
QEDMatrixDOSSpectrum	block	no	/	/

Table 3.4: Input variables that define the parameters for the linear optical response and for the DOS.

Finally, in table 3.4 the variables that define the output are listed. For a detailed description please refer to section 3.2.2 and 3.2.1. The first three variables refer to the linear

response function. In particular, *QEDMatrixEta* defines an artificial broadening, *QEDMatrixOpticalSpectrum* and *QEDMatrixProbePolarization* are blocks with the same shape as the ones defined in table 3.2 and define the range of energies covered for computing the spectrum and the polarization of the probe beam. The last two variables refer to the DOS, in particular *QEDMatrixGamma* defines again an artificial broadening for the Lorentzians, while *QEDMatrixDOSSpectrum* has the same meaning as *QEDMatrixOpticalSpectrum*. After reading the input file, the *QED Solver* initializes the parallelization scheme (if requested) and finally reads the Kohn-Sham states from Octopus. Subsequently it either proceeds to the definition and diagonalization of the QED Matrix (if requested with the variable *QEDMatrixDiagonalizeMatrix*) and finally to the calculation of the output (if they were requested with the variables *QEDMatrixOpticalResponse* and *QEDMatrixDOS*). A representation of the flow of the software is given in figure 3.1.

3.2.1. Density Of States

The first output that the present utility can compute is the Density of States (DOS). This quantity represents the number of states per unit of volume V and at a certain energy E . For a three-dimensional periodic system, we can formulate it as [39]

$$D(E) = 2 \sum_{\mathbf{k}} \delta(E(\mathbf{k}) - E) = 2 \int_{B.Z.} \frac{V}{(2\pi)^3} \delta(E(\mathbf{k}) - E) d\mathbf{k} \quad (3.1)$$

where the factor 2 accounts for the spin and \mathbf{k} is the \mathbf{k} vector of the reciprocal space. The term $E(\mathbf{k})$ represents the eigenvalues of the states in the system. To compute the DOS, one should scan over a wide range of energies E (this is controlled with the input parameter *QEDMatrixDOSSpectrum*). If there is a state at that energy then Dirac's delta will be non-zero, so there will be a state count. However, in computational physics it is not possible to use the Delta function since one cannot have a cycle over an infinite number of energies and also because floating point numbers cannot be represented with infinite precision on a computer. Since the delta to be non-zero requires that the argument is *exactly* zero, this condition would never be satisfied. As a consequence, instead of using a delta we use a Lorentzian function, which has a similar shape (but with a parameterized broadening):

$$D(E) = \frac{1}{n\pi} \sum_{\mathbf{k}} \frac{\gamma}{(E(\mathbf{k}) - E)^2 + \gamma^2} \quad (3.2)$$

where n is the matrix dimension and γ is the broadening defined with the input parameter *QEDMatrixGamma*. The software *QED Solver* is able to compute only the total density of states (tDOS) and the joint density of states (jDOS) [39]. Since both of them are computed

after the diagonalization, they represent the DOS of the polaritonic states, so instead of having the index \mathbf{k} we will have the index I (also because after the diagonalization we lose the information about the \mathbf{k} points). Also, for the tDOS we shift all the energies by the electronic ground state, so that the tDOS starts from zero. This is computed as $E_{GS,el} = \sum_{j,\mathbf{k}} \epsilon_{j,\mathbf{k}}^{KS}$, where ϵ^{KS} is the energy of the single-particle Kohn-Sham state and the index j runs only on the occupied states (valence band). This shift implies that when the cavity is turned off ($A_0 = 0, \omega = 0$) then the ground state is only electronic, so jDOS and the tDOS represent the same quantity. It should be stressed that this is true only because we chose as a basis for the Hamiltonian the Slater determinants representing transitions. Finally, we state the formulas for the tDOS and jDOS implemented in the code.

$$D_t(E) = \frac{1}{n\pi} \sum_I \frac{\gamma}{[(E_{pol,I} - E_{GS,el}) - E]^2 + \gamma^2} \quad (3.3)$$

$$D_j(E) = \frac{1}{n\pi} \sum_{I>1} \frac{\gamma}{[(E_{pol,I} - E_{pol,0}) - E]^2 + \gamma^2} \quad (3.4)$$

3.2.2. Linear Optical Response

The other quantity that the software is able to compute is the linear response function, which measures how the system responds to a perturbation. This latter is represented by a probe beam of light, which in general can have a different polarization with respect to the light in the cavity. The polarization can be controlled with the input block *QEDMatrixProbePolarization*, while the range of energies (ω) for which this the linear response function should be calculated is controlled by the input block *QEDMatrixOpticalSpectrum*. By applying linear response theory on the polaritonic states, the formula for the matter component of the linear response function becomes [7, 40]

$$\chi(\Omega, \omega) = \frac{1}{n} \sum_{I>1} \frac{\left| \langle \Psi_I | \hat{\mathbf{P}} \cdot \mathbf{e}_{probe} | \Psi_0 \rangle \right|^2}{\omega - (E_{pol,I}(\Omega) - E_{pol,0}(\Omega)) + i\eta} \quad (3.5)$$

where Ω is the energy of the cavity mode, ω is the energy of the probe beam, η is an artificial broadening (controlled by the input variable *QEDMatrixEta*), \mathbf{e}_{probe} is the polarization vector of the probe beam and n is the matrix dimension. Furthermore, Ψ_0 represents the polaritonic ground state, while Ψ_I is the excited polaritonic state. The operator $\hat{\mathbf{P}}$ is the momentum operator between Slater determinants, the same that appears in equation (2.3). This means that the matrix representation of such operator would have a dimension equal to (2.8), coherently with the fact that we are calculating the matter

component of the linear response function. However, the polaritonic states $|\Psi_0\rangle, \{|\Psi_I\rangle\}$ that come from the diagonalization of the QED Hamiltonian build on the basis (2.5), have dimension (2.7). In order to account for this difference, the operator \hat{P} in equation (3.5) is actually $\hat{P} \otimes \hat{\mathbb{I}}$ where $\hat{\mathbb{I}}$ represents the identity operator for the photonic part. Consequently, the operator $\hat{P} \otimes \hat{\mathbb{I}}$ will have the correct dimension (2.7), and its matrix representation will be:

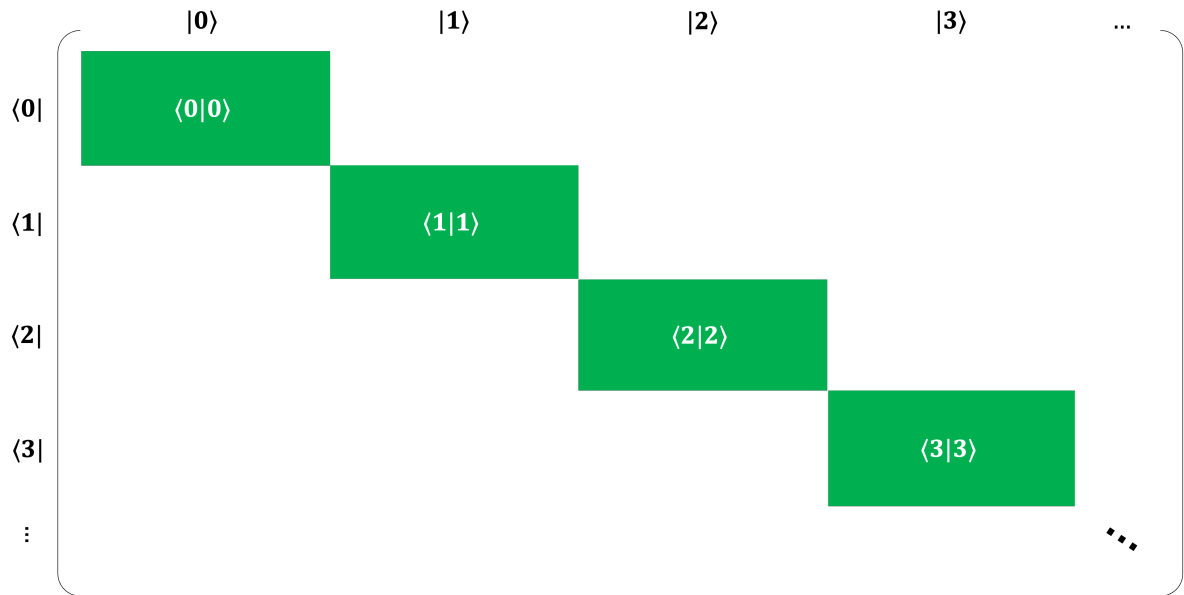


Figure 3.3: Structure of the matrix for the linear optical response. The only blocks that contain non-zero elements are located on the main diagonal. The meaning of the color is the same of figure 2.1, so the green blocks represent the bi-linear coupling shifted on the main diagonal (due to the identity operator in the photon part)

3.3. Parallelization of the code

Up to now we intended the code for this utility as a serial set of instructions to be executed in sequential order by the CPU of the computer. This is the case for the majority of software in the world, when the user launches them, the operating system loads the data and the instructions on the run-time memory (the RAM) and assigns the execution to a processor of the CPU. This goes through all the instructions and performs the necessary operations. The communication between memory and CPU takes place thanks to a bus, according to the Von Neumann architecture [41]. After the execution is terminated, another task is assigned to the processor and so on. We will refer to this as *serial approach*, and for most application it works and there is no need to introduce extra complexity. However the physical systems we deal with are complicated, so they

require much more computational resources to be successfully executed. We will discuss this in-depth in section 3.3.1. This extra power can be reached by increasing the number of processors that work on different parts of the same problem. However, telling the operating system to allocate many processes to the same problem is not enough, because each of them needs to be aware of the work that the others are doing. For instance, let us consider the complex problem of summing all natural numbers from 0 to 100. We can split it into two simpler problems by using two processes. But if we simply allocated these two without making them aware of each other, then the first would sum from 0 to 50, thus obtaining $\sum_{n=0}^{50} n = 1275$ and the second from 51 to 100, thus obtaining $\sum_{n=51}^{100} n = 3775$. The final result would depend on which process we use to read the output, while it should always be 5050. This happens because the two nodes need to communicate at the end to combine their work. We will refer to this paradigm as *parallel approach*, or as it is commonly called, *MPI programming*. MPI stands from *Message Passing Interface*, from the first standard library for parallel programming.

In this section we will deal with the parallelization of the code, firstly discussing why we need it for the problem in this work, and then explaining the main ideas of the parallel approach.

3.3.1. Limitations of the serial approach

In figure 3.1 the flow diagram of the *QED Solver* was presented. From that picture it is evident that the software can be divided into three main sections, the initialization of the system, the diagonalization of the QED matrix and finally the calculation of the output. The former has a little complexity, as the only operations that are done are the reading of the *inp* file (which assigns the values to the variables that define the executing as discussed in section 3.2) and of the Kohn-Sham states. Also, the parallel layout is initialized. The execution of this block takes some seconds even on the CPU of a normal computer, therefore no further discussion is needed. On the other hand, by looking at the equations for computing the DOS (3.3) (3.4) in the output box, one can see that their complexity is quite small. The software only has to perform a sum of real numbers. Therefore, the computational complexity of the *QED Solver* is due to the diagonalization of the QED matrix and to the linear response function. Let us consider the serial approach and let us analyze the two problems in terms of the operation to be performed (algorithmic complexity) and the memory required.

For what concerns the diagonalization problem, the software only needs to store the full QED Matrix (as of figure 2.1) which has dimension (2.7). If we consider Graphene, with four bands in the valence band and the conduction band, with a sampling of the Brillouin

zone using a 60×60 k points grid and with 2 photons in the cavity (which is the minimum to get all the non zero blocks), we have

$$\begin{aligned} DIM_{Graphene} &= (1 + VB_{states} * CB_{states} * k_{points}) * (N_{ph} + 1) = \\ &(1 + 4 * 4 * 3600) * (2 + 1) = 172803 \end{aligned} \quad (3.6)$$

Therefore, the QED matrix has $172803^2 = 29860876809$ elements. Since the states are complex and since in scientific software one always wants the maximum precision, each of those elements will be a *Complex Double*, which is represented with 16 *bytes*. This leads to a main memory (RAM) requirement of 477.77 *GB*, entirely dedicated to this task. Normal computers usually have 16 *GB* or 32 *GB* of RAM. Apart from requiring a lot of memory, the eigenvalue problem has a complexity that scales as [42] $\mathcal{O}(N^3)$, where N is the matrix dimension (3.6). This means that roughly N^3 operations are required to successfully diagonalize the matrix (the exact number depends on the algorithm and on the assumption that one can make on the shape of the matrix).

For what concerns the linear response function, the term that defines the complexity is the numerator, which is a matrix element between two polaritonic states and the matrix in figure 3.3, which has the same dimension of the QED matrix. Then, each element requires the *QED Solver* to store the full matrix plus the two polaritonic states. This leads to a total of $N^2 + 2N = 29861222415$ elements, which is bigger than the diagonalization problem. To solve this problem, in the *QED Solver* the shape of the matrix is exploited. By looking at figure 3.3, if one considers the first row, only the first $\frac{N}{N_{ph}+1} = 1 + 4 * 4 * 3600$ elements can be non zero. Therefore, only the small matrix of dimensions $\frac{N}{N_{ph}+1} \times \frac{N}{N_{ph}+1}$ is stored and then this is accounted when performing the matrix-vector multiplication of the matrix element. As for the computational cost, one has to perform firstly a matrix-vector multiplication and then a vector-vector multiplication, so the total number of required operations is $N^2 + N \ll N^3$. Since the computational cost of the linear optical response is lower than the diagonalization and the memory requirement is also reduced thanks to the shape of the matrix. Therefore, in the following discussion we will refer to the diagonalization.

From this discussion, it can be understood that the serial approach is not suitable for the dimension of the problem. On the other hand, the parallel approach allows dividing the QED matrix into many processors, thus linearly reducing the computational cost. Also the memory requirements can be reduced if one uses many nodes, as we will discuss in section 3.3.2.

3.3.2. High Performance Computing

In the previous section we already discussed that the parallel approach consists of dividing the execution of the software into many processors. When dealing with parallel programming, it is common to use clusters which can be seen as a network of computers. A cluster is composed of many nodes, each of which has a certain number of CPUs and a certain amount of main memory. A node is the smallest processing unit that can be assigned to a single user [43]. The assignment is done by the scheduler of the cluster and it is based on the resources asked by the user. The request is done using a *batch* script (see algorithm 3.2). Another concept that will be used in the following discussion is the one of task, which can be defined as the smallest unit of instructions that needs to be executed on a node [43]. In the batch script mentioned above, the user should specify how many nodes should be used in the calculation and how much memory per node is required. Further, the number of tasks per node and the number of processors (CPU) per task should be specified. Finally, one has to declare what is the maximum time required for the calculation.

Algorithm 3.2 Example of a part of *batch* script for submitting a job

```

1: #SBATCH --nodes=6
2: #SBATCH --ntasks-per-node=15
3: #SBATCH --cpus-per-task=2
4: #SBATCH --mem=170G
5: #SBATCH --time=10:00:00

```

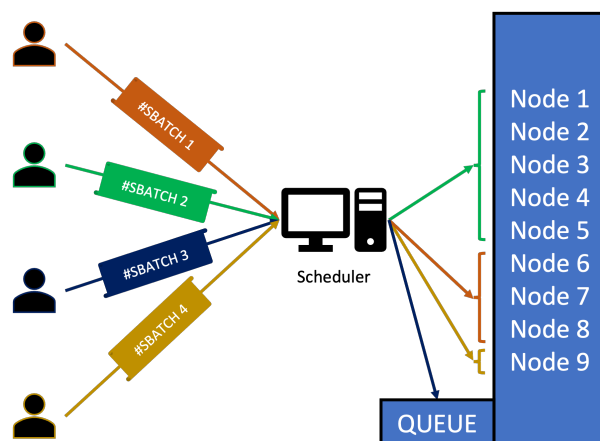
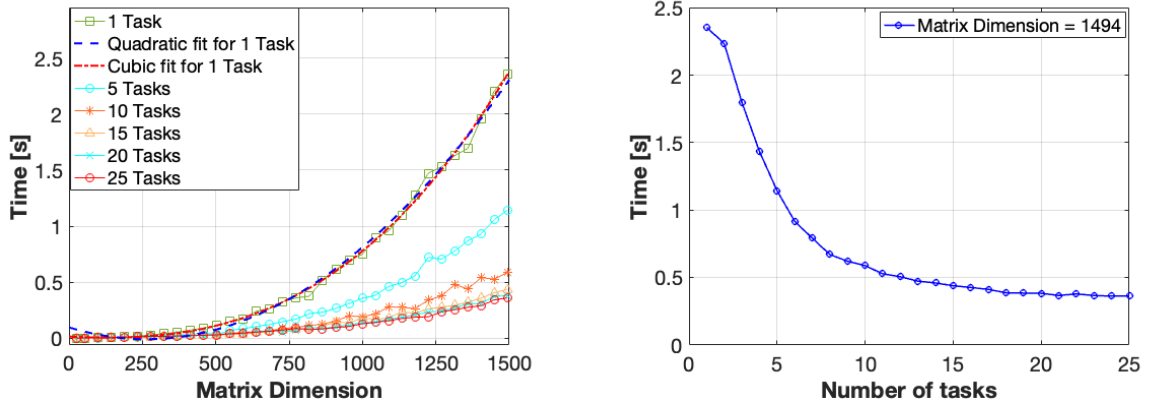


Figure 3.4: Assignment of computing resources in an HPC cluster. Each user submits a *batch* script, then the scheduler assigns the computing nodes considering the number of requested nodes, the memory request and the maximum execution time

In algorithm 3.2 a part of a batch script is reported. In that job, 6 nodes were requested each with 170 *GB* of main memory and 15 tasks. Therefore, the total memory allocated is $170 \text{ GB} * 6 = 1.02 \text{ TB}$, and the problem is executed with 90 tasks (all running in parallel). Since 2 CPUs per tasks are assigned, then a total of 180 CPUs are dedicated to the problem. The maximum time is ten hours. The information present in this script is used by the scheduler of the cluster to define when the resources should be allocated to the user.

3.3.3. Serial vs Parallel code performance

In this section we compare the results in terms of performance for the *QED Solver* when executed in serial and in parallel. In particular, the measurements were performed using the *ProfilingMode* of Octopus Code on the MPCDF cluster Ada [44] while requesting a single node with 200 *GB* of main memory. A simple system was defined for this task, which was a 1D LiH chain with 2 k points, 1 state in the valence band and four states in the conduction bands. According to equation (2.8), this leads to a block dimension of 9. The variable *QEDMatrixNumberOfPhotons* is used to control the dimension of the global matrix (2.7). The calculations were repeated for 1 task (serial) and for 5, 10, 15, 20, 25 tasks.



(a) Diagonalization time as a function of the matrix dimension for many numbers of tasks.

(b) Diagonalization time as a function of the number of tasks for the matrix dimension of 1494

Figure 3.5: Performance of the code for the diagonalization of the QED matrix in the serial and parallel case

We measured the time for the subroutine *qed_solve* (which diagonalizes the Hamiltonian using the eigensolver ELPA [37]) and for the subroutine *qed_get_matrix* (which defines the QED matrix). No measurements were performed on the subroutine *qed_optical_response*

(which computes the linear optical response) because its performance greatly depends on reading the polaritonic states from binary files. This operation depends on the bus of the cluster, which is shared between all users. Let us start with the diagonalization time.

As for the diagonalization, despite the presence of noise, it can be seen that the time needed grows with the cube of the matrix dimension N . The cubic fitting of the curve (dotted blue curve) is much more precise than the quadratic one (dotted red curve), especially in the first half of the graph. Since the fluctuations are minor if compared to the trend, it can be argued that they are due to cluster usage at the moment of measurement. This is particularly true for the parallel case, as the tasks need to communicate. It is interesting to note that when the matrix dimension is small compared to the number of tasks, then increasing the number of tasks does not lead to an improvement in performance. This is partly due to the communication time, and partly because with modern CPUs the difference of elements in the matrix dimension must be significant to generate an effect. In the figure 3.5a, when the matrix dimension is 600, if we are using 25 tasks then each of them manages $\frac{600^2}{25} = 14400$ elements, while by using 15 tasks each of them manages $\frac{600^2}{15} = 24000$ elements. The difference is minor also considering that the majority of them are zeros.

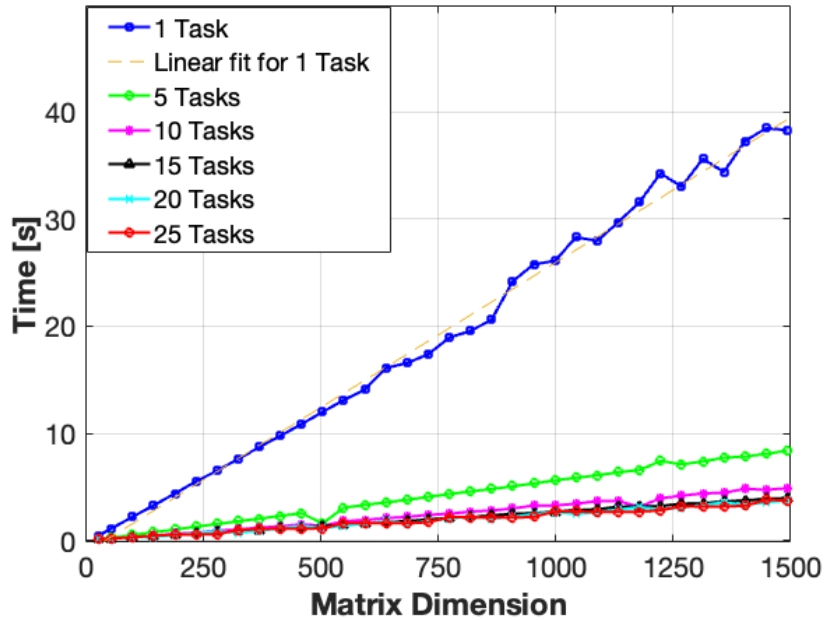


Figure 3.6: QED matrix build time. The trend is linear as shown by the linear fitting for the 1 task case.

Let us now consider the matrix build time. Since the number of elements in a square matrix is N^2 , N being the matrix dimension, one would expect a quadratic scaling for the

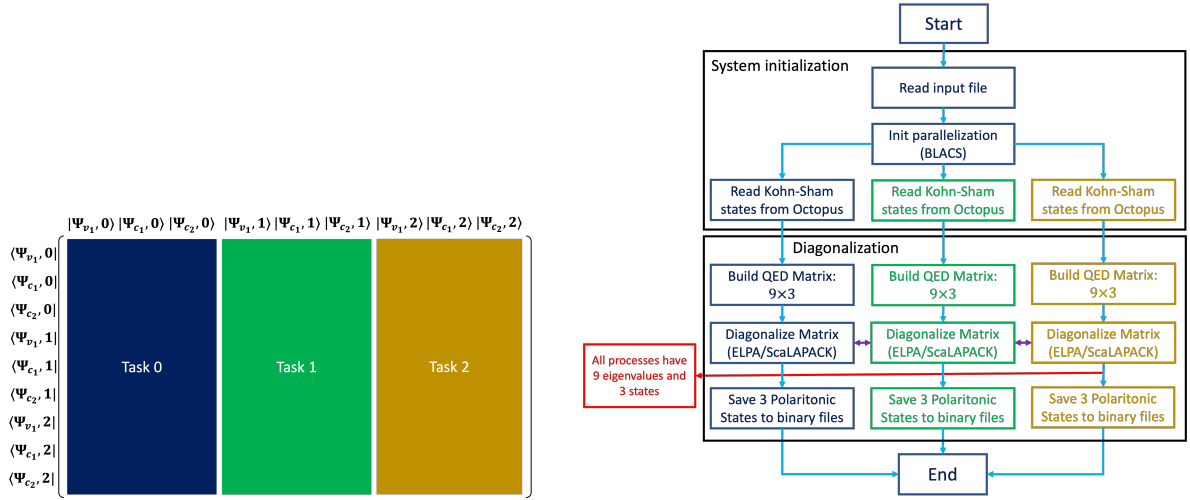
subroutine `qed_get_matrix`. In the parallel case, each task would manage $\frac{N^2}{n_t}$ elements, which is still quadratic. This is indeed the scaling of the *DO* cycles for the rows and the columns. However figure 3.6 clearly shows that the time scales linearly with the matrix dimension. To understand this behavior, one should look carefully at the structure of the QED matrix, so let us consider the Hydrogen example (2.2.3). First of all, one can see that the majority of the elements is 0, so in that case the algorithm does not do anything. Further, the terms on the main diagonal of the blocks are a simple sum of known quantities, so also in that case the code is quite fast. The real complexity is given by the bi-linear coupling block because to compute its entries one has to perform a matrix element between Kohn-Sham states. This operation requires performing a derivative and then an integral. In the system used to produce figure 3.6, each block has a dimension of 9, and the bi-linear coupling block has only 36 non-zero elements (out of 81 entries). Therefore, adding a photon to the cavity implies adding 72 matrix elements to compute, and adding 5 photons to the cavity means adding $72*5$ matrix elements to compute. This explains the linear scaling for the subroutine `qed_get_matrix`.

3.4. Parallel code examples

In this section we will explore how the code of *QED Solver* was parallelized. We will only discuss the diagonalization and the linear optical response, as each of them introduces important concepts of parallel programming. For the sake of simplicity, let us consider the system discussed in section 2.2.3 where the Hamiltonian has dimension 9×9 , and it is represented in equation (2.2.3). Let us divide this problem into three tasks and start by the diagonalization.

The subdivision of the matrix is performed thanks to the BLACS library (Basic Linear Algebra Communication Subprograms), which creates a *grid* of processors. There are many possibilities to do that, but in this software it was decided to allocate all tasks to the columns, so that in the example that we are considering each task would manage three columns and nine rows. A visual representation of the flow chart and the matrix division is provided in figure 3.7a. Within the BLACS grid, each task has a unique rank and knows how many rows and columns it manages. One can easily iterate through them using a standard Fortran *do* loop. However when building the QED Matrix the task also needs to know the global indexes, otherwise they would build the same matrix. In fact, by looking at figure 3.7a, and comparing it with the equation (2.2.3), one can see that for Task 0 the element (1, 1) should be $H_{1,1} = \epsilon_{v_1} + \frac{\Omega_1}{2}$, while for task 1 the element (1, 1) should be $H_{1,1} = 0$. This is because the local element $H_{1,1}$ of task 1 corresponds to the global element $H_{1,4}$ of the QED matrix. The BLACS grid provides a function that allows

the tasks to know about the global indexes they are managing. From this discussion it emerged the most important concept of parallel programming, which is that all tasks run the same algorithm, but manage different data. As a consequence, each task will produce a different result, which then should be properly combined with the ones generated by the others tasks. Considering again the example of the Hydrogen atom, all nodes will read all the Kohn-Sham states because each of them has to build some part of the bilinear coupling block. Subsequently, they all build different parts of the QED matrix and then begin the diagonalization. While diagonalizing, each task communicates with the others to share the matrix element they manage. Once this step is completed, each task will have all the eigenvalues and some eigenvectors (in this case three). Finally, each task writes the polaritonic states that it has to binary files. It should be stressed again that the code is the same for every task, the difference only comes from the fact that each task is assigned to a different part of the matrix. A visual representation of the flow is given in figure 3.7b.



(a) BLACS subdivision of the QED Matrix. Each task has a certain number of columns (in this example three) and all the rows

(b) Flow chart for the parallelization of the diagonalization. The purple arrows represent a communication between tasks

Figure 3.7: In fig a the flow diagram is represented, where it should be noted that the BLACS grid is generated at very beginning of software. Then, the Kohn-Sham states are read, followed by the definition of the QED Matrix, the diagonalization. Finally the polaritonic states are saved and the BLACS grid is de-allocated. In figure b, the BLACS grid for the QED Matrix is represented. Each task manages 3 columns and 9 rows. Before the diagonalization, the QED Matrix contains the matrix elements, after the diagonalization it contains the polaritonic states. Therefore, each task manages 3 polaritonic states

The chosen subdivision of the QED Matrix is particularly advantageous in the last step, which is the writing of the polaritonic states to binary files. In fact, for both eigensolvers (ELPA and ScaLAPACK), after the diagonalization the eigenvectors are along the columns of the matrix. As a consequence, with the chosen parallel layout each task has a certain number of states that can immediately be written to files, without any communication needed.

Let us now consider the linear optical response. The code implements the formula presented in section 3.2.2, which has a lower algorithmic complexity compared to the diagonalization. By looking at equation (3.5), one can see that the sum has $N - 1$ terms, where N is the matrix dimension (2.7). Therefore, in the Hydrogen example we are considering there will be 8 terms. The complexity of the linear response function code is mainly due to the numerator, therefore that is the part that is parallelized. Computing the denominator and performing the actual sum are cheap operations that can be executed by a single task.

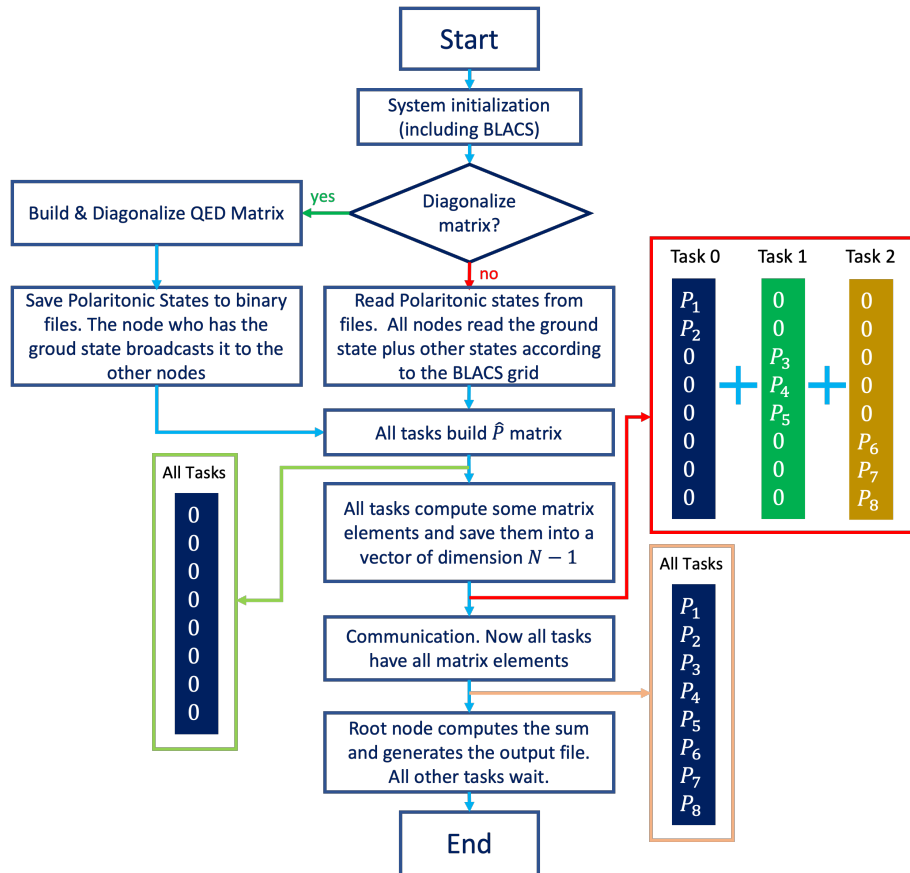


Figure 3.8: Flow diagram for the parallelized linear optical response

Let us now explore the algorithm. Firstly, one can see that the matrix elements are always

between the polaritonic ground state Ψ_0 and an excited state. As a consequence, every task should have the polaritonic ground state plus a certain number of excited state, depending on the dimension of the matrix and on the number of tasks assigned to the problem. Since the linear optical response is computed after the diagonalization of the matrix, the tasks are already divided into a BLACS grid. Therefore, if the matrix was diagonalized it makes sense to keep using the same grid, with the addition that the task that has the polaritonic ground state has to broadcast such state to all other tasks. This is a standard MPI operation, that is indeed called *broadcast*. If the QED matrix was not diagonalized, then all the states were previously saved to binary files, so all tasks simply have to read the file containing the polaritonic ground state. After this operation, all tasks should build the \hat{P} matrix. One can note that the numerator does not depend on the probe energy ω , therefore it is enough to compute it once. Subsequently, all tasks initialize a vector of dimension $N - 1$ which has zeros on all entries. It will contain the polaritonic matrix elements in the numerator of equation (3.5). Each task should compute the matrix element between the polaritonic ground state and the excited states that it manages. In the example of the Hydrogen atom, as of figure 3.7a, the task 0 will compute two matrix elements, that are $\langle \Psi_{GS} | \hat{P} | \Psi_1 \rangle$, $\langle \Psi_{GS} | \hat{P} | \Psi_2 \rangle$, while the tasks 1 and 2 will compute three matrix elements each. After this operation is completed, each task will have some elements of the aforementioned array equal to zero, and others containing the computed matrix elements. For the example of Hydrogen atoms, the situation is represented in the red box in figure 3.8. Finally, we have to combine the information of all tasks so that the one that has to compute the sum can have all the information. This is again a standard MPI operation, called *MPI_Allreduce*, in which all tasks sum their array (or number or matrix) with the same array held by all the other tasks. The situation after this operation is shown in the orange box in figure 3.8. After that, the task assigned to the calculation of the sum can perform the remaining operations, which are the cycle over ω , the definition of the denominator, the actual sum and the output to text file.

4 | Results & Discussion

After describing the theory and the implementation, we shall now discuss the results obtained. We will present three systems, with increasing complexity. For each of them, firstly we state the parameters of the simulation, then we discuss the band structure to rationalize the formation of polaritons. Subsequently, we analyze the linear response function as a function of the light-matter coupling constant (the term A_0 in equation (2.4)).

4.1. Benzene molecule

The first system discussed in this work is the Benzene molecule, which is a finite system. The setup is taken from the paper *Light-Matter Response in Nonrelativistic Quantum Electrodynamics* [45] and it is reported in the figure below.

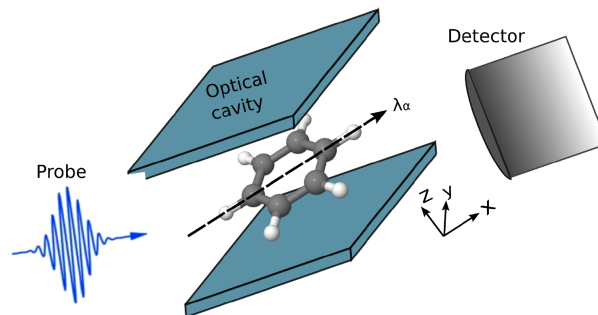


Figure 4.1: Set up for the Benzene molecule. This image is taken from [45], while the coordinates for the atoms are taken from [46]. In the image, λ_α represents the polarization direction of the light in the cavity

The benzene molecule is parallel to the cavity mirrors, as it lies in the xy plane, while the cavity is a Fabry-Perot resonator which confines the light in z direction. The photon mode is polarized in the x direction (as indicated by λ_α in figure 4.1), and the photon basis was truncated to $n = 5$, thus $\{|0\rangle, |1\rangle, |2\rangle, |3\rangle, |4\rangle, |5\rangle\}$. This was decided after a test on the convergence. The ground state of the benzene molecule has 15 occupied

states, which were all included in the calculation. As for the unoccupied states, 10 were considered. Since benzene is a finite system, we performed simulations with periodic boundary conditions on a single k-point grid. According to equation (2.7), the matrix dimension is $DIM_{H_{C_6H_6}} = 906$.

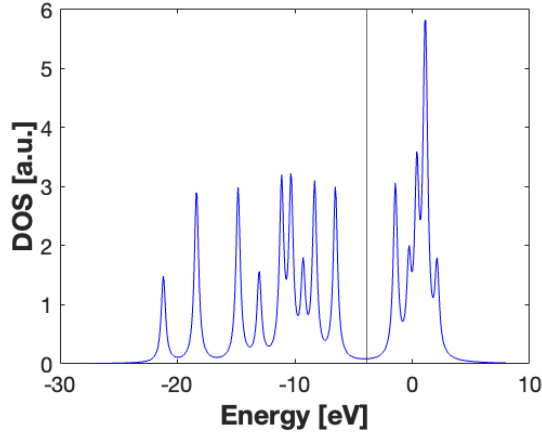


Figure 4.2: Single particle density of states for Benzene molecule. The peaks in this plot do not represent the polaritonic states of equation (3.3), but only the electronic states. The vertical line at $-3.9eV$ is the Fermi level

In figure 4.2, the density of states for the Benzene molecule is reported. The vertical line at $-3.9eV$ is the Fermi level, therefore from this plot the HOMO-LUMO transition, that is the transition between the highest occupied state to the lowest unoccupied state, is expected to be at $5.11eV$ which is accordance with the literature (the small difference is due to the number of unoccupied states included in the calculation) [47]. This transition is the $\pi - \pi^*$, and in the following discussion we tune the cavity to this frequency thus focusing on this transition, rather than on the ones at higher energy.

Let us now consider the absorption of benzene without the cavity. To do that it is enough to set the coupling strength A_0 to zero. As one would expect from the energies of the states, the $\pi - \pi^*$ peak in both the linear optical response (figure 4.3a) and the joint DOS (figure 4.3b) takes place at $5.12eV$. However, if one compares this result with the literature [45, 47], the transition should happen at $6.9eV$. This difference can be explained by the fact that in the present work the dynamic response was disregarded, while that was accounted for in both reference papers (which were using a time-dependent approach). In such a framework, they included the variation of the exchange-correlation potential that happens after the optical response, which gives the difference in the transition energy. It is worth noticing that in principle this effect is present also in solids, but due to the presence of a much higher number of electrons it is usually negligible. On the contrary,

for finite systems like molecules, the effect is much bigger. Another interesting feature is to observe that there are almost no transitions between $5eV$ and $10eV$ and then after $15eV$, while the joint DOS is quite big. This is due to the matrix elements in the linear optical response, which are zero due to the symmetries of the orbitals.

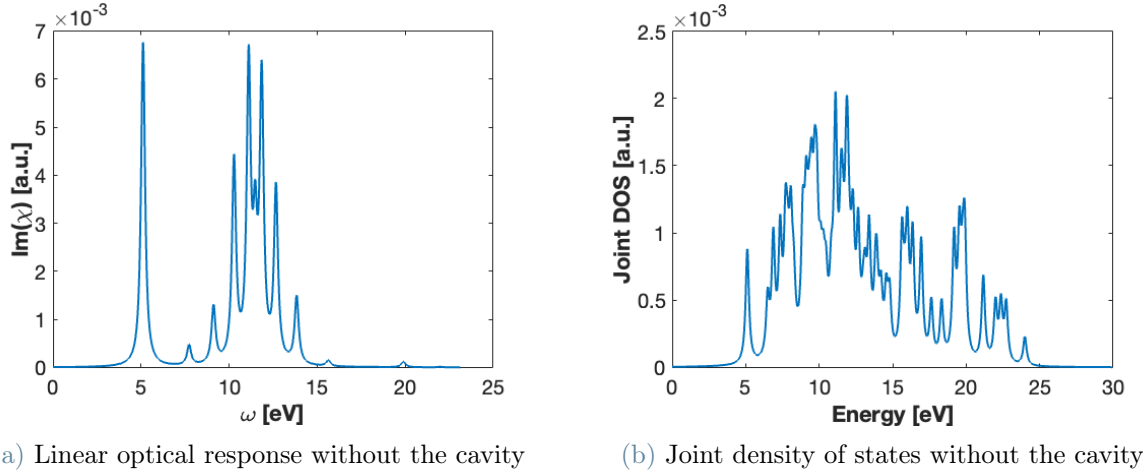


Figure 4.3: In panel (a) the linear optical response of the Benzene molecule is shown. The first peak is roughly at $5.12eV$, which corresponds to the $\pi - \pi^*$. Conversely, the series of peaks between $10eV$ and $14eV$ correspond to the $\sigma - \sigma^*$ transitions. In panel (b) the Joint DOS is represented. It is possible to observe the peaks corresponding to the $\pi - \pi^*$ and $\sigma - \sigma^*$ transitions. The value of the Lorentzian broadening was $\eta = 135meV$

Let us now turn on the cavity and consider the linear optical response. As it was expected (figure 4.4), as soon as the coupling is non zero then the polaritonic split appears. If one looks at the Rabi splitting in the absorption line at the lowest energy (the $\pi - \pi^*$), one can see that it increases with A_0 . Before analyzing this splitting in detail, it is worth noticing that apart from the main photonic line there are other ones in the left part of the graphs. They are highlighted in the panel corresponding to $A_0 = 0.06$. The physical interpretation for those is that the line at the lowest energy is due to the coupling of the electronic states with the Fock state $|1\rangle$, the second line corresponds to the coupling with the Fock state $|2\rangle$ and so on. These resonances have a lower intensity than the primary ones, and the steepness of the line describing them is much higher, which is why they are harder to see and they are not present in every panel. In fact, for $A_0 = 0.02$ they are too weak, while for $A_0 = 0.08, A_0 = 0.1$ they are shifted out to the left side of the graph.

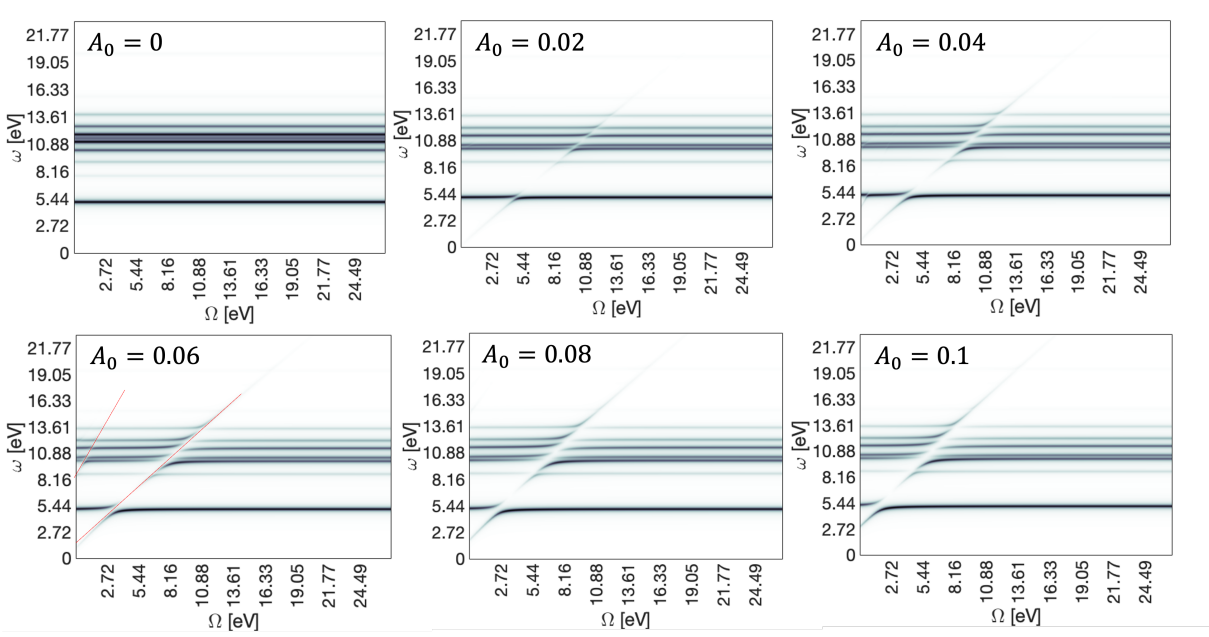


Figure 4.4: Contour plot of the linear optical response for some values of the coupling strength A_0 . On the x-axis there is the resonance energy of the cavity and on the y-axis the energy of the probe. The value of the Lorentzian broadening was $\eta = 135meV$

Let us briefly analyze the steepness of those two red lines. The lower one forms an angle of 42° , while the second has an angle of 64° , thus their ratio is 1.52. To understand whether it is correct, one should consider the matrix elements of the main diagonal of the QED matrix. Since those are the photon lines, they must be described by the photonic part of the matrix elements of the Hamiltonian. By looking at equation (2.4), and remembering that the operator $\hat{a}^\dagger \hat{a}$ applied to a Fock state gives the number of photons, then the photonic part of the elements is given by

$$\langle n | H_{QED} | n \rangle = E_n = \Omega \left(n_{ph} + \frac{1}{2} \right) + N_{el} A_0^2 \left(n_{ph} + \frac{1}{2} \right) \quad (4.1)$$

For the first photon line clearly one has that $n_{ph} = 1$, while for the second $n_{ph} = 2$. As a consequence, the two lines will be:

$$\langle 1 | H_{QED} | 1 \rangle = E_{ph,1} = \frac{3}{2} \Omega + \frac{3N_{el}A_0^2}{2} \quad (4.2)$$

$$\langle 2 | H_{QED} | 2 \rangle = E_{ph,2} = \frac{5}{2} \Omega + \frac{5N_{el}A_0^2}{2} \quad (4.3)$$

The ratio between the two angular coefficients is $\frac{5}{3} = 1.67$, which is comparable with the one obtained with the two lines.

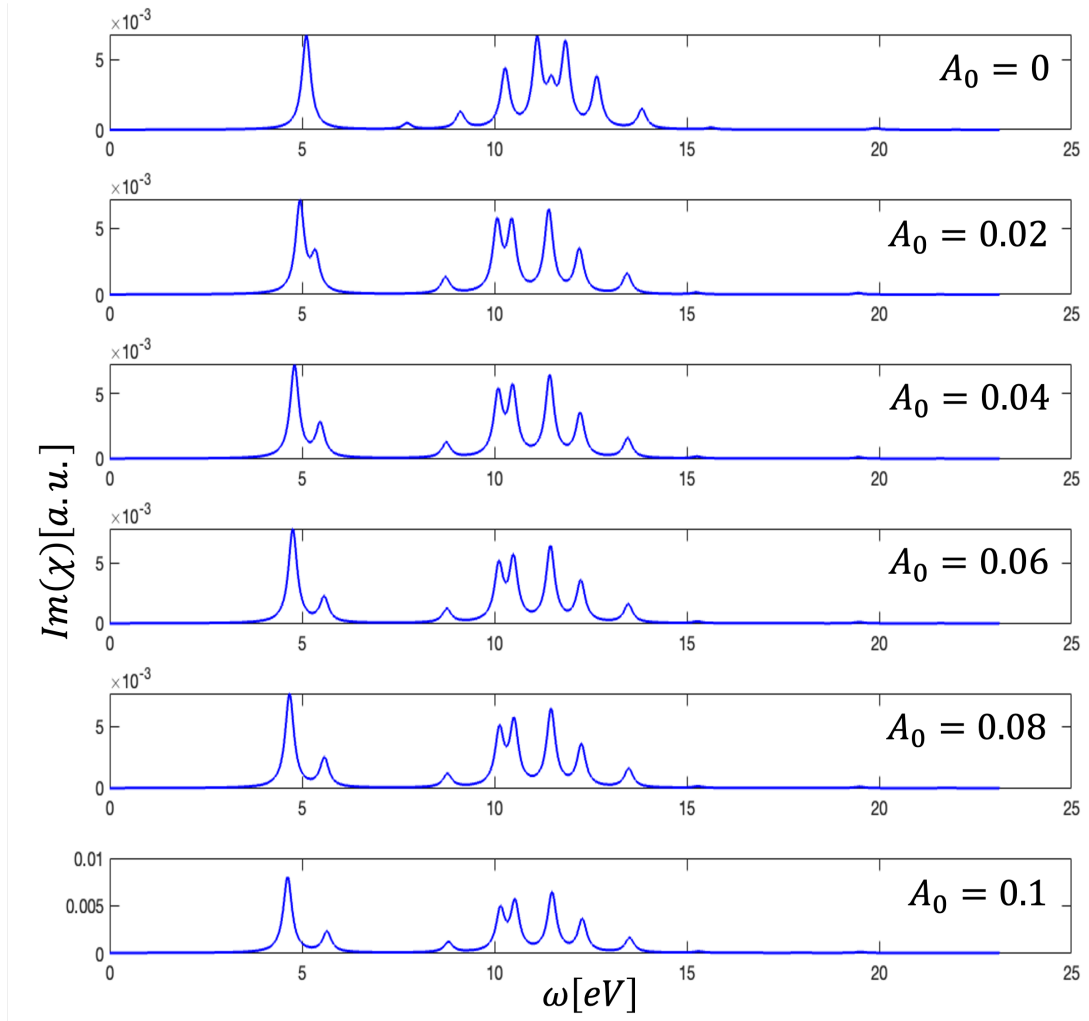


Figure 4.5: Comparison of the Rabi splitting for the $\pi - \pi^*$ transition

Finally, as for the Rabi splitting of the $\pi - \pi^*$ transition, it can be seen from figure 4.5 that the lower polariton is always more intense than the upper one which is in accordance with what is found in literature [45]. As for the value of the splitting, it increases linearly with the coupling strength A_0 , which is in accordance with equation (1.56). The values are reported in the table below.

	$A_0 = 0$	$A_0 = 0.02$	$A_0 = 0.04$	$A_0 = 0.06$	$A_0 = 0.08$	$A_0 = 0.1$
$\pi - \pi^*$	0	0.36	0.68	0.85	0.93	1.03

Table 4.1: Rabi splitting (in eV) as a function of the coupling strength

4.2. LiH 1D chain

The second system we discuss is a simple 1D linear chain of Lithium and Hydrogen. The system is non-physical (as we will discuss), nevertheless it constitutes a good introduction to periodic systems because of its simple structure. Moreover, this was the system that was used to debug the implementation of the software, as it was possible to test observables even with a very small matrix (as small as 14×14).

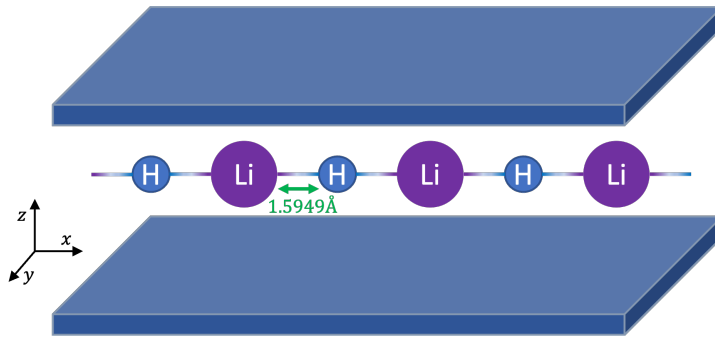


Figure 4.6: Set up of the LiH 1D chain. The cavity confines the photon mode in the z -direction, while the chain is periodic in the x -direction. The distance between Lithium and Hydrogen atom is 1.5949 \AA

The setup used is represented in the figure above. The distance for the Li-H bond is the one of the Lithium Hydride molecule [48], and the chain is periodic in the x direction.

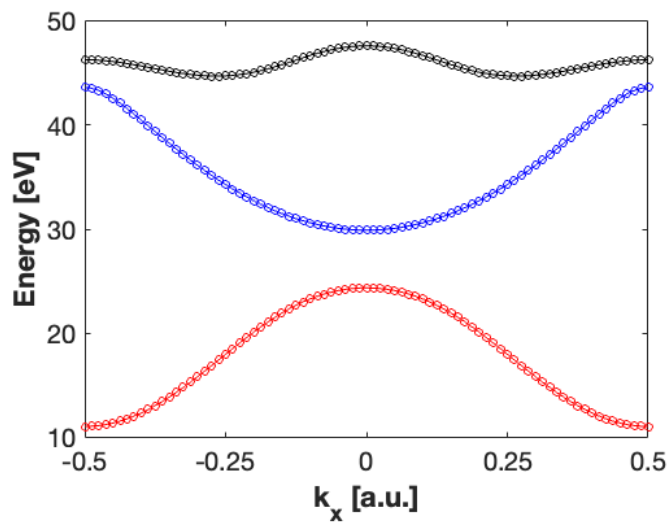


Figure 4.7: Band structure of the LiH 1D chain. The red state is the valence band, which is fully occupied, while the other constitutes the conduction band. The blue state is double degenerate. The presence of a gap indicates a insulating behavior

On the other hand, the cavity is a Fabry-Perot resonator which confines the light in z direction. The photon mode is polarized in the x direction, and the photon basis was truncated to $n = 5$, thus $\{|0\rangle, |1\rangle, |2\rangle, |3\rangle, |4\rangle, |5\rangle\}$. As for the property of the material, both the Lithium and the Hydrogen have 1 electron available for bonds (for Lithium is the $2s$, for Hydrogen the $1s$). As a consequence, there will be only 1 valence band (which will be full), and we can expect a semiconducting behavior. As for the unoccupied states, 3 states were used for the conduction bands and the Brillouin zone was sampled with 81 k points. From equation (2.7), the matrix dimension is $DIM_{H_{LiH}} = 1464$.

In figure 4.7 the band structure of the system is reported. The presence of an energy gap of $5.53eV$ between valence (red state) and conduction band indicates that the material behaves as an insulator, as it was expected from the electronic valence of Li and H atoms. Moreover, it should be noted that the blue band is double degenerate. Let us now consider the linear optical response and the joint density of states without coupling with the cavity. To do that, it is enough to set $A_0 = 0$ in the calculation.

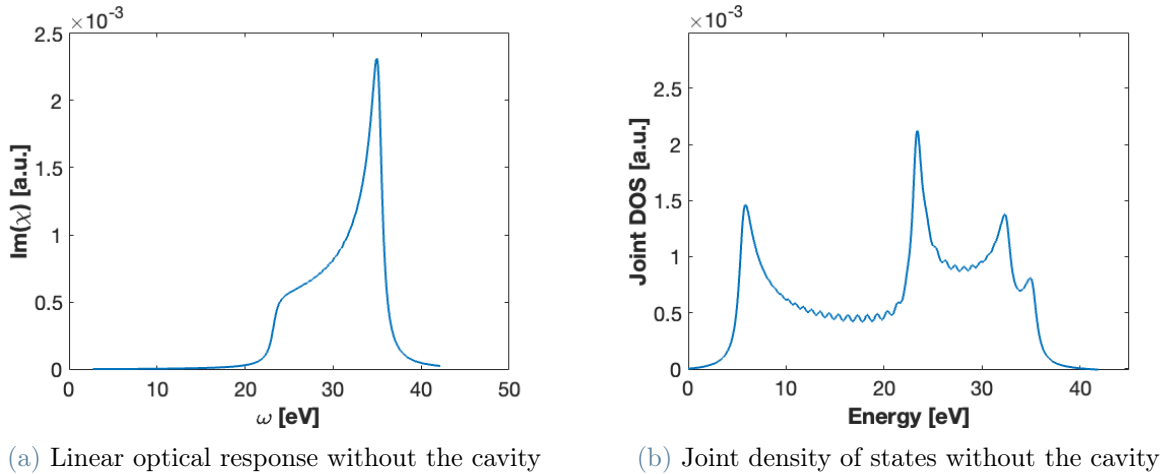


Figure 4.8: In panel (a) the linear optical response of the LiH 1D chain is shown. The onset is roughly at $23.5eV$, which corresponds to the transition from the red band to the black band at $k_x = 0$. Conversely, the highest peak corresponds to the transition between the same bands, but at the border of the Brillouin zone. In panel (b) the Joint DOS is represented. The first peak corresponds to the band gap, while the second corresponds to the onset of the optical absorption. The value of the Lorentzian broadening was $\eta = 544meV$

In figure 4.8a and 4.8b the linear optical response and the joint DOS are shown, respectively. From the joint DOS it is possible to recognize the first peak as the band gap of the system at $5.53eV$, followed by a decrease that goes as $D(E) \sim \frac{1}{\sqrt{E}}$ as it is expected for 1D

systems [39]. The small undulations between $10eV$ and $20eV$ are due to the finite k-point sampling in the simulation. Interestingly, the transitions between these two bands (the valence and the first conduction band) are not present in the optical response 4.8a. This is due to the fact that the matrix elements between the polaritonic states in equation (3.5) are zero. This can be interpreted by considering the symmetries of the bands, which would justify the zero in the matrix elements. The $\frac{1}{\sqrt{E}}$ trend continues until the first transition from the red band to the black band, which generates the peak at $23.5eV$, and it is the onset of the optical response. Finally, the two peaks at higher energy correspond to transitions happening at $k_x = \pm 0.25$ and at the border of the Brillouin zone. In particular, the latter generates the biggest absorption peak.

Let us now turn on the cavity. Firstly the linear optical response will be analyzed. As one can see from figure 4.9, while without cavity coupling the material response is independent of the cavity frequency, when the cavity is turned on, the linear response band is divided into two branches, separated by a region with a much lower optical response. This trend increases with the coupling strength A_0 . If one recalls figure 1.4, then the upper band can be identified with the upper polariton, the lower with the lower polariton. The fact that there is a region with lower absorption is coherent with the fact when there is strong coupling, the dressed states are split by the Rabi splitting, which is also supposed to increase linearly with the coupling strength A_0 , according to equation (1.56).

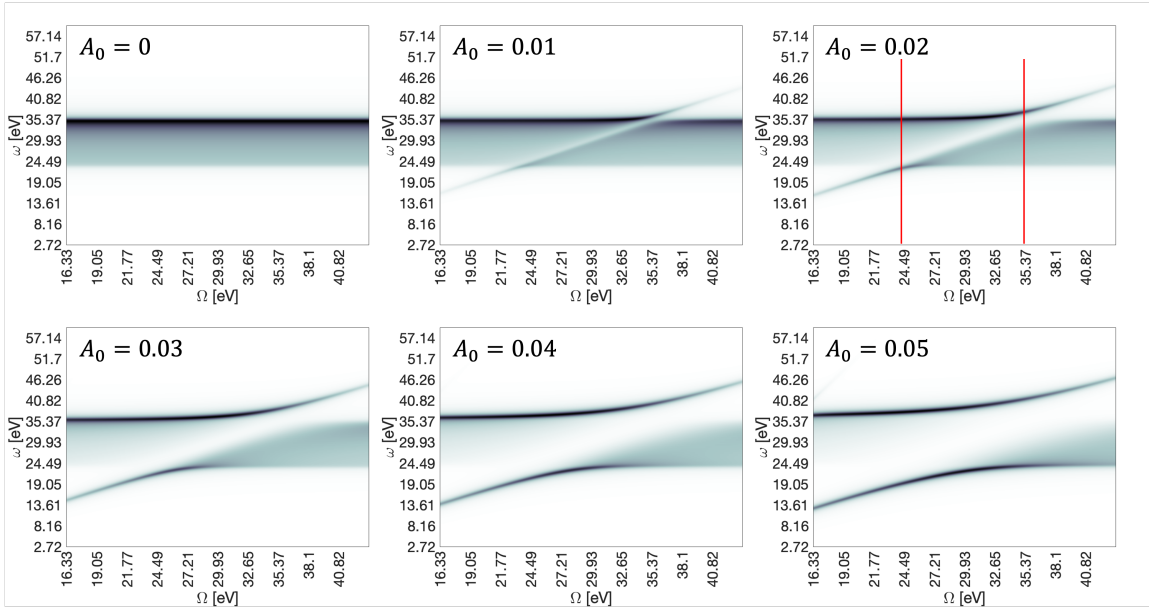


Figure 4.9: Contour plot of the linear optical response for many values of the coupling strength A_0 . On the x-axis there is the resonance energy of the cavity and on the y-axis the energy of the probe. The value of the Lorentzian broadening was $\eta = 544meV$

To prove that the Rabi splitting is indeed linear, let us consider two vertical cuts of the linear optical response (i.e. at two fixed cavity energies). The cuts are represented by the red lines in figure 4.9.

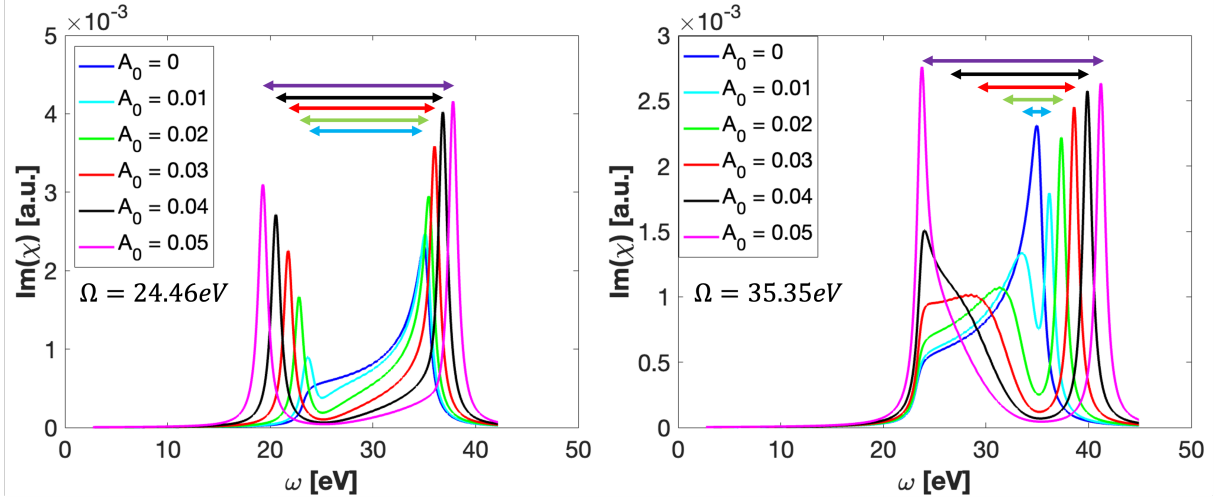


Figure 4.10: Comparison between two vertical cuts (i.e. at fixed cavity frequency) for the linear optical response. The arrows represent the Rabi splitting

The first cut is taken at $\Omega = 24.46\text{eV}$, which means where the lower polariton splits. The second is taken at $\Omega = 35.35\text{eV}$, where the upper polariton splits. In both cases, the increasing length of the arrows (which represent the Rabi splitting) increases linearly as shown in the table below.

	$A_0 = 0$	$A_0 = 0.01$	$A_0 = 0.02$	$A_0 = 0.03$	$A_0 = 0.04$	$A_0 = 0.05$
$\Omega = 24.46\text{eV}$	0	11.41	12.98	14.28	16.23	18.56
$\Omega = 35.35\text{eV}$	0	3.97	5.98	9.59	13.58	17.43

Table 4.2: Rabi splitting (in eV) as a function of the coupling strength

4.3. Graphene

The last system studied in this work is Graphene, which is a 2D material constituted only by Carbon atoms arranged in hexagons. Due to its properties, it is probably the most studied 2D material. The main characteristic of its band structure is the presence of the Dirac points (and Dirac cones), where the valence band and the conduction band touch. From those points, two cones are originated, where the dispersion relation of the

electron is linear. As a consequence, since the mass is the second derivative of the energy dispersion relation with respect to k [39], the mass of electron inside these cones is zero, which means that the fermions cannot accelerate nor decelerate.

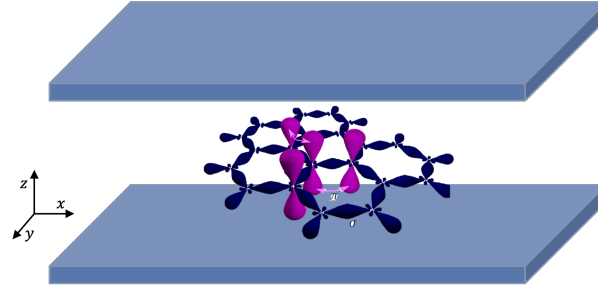


Figure 4.11: FP Cavity containing the Graphene used to simulate this system. The lattice of Graphene is taken from <https://en.wikipedia.org/wiki/Graphene>

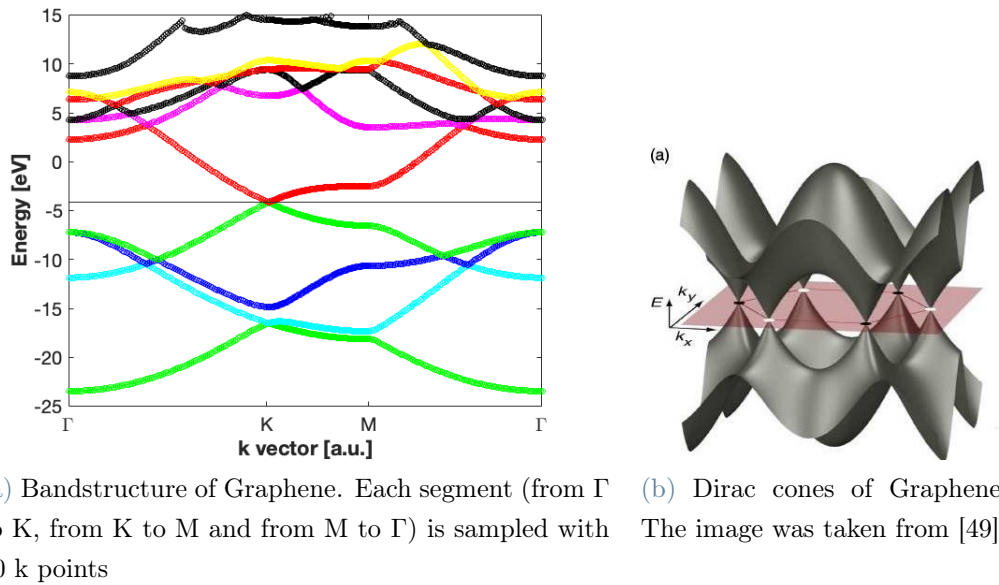


Figure 4.12: In panel (a) the band structure with 4 states in the valence band and 6 states in the conduction band is shown. The line at $-4.17eV$ represents the Fermi level. In panel (b) a 3D representation of the π bands, with a focus on the Dirac points

Due to the presence of these cones, this material has a very high computational complexity. In fact, one has to use a fine k-point sampling to correctly describe the region around the cones. At the same time, one can see that the conduction bands from number 2 to number 5 are very close in energy both at Γ and K, which means that to get a coherent quantitative description one has to include most of them. In particular, for the following results all the states in the valence were included, as well as 4 states in the conduction

band. As for the k points sampling, a grid of 60×60 points in the xy plane was used, for a total of 3600 points. Finally, the photonic base was truncated to 4 states, thus $\{|0\rangle, |1\rangle, |2\rangle, |3\rangle\}$. As a consequence, according to equation (2.7), the matrix dimension is $DIM_{H_{Graphene}} = 230404$. The computational complexity of the system is extremely high compared to the LiH chain or the Benzene molecule. For such reason, it was not possible to include 6 photonic states like in the previous page, as well as the 5th conduction band had to be left out.

Let us now consider the properties of Graphene without the presence of the cavity.

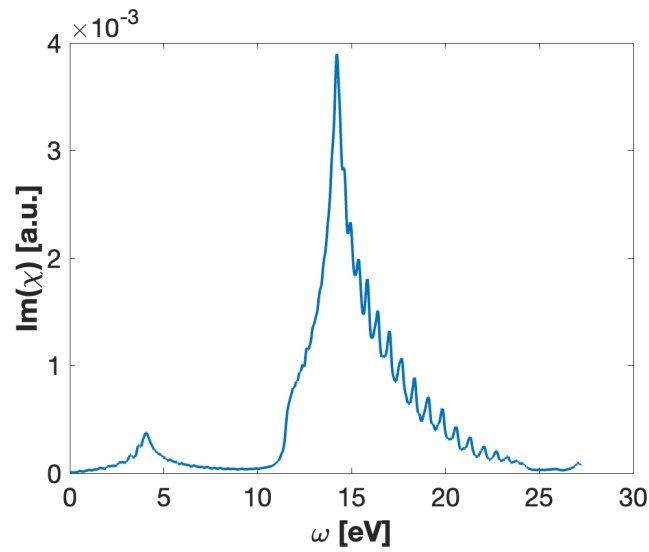
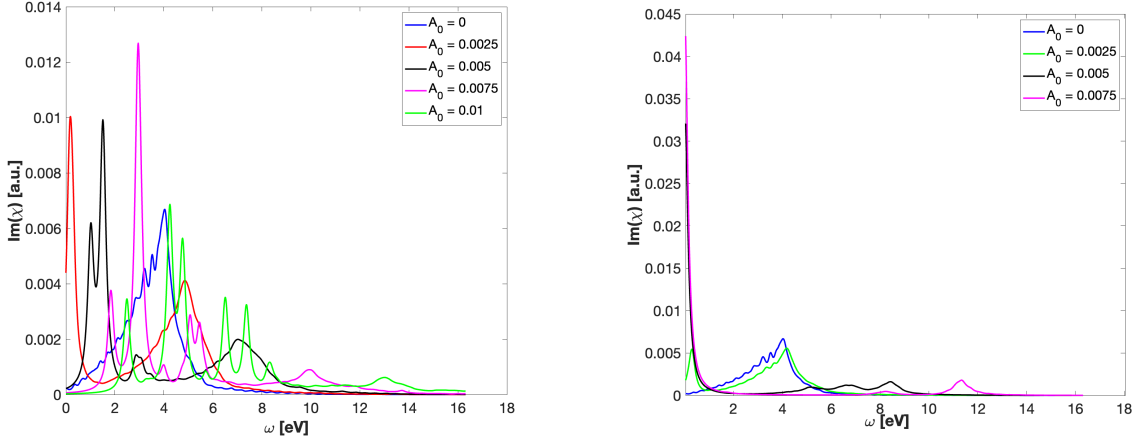


Figure 4.13: Linear optical response of Graphene without the cavity. The value of the Lorentzian broadening was $\eta = 150meV$

As it can be seen, the onset of the linear response is at $0eV$, as one would expect due to the fact that the valence and the conduction band touch each other at the K point. Subsequently the first peak is at about $4.2eV$, which according to the literature [50, 51] corresponds to the $\pi - \pi^*$ around the M point. The intensity calculated in this work is lower than the one present in the literature. Finally, the highest absorption peak at $14.35eV$ is given by the $\sigma - \sigma^*$ transition. In one recalls how dense the conduction bands from 2 to 5 are (figure 4.12a), then it is easy to see that this peak is supposed to be much higher than the $\pi - \pi^*$ one. The fact that the intensity of the $\pi - \pi^*$ is much lower than the one that can be found in literature is due to the fact that the matrix element at the numerator of equation (3.5) should include a term $\propto \frac{1}{E_I - E_1}$. Since its value is $\frac{1}{4eV}$ for the $\pi - \pi^*$ and $\frac{1}{15eV}$ for the $\sigma - \sigma^*$, then the two peaks get rescaled and yield the expected result.

Let us now turn on the cavity. In all the following discussions, the polarization of the light

in the cavity was circular, thus the polarization vector was $\mathbf{e} = \frac{1}{\sqrt{2}}(\mathbf{e}_x + i\mathbf{e}_y)$. Due to the computational complexity of this problem it was not possible to produce the contour plots for observing the polaritonic split in the bands. Therefore, it will only be possible to consider plots at certain cavity energy. Moreover, in order to study the modification of the Dirac cone it was decided to sample the Brillouin zone only around the K point. This allowed to strongly simplify the computational complexity, as the number of k points needed was 973. In addition, it was also decided to focus only on the bands which form the Dirac cone, which means the last valence band and the first conduction band. This contributed to simplify the problem from both a computational and a physical point of view.



(a) Linear optical response of Graphene using circularly polarized light $\mathbf{e} = \frac{1}{\sqrt{2}}(\mathbf{e}_x + i\mathbf{e}_y)$

(b) Linear optical response of Graphene using linearly polarized light in the x direction

Figure 4.14: In panel (a) the linear optical response using circularly polarized light is shown. In panel (b) a 3D representation of the π bands, with a focus on the Dirac points. For both panels, the cavity energy is $27.2meV$ and the Lorentzian broadening is $\eta = 150meV$.

Let us start by analyzing the panel 4.14a, which is for circularly polarized light. When the cavity is turned on, like in the previous systems the peak at $4eV$ is split into an upper polariton and a lower polariton (red curve). This split pushes the lower branch very close to the $\omega = 0eV$, which prevents the gap from opening for such value of A_0 . However, by increasing the coupling strength one can see that the response for small values of ω decreases, and for $A_0 = 0.01$ the onset on $Im(\chi)$ is at around $2eV$. This witnesses the gap opening in the band structure. However, one can observe other interesting features. In fact, by considering the black curve ($A_0 = 0.005$), it can be seen that the first peak

corresponding to the lower polariton is shifted with respect the same peak of the red curve ($A_0 = 0.0025$), coherently with the expectations. However, that peak is itself split into two peaks, which is a feature that was not observed in the previous systems. By looking at the magenta and green curves, this sub-split increases and it also appears in the upper polariton peak ($5.5eV$ for $A_0 = 0.0075$ and between $6eV$ and $8eV$ for the green curve). On the contrary, if the polarization of the light in the cavity is linear (figure 4.14b), as soon as the coupling strength is greater than zero the optical response in the region $\omega = 0eV$ increases. For small values of A_0 (green curve) a small peak appears, which later grows exponentially when A_0 is increased. This shows that linearly polarized light is not suitable for opening a gap in the band structure of Graphene.

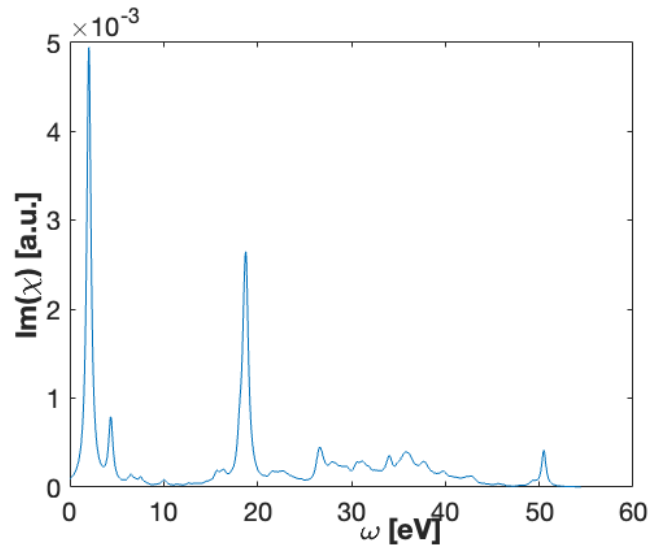


Figure 4.15: Linear optical response of Graphene. The value of the coupling strength was $A_0 = 0.005$, the cavity energy was $\Omega = 272meV$ and the Lorentzian broadening was $\eta = 272meV$

Finally, to confirm what was observed for the Graphene for the simulations in which the k-point sampling was performed only around a small region centered at the K-point, in the figure 4.15 the results for the case of full sampling of the Brillouin zone are reported. The plot should be compared with the black curve in figure 4.14a. It can be seen that the onset at zero is at the same height, which suggests that by using higher values of A_0 a gap would appear. As for the position of the peaks, it can be noted the splitted peak in figure 4.15 corresponds to the highest peak in figure 4.14a, which however has no splitting. Subsequently, the peak around $3eV$ in 4.14a corresponds to the second peak in 4.15, which however is shifted at $4eV$. Finally, in figure 4.15 it is possible to recognize the $\sigma - \sigma^*$ peak, which is shifted from around $14eV$ to around $19eV$.

As it might be clear from the discussion on Graphene, the system is quite complex as plenty of different phenomena (which are not observed for Benzene or the LiH chain) take place. Nevertheless, there is an indication that by using circularly polarized light a gap is opened, which should be considered a remarkable result. The understanding of the full physics of the system should be considered a future development of this work.

5 | Conclusions and future developments

In this thesis work we presented a new software for studying materials in the framework of cavity QED. We started by exploring the theoretical background of cavity QED, that is by quantizing the electromagnetic field and by describing the behavior of electrons in both finite and periodic systems. Afterward, we combined the radiation field and the matter by deriving the QED Hamiltonian starting from the canonical momentum substitution and arriving at the dressed states, which are a mix of the electronic states and the photonic states. This led to the introduction of the concept of polaritons. Subsequently, we discussed the methods and the assumption used to study the problem, among which the one of taking only the photonic mode at $q = 0$. Then, we discussed the structure of the problem and how the code was implemented, firstly by giving the shape of the QED matrix, then by discussing the serial implementation of the code and finally discussing the limitation of such an approach, which led to its parallelization.

Finally, we used the software to study three systems, the LiH 1D chain, the Benzene molecule and Graphene. To study those systems, it was enough to enter the parameters of the material in a simple input file. For each system we showed that by increasing the coupling strength A_0 we increase the Rabi splitting of the peak at resonance, and this increase is linear. The fact that we were able to do this for Graphene is a significant result because the computational complexity of studying such a system is very high due to the number of k points required to successfully sample the Dirac cone. For Graphene, we also showed that by using chiral light it is possible to open a gap at the Dirac cone, which is in accordance with what is found in literature. On the other hand, for both the LiH chain and the Benzene molecule we were able to see the polaritonic splitting by plotting the linear response function against the cavity resonance and the probe energy. This result is also computationally significant because the QED matrix had to be diagonalized about one thousand times for each value of the coupling parameter.

In conclusion, in this work we developed a software that allows studying any material in a QED cavity, starting only from the Kohn-Sham states (which can be easily computed

using DFT). This is relevant because the flexibility of the code allows approaching systems spanning from molecular to bulk in an efficient and controllable way for any light-matter coupling regime. Moreover, since the code was parallelized and it was written with a programming language highly optimized for numeric computation, the complexity of the systems that we will be able to study in the future will increase significantly as scientists will be able to make use of this code in the computer clusters of their institutes.

Finally, the future developments of this project are twofold. On one hand, it will be interesting to use the software to study more complex systems such as Weyl semi-metals. For those, the number of k points required to correctly sample the Weyl points is very high due to the extra dimension (the material is 3D), which will require a big computational effort. The hope is to control the position of such points and affect the topological chiral currents associated with them. On the other hand, the development of the software will continue to include new features, such as the correlation between electrons and the possibility of computing the ground-state electronic density from the polaritonic states and exploiting it to develop DFT functional with built-in light-matter correlation.

There will also be improvements regarding the diagonalization of the QED matrix, as it is possible to fully exploit its sparse structure. However, the most exciting development will be overcoming the single-mode approximation. To do that, it is possible to make use of a Quantum Computer to delegate the calculation of the Fock states, which are very expensive for classical computing (as shown through this work) but are quite cheap for quantum hardware. This will constitute an absolute first in the use of a quantum computer and will open many possibilities to study systems whose complexity will always be prohibitive for a classical supercomputer. This will be an actual development of this thesis work, as I will begin a Ph.D. jointly between the Max Planck Institute for the Structure and Dynamics of Matter and IBM Research Zurich. This collaboration will bring together the expertise from both institutions, and eventually will allow studying cavity QED materials by interfacing a quantum computer with the TDDFT code Octopus.

Bibliography

- [1] M. Radivojević and T. Rehren, “Tainted ores and the rise of tin bronzes in eurasia, c. 6500 years ago,” *Antiquity Publications Ltd.*, December 2013.
- [2] D. Johnson, “Ibm introduces the world’s first 2-nm node chip,” 2021.
- [3] J. Faist, F. Capasso, D. L. Sivco, C. Sirtori, A. L. Hutchinson, and A. Y. Cho, “Quantum cascade laser,” *Science*, vol. 264, no. 5158, pp. 553–556, 1994.
- [4] H. Hübener, M. A. Sentef, U. De Giovannini, A. F. Kemper, and A. Rubio, “Creating stable floquet–weyl semimetals by laser-driving of 3d dirac materials,” *Nature Communications*, vol. 8, 2017.
- [5] A. L. Schawlow and C. H. Townes, “Infrared and optical masers,” *Phys. Rev.*, vol. 112, pp. 1940–1949, Dec 1958.
- [6] S. Latini, D. Shin, S. A. Sato, C. Schäfer, U. D. Giovannini, H. Hübener, and A. Rubio, “The ferroelectric photo ground state of SrTiO_3 : Cavity materials engineering,” *Proceedings of the National Academy of Sciences*, vol. 118, no. 31, p. e2105618118, 2021.
- [7] S. Latini, E. Ronca, U. De Giovannini, H. Hübener, and A. Rubio, “Cavity control of excitons in two-dimensional materials,” *Nano Letters*, vol. 19, no. 6, pp. 3473–3479, 2019.
- [8] G. Mazza and A. Georges, “Superradiant quantum materials,” *Phys. Rev. Lett.*, vol. 122, p. 017401, Jan 2019.
- [9] M. A. Sentef, M. Ruggenthaler, and A. Rubio, “Cavity quantum-electrodynamical polaritonically enhanced electron-phonon coupling and its influence on superconductivity,” *Science Advances*, vol. 4, no. 11, p. eaau6969, 2018.
- [10] Y. A. et al., “Quantum electrodynamic control of matter: Cavity-enhanced ferroelectric phase transition,” *Phys. Rev. X*, vol. 10, p. 041027, 2020.
- [11] E. R. Xiao Wang and M. A. Sentef, “Cavity quantum electrodynamic chern insu-

- lator: Towards light-induced quantized anomalous hall effect in graphene,” *Physical Review B*, vol. 99, p. 235156, 2019.
- [12] R. G. Lindner N. and G. V., “Floquet topological insulator in semiconductor quantum wells,” *Nature Physics*, vol. 7, p. 490–495, 2011.
- [13] A. Cavalleri, “Photo-induced superconductivity,” *Contemporary Physics*, 2017.
- [14] S. Kaiser, “Light-induced superconductivity in high-*t_c* cuprates,” *Physica Scripta*, vol. 92, p. 103001, 2017.
- [15] A. Kavokin, “Exciton–polaritons in microcavities: Recent discoveries and perspectives,” *Phys. Status Solidi B*, vol. 247, p. 1898–1906, 2010.
- [16] D. N. Basov, A. Asenjo-Garcia, P. J. Schuck, X. Zhu, and A. Rubio, “Polariton panorama,” *Nanophotonics*, vol. 10, no. 1, pp. 549–577, 2021.
- [17] S. Latini, U. De Giovannini, E. J. Sie, N. Gedik, H. Hübener, and A. Rubio, “Phonon polaritons as hybridized exciton-photon-phonon excitations in a monolayer *h*-bn optical cavity,” *Phys. Rev. Lett.*, vol. 126, p. 227401, Jun 2021.
- [18] R. A. Meyers, *Encyclopedia of Physical Science and Technology*. Academic Press, 2001.
- [19] P. Dirac, *Principles of Quantum Mechanics*. Oxford University Press, 1982.
- [20] R. Loudon, *The Quantum Theory of Light*. Oxford Science Publications, 2000.
- [21] H. B. G. Casimir and D. Polder, “The influence of retardation on the london-van der waals forces,” *Phys. Rev.*, vol. 73, pp. 360–372, Feb 1948.
- [22] T. A. Welton, “Some observable effects of the quantum-mechanical fluctuations of the electromagnetic field,” *Phys. Rev.*, vol. 74, pp. 1157–1167, Nov 1948.
- [23] F. Giustino, *Materials Modelling using Density Functional Theory*. Oxford University Press, 2014.
- [24] D. J. Griffiths and D. F. Schroeter, *Introduction to Quantum Mechanics*. Cambridge University Press, 2018.
- [25] P. Hohenberg and W. Kohn, “Inhomogeneous electron gas,” *Phys. Rev.*, vol. 136, pp. B864–B871, Nov 1964.
- [26] G. Stefanucci and R. van Leeuwen, *Nonequilibrium Many-Body Theory of Quantum Systems*. Cambridge, 2013.

- [27] M. Fox, *Quantum Optics: an introduction*. Oxford University Press, 2006.
- [28] A. Boca, R. Miller, K. M. Birnbaum, A. D. Boozer, J. McKeever, and H. J. Kimble, “Observation of the vacuum rabi spectrum for one trapped atom,” *Phys. Rev. Lett.*, vol. 93, p. 233603, Dec 2004.
- [29] J. Reithmaier, G. Sek, A. Löffler, and et al., “Strong coupling in a single quantum dot–semiconductor microcavity system,” *Nature*, vol. 432, pp. 197–200, 2004.
- [30] Y. Y. Tim Byrnes, Na Young Kim, “Exciton–polariton condensates,” *Nature Physics*, vol. 10, pp. 803–813, 2014.
- [31] C. F. Klingshirn, *Semiconductor optics*. Springer, 2004.
- [32] P. Hasnip, “What is the kpoints in electronic structure calculations?,” 04 2015.
- [33] “Octopus code,” 2022.
- [34] M. A. Marques, A. Castro, G. F. Bertsch, and A. Rubio, “Octopus: a first-principles tool for excited electron–ion,” *Computer Physics Communications*, vol. 151, no. 1, pp. 60–78, 2003.
- [35] G. B. Bachelet, D. R. Hamann, and M. Schlüter, “Pseudopotentials that work: From h to pu,” *Phys. Rev. B*, vol. 26, pp. 4199–4228, Oct 1982.
- [36] X. Andrade, D. Strubbe, U. De Giovannini, A. H. Larsen, M. J. T. Oliveira, J. Alberdi-Rodriguez, A. Varas, I. Theophilou, N. Helbig, M. J. Verstraete, L. Stella, F. Nogueira, A. Aspuru-Guzik, A. Castro, M. A. L. Marques, and A. Rubio, “Real-space grids and the octopus code as tools for the development of new simulation approaches for electronic systems,” *Phys. Chem. Chem. Phys.*, vol. 17, pp. 31371–31396, 2015.
- [37] M. P. Computing and D. F. (MPCDF), “Eigenvalue solvers for petaflop application,” 2022.
- [38] U. o. C. D. Univ. of Tennessee, Univ. of California Berkeley and N. Ltd., “Scalable linear algebra package,” 2022.
- [39] G. Grosso and G. P. Parravicini, *Solid State Physics*. Academic Press, 2000.
- [40] F. J. e. a. Ruggenthaler M., Tancogne-Dejean N., “From a quantum-electrodynamical light–matter description to novel spectroscopies,” *Nat Rev Chem*, vol. 2, p. 0118, 2018.
- [41] P. Pacheco, *An introduction to parallel programming*. Morgan Kaufmann Publishers, 2011.

- [42] C. K. Yap, *Fundamental Problems in Algorithmic Algebra*. Princeton University Press, 1993.
- [43] A. Sedighi, Y. Deng, and P. Zhang, “Fairness of task scheduling in high performance computing environments,” *Scalable Computing: Practice and Experience*, vol. 15, pp. 273–285, 09 2014.
- [44] M. P. Computing and D. F. (MPCDF), “Ada cluster documentation,” 2022.
- [45] J. Flick, D. M. Welakuh, M. Ruggenthaler, H. Appel, and A. Rubio, “Light–matter response in nonrelativistic quantum electrodynamics,” *ACS Photonics*, vol. 6, no. 11, pp. 2757–2778, 2019.
- [46] C. C. Comparison and B. D. (NIST), “Listing of experimental geometry data for c6h6 (benzene),” 2022.
- [47] K. Yabana and G. F. Bertsch, “Time-dependent local-density approximation in real time: Application to conjugated molecules,” *International Journal of Quantum Chemistry*, vol. 75, pp. 55–66, 1999.
- [48] C. C. Comparison and B. D. (NIST), “Experimental data for lih (lithium hydride),” 2022.
- [49] H. Pandey, *Fabrication, Characterization & Simulation of Graphene Field Effect Transistors operating at Microwave Frequencies*. PhD thesis, 08 2013.
- [50] D. Novko, M. Sunjic, and V. Despoja, “Optical absorption and conductivity in quasi-two-dimensional crystals from first principles: Application to graphene,” *Physical Review B*, vol. 93, p. 125413, 03 2016.
- [51] M. C. Paolo E. Trevisanutto, Markus Holzmann and V. Olevano, “Ab initio high-energy excitonic effects in graphite and graphene,” *Physical Review B: Condensed Matter and Materials Physics*, vol. 81, p. 121405, 2010.

A | Derivation of QED matrix elements

In this appendix we will explicitly calculate the generic matrix element for a solid in an optical cavity starting from equation (2.4) and from the chosen basis (2.5). A generic matrix element for this problem is defined as $H_{I,J,m,n}$, where I, J are the indexes for the electronic states and m, n are the ones for the photon number states. Since we are interested in studying solids, the generic index I (and J) should be further specified in the index of the conduction band in which we put the electron, the index of the valence band from which we remove the electron and finally the k point. Therefore, each electronic state will be characterized by c_I, v_I, k_I .

Before starting calculating the matrix element, it is useful to recall the communication rules for the bosonic \hat{a}, \hat{a}^\dagger and fermionic \hat{c}, \hat{c}^\dagger creation and annihilation operators:

$$\left[\hat{a}_i, \hat{a}_j^\dagger \right] = \hat{a}_i \hat{a}_j^\dagger - \hat{a}_j^\dagger \hat{a}_i = \delta_{i,j}, \left[\hat{a}_i, \hat{a}_j \right] = \left[\hat{a}_i^\dagger, \hat{a}_j^\dagger \right] = 0 \quad (\text{A.1})$$

$$\left[\hat{c}_i, \hat{c}_j^\dagger \right] = \hat{c}_i \hat{c}_j^\dagger + \hat{c}_j^\dagger \hat{c}_i = \delta_{i,j}, \left[\hat{c}_i, \hat{c}_j \right] = \left[\hat{c}_i^\dagger, \hat{c}_j^\dagger \right] = 0 \quad (\text{A.2})$$

Their action on a generic state is to add or remove a particle from the initial state. In the case of fermions, one can either have zero or one particle in a state due to Pauli exclusion principle while in bosonic case the only constraint is that the number of particles is non-negative. As a consequence, it holds that if we apply the annihilation operator to an empty state we get zero: $\hat{a}|0\rangle = 0$. Finally, the action of such operators on a generic state is given by the following relations:

$$\hat{a}^\dagger |n\rangle = \sqrt{n+1} |n+1\rangle \quad (\text{A.3})$$

$$\hat{a} |n\rangle = \sqrt{n} |n-1\rangle, \hat{a} |0\rangle = 0 \quad (\text{A.4})$$

Moreover, we recall that the momentum operator between Slater determinants with vertical transitions and the single-mode vector potential operator are defined as:

$$\widehat{P}_{i,j,k} = \sum_{i,j,k'} \langle \phi_{i,k} | \widehat{\mathbf{p}} | \phi_{j,k} \rangle \widehat{c}_{i,k}^\dagger \widehat{c}_{j,k} \quad (\text{A.5})$$

$$\widehat{A} = A_0 (\widehat{a}^\dagger + \widehat{a}) \quad (\text{A.6})$$

After recalling these relations we can start deriving the expression for the general matrix element. Let us consider two states $|\Psi_{a,k}\rangle |n\rangle$ and $|\Psi_{b,k'}\rangle |m\rangle$. Then we have:

$$\begin{aligned} \langle n | \langle \Psi_{a,k} | \widehat{H}_{QED} | \Psi_{b,k'} \rangle | m \rangle &= \langle n | \langle \Psi_{a,k} | \sum_{i,k} \epsilon_{i,k}^{KS} \widehat{c}_{i,k}^\dagger \widehat{c}_{i,k} | \Psi_{b,k'} \rangle | m \rangle + \\ \langle n | \langle \Psi_{a,k} | \frac{N_{el} A_0^2}{2} (\widehat{a}^{\dagger 2} + \widehat{a}^2 + 2\widehat{a}^\dagger \widehat{a} + 1) + \omega \left(\frac{1}{2} + \widehat{a}^\dagger \widehat{a} \right) | \Psi_{b,k'} \rangle | m \rangle & \quad (\text{A.7}) \\ - A_0 \langle n | \langle \Psi_{a,k} | \sum_{i \neq j,k} \langle \phi_{i,k} | \widehat{\mathbf{p}} \cdot \mathbf{e} | \phi_{j,k} \rangle \widehat{c}_{i,k}^\dagger \widehat{c}_{j,k} (\widehat{a}^\dagger + \widehat{a}) | \Psi_{b,k'} \rangle | m \rangle \end{aligned}$$

Let us now examine the previous expression term by term. The operators in the first term act only on the electronic states, so we can extract the photon part. Furthermore, the creation and annihilation operators act on the same same (that is actually the density operator), therefore this term can only be non-zero if both the electronic and photonic states are the same. Therefore we have:

$$\begin{aligned} \langle n | \langle \Psi_{a,k} | \widehat{H}_{el} | \Psi_{b,k'} \rangle | m \rangle &= \langle n | m \rangle \langle \Psi_{a,k} | \sum_{i,k} \epsilon_{i,k}^{KS} \widehat{c}_{i,k}^\dagger \widehat{c}_{i,k} | \Psi_{b,k'} \rangle = \\ \delta_{n,m} \sum_{i,k} \epsilon_{i,k}^{KS} \langle \Psi_{a,k} | \widehat{c}_{i,k}^\dagger \widehat{c}_{i,k} | \Psi_{b,k'} \rangle &= \delta_{n,m} \delta_{a,b} \delta_{k,k'} \sum_{i,k} \epsilon_{i,k}^{KS} n_{i,k} \end{aligned} \quad (\text{A.8})$$

Where $n_{i,k}$ is the number of particle in the state i, k and the index i runs over all states, both in valence and conduction band. By looking at the Kronecker's deltas in the previous expression, one can see that this part of the Hamiltonian only yields terms on the main diagonal of the matrix.

Let us now consider the second term of the Hamiltonian, which corresponds to the photon part. Similarly to the previous term, since the operators do not act on the electronic states

we can extract the electronic part. Therefore we have:

$$\begin{aligned}
& \langle n | \langle \Psi_{a,k} | \hat{H}_{el} | \Psi_{b,k'} \rangle | m \rangle = \\
& \langle n | m \rangle \langle \Psi_{a,k} | \frac{N_{el} A_0^2}{2} \left(\hat{a}^{\dagger 2} + \hat{a}^2 + 2\hat{a}^{\dagger} \hat{a} + 1 \right) + \omega \left(\frac{1}{2} + \hat{a}^{\dagger} \hat{a} \right) | \Psi_{b,k'} \rangle | m \rangle = \\
& \langle \Psi_{a,k} | \Psi_{b,k'} \rangle \frac{N_{el} A_0^2}{2} \left(\langle n | \hat{a}^{\dagger 2} + \hat{a}^2 + 2\hat{a}^{\dagger} \hat{a} + 1 | m \rangle \right) + \omega \left(\frac{1}{2} + \langle n | \hat{a}^{\dagger} \hat{a} | m \rangle \right) = \quad (A.9) \\
& \delta_{a,b} \delta_{k,k'} \frac{N_{el} A_0^2}{2} \left(\sqrt{(m+1)(m+2)} \delta_{n,m+2} + \sqrt{m(m-1)} \delta_{n,m-2} + (2m+1) \delta_{n,m} \right) + \\
& \omega \left(\frac{1}{2} + m \right) \delta_{n,m}
\end{aligned}$$

Where m is the number of photons in the state $|m\rangle$. By looking at this expression, one can see (thank to the deltas of the electronic part) that this term only yield non zero element on the main diagonal of block located either on the main diagonal (the red blocks of fig 2.1) or on the second diagonal (the blue blocks of fig 2.1).

Finally, we shall consider the last term of equation (A.7), the bi-linear coupling. In this case, the operators act on both the electronic and the photonic part, so we cannot do any *a priori* assumption.

$$\begin{aligned}
& \langle n | \langle \Psi_{a,k} | \hat{H}_{el} | \Psi_{b,k'} \rangle | m \rangle = \\
& - A_0 \langle n | m \rangle \langle \Psi_{a,k} | \sum_{i \neq j,k} \langle \phi_{i,k} | \hat{\mathbf{p}} \cdot \mathbf{e} | \phi_{j,k} \rangle \hat{c}_{i,k}^{\dagger} \hat{c}_{j,k} (\hat{a}^{\dagger} + \hat{a}) | \Psi_{b,k'} \rangle | m \rangle = \\
& - A_0 \sum_{i \neq j,k} \langle \phi_{i,k} | \hat{\mathbf{p}} \cdot \mathbf{e} | \phi_{j,k} \rangle \langle \Psi_{a,k} | \hat{c}_{i,k}^{\dagger} \hat{c}_{j,k} | \Psi_{b,k'} \rangle \langle n | \hat{a}^{\dagger} + \hat{a} | m \rangle = \quad (A.10) \\
& - A_0 \sum_{i \neq j,k} \langle \phi_{i,k} | \hat{\mathbf{p}} \cdot \mathbf{e} | \phi_{j,k} \rangle \langle \Psi_{a,k} | \hat{c}_{i,k}^{\dagger} \hat{c}_{j,k} | \Psi_{b,k'} \rangle \left(\sqrt{m+1} \delta_{n,m+1} + \sqrt{m} \delta_{n,m-1} \right)
\end{aligned}$$

By looking at this expression above one can see that, due to the deltas on the photonic part, this terms yields non-zero elements only on the blocks located on the first diagonal of the matrix (the green blocks in fig 2.1). The electronic part is more complicated, and needs further discussion. The operator $\hat{c}_{i,k}^{\dagger} \hat{c}_{j,k}$ removes an electron from the state j, k and places it on the state i, k . This suggests that we should look for non-zero elements between Slater determinants that represent having all electrons in the valence band state (the ground state) and others that represent an excitation from the valence band to the conduction band. As a matter of fact, if we consider consider the bilinear coupling between the Slater determinants representing the ground state we would get zero. Indeed, saying $\langle \Psi_{GS} | \hat{c}_{i,k}^{\dagger} \hat{c}_{j,k} | \Psi_{GS} \rangle$ means that we are taking the bracket between a state that has a vacancy in the state j, k and another that has a vacancy in the state i, k . Due to the

fact that the states are orthonormal this would yield zero. Let us now consider the matrix element between the Slater determinant of the ground state and of a generic excitation. Then we would have:

$$\begin{aligned}
\langle \Psi_{GS} | \hat{c}_{i,k}^\dagger \hat{c}_{j,k} | \Psi_{c_1,k} \rangle &= \langle \Psi_{GS} | \hat{c}_{i,k}^\dagger \hat{c}_{j,k} \hat{c}_{c_1,k}^\dagger \hat{c}_{v_i,k} | \Psi_{GS} \rangle = \\
\langle \Psi_{GS} | \hat{c}_{i,k}^\dagger \left[\delta_{j,c_1} - \hat{c}_{c_1,k}^\dagger \hat{c}_{j,k} \right] \hat{c}_{v_i,k} | \Psi_{GS} \rangle &= \\
\delta_{j,c_1} \langle \Psi_{GS} | \hat{c}_{i,k}^\dagger \hat{c}_{v_i,k} | \Psi_{GS} \rangle - \langle \Psi_{GS} | \hat{c}_{i,k}^\dagger \hat{c}_{c_1,k}^\dagger \hat{c}_{j,k} \hat{c}_{v_i,k} | \Psi_{GS} \rangle &= \delta_{j,c_1} \delta_{i,v_i}
\end{aligned} \tag{A.11}$$

where we used the commutation relation (A.2) and the last term is zero because $\hat{c}_{j,k}$ acts on a conduction band state. It should be noted that there should also be a delta for the k point, which is not present because we chose the creation and annihilation operators to act on the same k point. Finally, we can write the full expression for the matrix element of the first row or column of a bi-linear coupling block:

$$\begin{aligned}
\langle \Psi_{GS} | \hat{c}_{i,k}^\dagger \hat{c}_{j,k} | \Psi_{c_1,k} \rangle &= \langle \Psi_{GS} | \hat{c}_{i,k}^\dagger \hat{c}_{j,k} \hat{c}_{c_1,k}^\dagger \hat{c}_{v_i,k} | \Psi_{GS} \rangle = \\
- A_0 \sum_{i \neq j,k} \langle \phi_{i,k} | \hat{\mathbf{p}} \cdot \mathbf{e} | \phi_{j,k} \rangle \langle \Psi_{a,k} | \hat{c}_{i,k}^\dagger \hat{c}_{j,k} | \Psi_{b,k'} \rangle \left(\sqrt{m+1} \delta_{n,m+1} + \sqrt{m} \delta_{n,m-1} \right) &= \\
- A_0 \sum_{i \neq j,k} \langle \phi_{i,k} | \hat{\mathbf{p}} \cdot \mathbf{e} | \phi_{j,k} \rangle \delta_{j,c_1} \delta_{i,v_i} \left(\sqrt{m+1} \delta_{n,m+1} + \sqrt{m} \delta_{n,m-1} \right) &= \\
- A_0 \langle \phi_{v_1,k} | \hat{\mathbf{p}} \cdot \mathbf{e} | \phi_{c_1,k} \rangle \left(\sqrt{m+1} \delta_{n,m+1} + \sqrt{m} \delta_{n,m-1} \right) &
\end{aligned} \tag{A.12}$$

With the above discussion we described the matrix element on the first row and on the first column of the bi-linear coupling block. However, if we look at (2.2.3) we notice that there are also non zero elements in that are not in those locations. In fact, they are matrix elements between Slater determinants representing excitation from the valence band to the conduction band, therefore they represent a double excitation of the system. To describe them, let us consider two Slater determinants $|\Psi_{c_a,k}\rangle = \hat{c}_{c_a,k}^\dagger \hat{c}_{v_a,k} | \Psi_{GS} \rangle$ and $|\Psi_{c_b,k}\rangle = \hat{c}_{c_b,k}^\dagger \hat{c}_{v_b,k} | \Psi_{GS} \rangle$. Then we have:

$$\begin{aligned}
\langle \Psi_{c_a,k} | \hat{c}_{i,k}^\dagger \hat{c}_{j,k} | \Psi_{c_b,k} \rangle &= \langle \Psi_{GS} | \hat{c}_{c_a,k}^\dagger \hat{c}_{v_a,k} \hat{c}_{i,k}^\dagger \hat{c}_{j,k} \hat{c}_{c_b,k}^\dagger \hat{c}_{v_b,k} | \Psi_{GS} \rangle = \\
\langle \Psi_{GS} | \hat{c}_{v_a,k}^\dagger \left[\delta_{i,c_a} - \hat{c}_{c_a,k}^\dagger \hat{c}_{i,k} \right] \left[\delta_{j,c_b} - \hat{c}_{c_b,k}^\dagger \hat{c}_{j,k} \right] \hat{c}_{v_b,k} | \Psi_{GS} \rangle &= \\
\delta_{j,c_b} \delta_{i,c_a} \langle \Psi_{GS} | \hat{c}_{v_a,k}^\dagger \hat{c}_{v_b,k} | \Psi_{GS} \rangle - \delta_{j,c_b} \langle \Psi_{GS} | \hat{c}_{v_a,k}^\dagger \hat{c}_{c_a,k}^\dagger \hat{c}_{i,k} \hat{c}_{v_b,k} | \Psi_{GS} \rangle - \\
\delta_{i,c_a} \langle \Psi_{GS} | \hat{c}_{v_a,k}^\dagger \hat{c}_{c_b,k}^\dagger \hat{c}_{j,k} \hat{c}_{v_b,k} | \Psi_{GS} \rangle + \langle \Psi_{GS} | \hat{c}_{v_a,k}^\dagger \hat{c}_{c_a,k}^\dagger \hat{c}_{i,k} \hat{c}_{c_b,k}^\dagger \hat{c}_{j,k} \hat{c}_{v_b,k} | \Psi_{GS} \rangle &= \\
\delta_{j,c_b} \delta_{i,c_a} \delta_{v_a,v_b} &
\end{aligned} \tag{A.13}$$

The last three terms are all zero because we are removing multiple electrons from a state, and then taking the bracket with a state from which we removed the same number of electrons from other states.

List of Figures

- 1.1 Representation of the Hohenberg-Kohn theorem. The green arrows representing the mapping from the external potential to the density are straightforward from the previous discussion. The Hohenberg-Kohn theorem proves the mapping from the density to the external potential. 12
- 1.2 FP cavity with a single atom (two-level system) inside. The yellow lines represent the round-trip of the light, while the red lines represent the losses κ and γ 19
- 1.3 Energy diagram for a single atom (represented by a two level system) in a QED Cavity in strong regime. The first two columns represent the bare states, which constitute the base for our interaction Hamiltonian. Their coupling generates a pairs of degenerate levels, which constitute the subspaces of our problem. The degeneracy is broken when $g_0 > 0$, and then we have the dressed states 21
- 1.4 The polariton dispersion in the vicinity of a single resonance for vanishing damping (solid lines) and finite damping (dashed lines) for $\epsilon_b = 1$. The dashed-dotted line gives the dispersion of photons in vacuum (a); real and imaginary parts of $\tilde{n}(\omega)$ for vanishing damping (b) and the creation of the polariton dispersion (solid lines) from those of excitons and photons (dashed lines) and the non-crossing rule: $\epsilon_b = 1$ (c). This figure is taken from [31] 23
- 2.1 Structure of the QED matrix as implemented in the code. If we put the photon number states on the rows/columns, then the matrix is penta-block-diagonal. The red block is diagonal and only terms from \hat{H}_{el} and \hat{H}_{ph} contribute to it. The green block is the bi-linear coupling block, whose elements are defined by \hat{H}_{int} . Finally, the blue blocks are again diagonal, and only the terms that contains $\hat{a}^{\dagger 2}, \hat{a}^2$ contribute to it 29
- 3.1 Flow chart of the software *QED Solver* 37

3.2	Schematic representation of the bands of Graphene for a DFT calculation with three unoccupied states. Since $QEDMatrixValenceBandStates = 3$ and $QEDMatrixConductionBandStates = 2$ the first and last states are excluded.	40
3.3	Structure of the matrix for the linear optical response. The only blocks that contain non-zero elements are located on the main diagonal. The meaning of the color is the same of figure 2.1, so the green blocks represent the bi-linear coupling shifted on the main diagonal (due to the identity operator in the photon part)	43
3.4	Assignment of computing resources in an HPC cluster. Each user submits a <i>batch</i> script, then the scheduler assigns the computing nodes considering the number of requested nodes, the memory request and the maximum execution time	46
3.5	Performance of the code for the diagonalization of the QED matrix	47
3.6	QED matrix build time. The trend is linear as shown by the linear fitting for the 1 task case.	48
3.7	Parallelization of the diagonalization.	50
3.8	Flow diagram for the parallelized linear optical response	51
4.1	Set up for the Benzene molecule. This image is taken from [45], while the coordinates for the atoms are taken from [46]. In the image, λ_α represents the polarization direction of the light in the cavity	53
4.2	Single particle density of states for Benzene molecule. The peaks in this plot do not represent the polaritonic states of equation (3.3), but only the electronic states. The vertical line at $-3.9eV$ is the Fermi level	54
4.3	Linear optical response and joint DOS for Benzene molecule without the cavity	55
4.4	Contour plot of the linear optical response for some values of the coupling strength A_0 . On the x-axis there is the resonance energy of the cavity and on the y-axis the energy of the probe. The value of the Lorentzian broadening was $\eta = 135meV$	56
4.5	Comparison of the Rabi splitting for the $\pi - \pi^*$ transition	57
4.6	Set up of the LiH 1D chain. The cavity confines the photon mode in the z-direction, while the chain is periodic in the x-direction. The distance between Lithium and Hydrogen atom is 1.5949 \AA	58

4.7	Band structure of the LiH 1D chain. The red state is the valence band, which is fully occupied, while the other constitutes the conduction band. The blue state is double degenerate. The presence of a gap indicates a insulating behavior	58
4.8	Linear optical response and joint DOS for LiH without the cavity	59
4.9	Contour plot of the linear optical response for many values of the coupling strength A_0 . On the x-axis there is the resonance energy of the cavity and on the y-axis the energy of the probe. The value of the Lorentzian broadening was $\eta = 544meV$	60
4.10	Comparison between two vertical cuts (i.e. at fixed cavity frequency) for the linear optical response. The arrows represent the Rabi splitting	61
4.11	FP Cavity containing the Graphene used to simulate this system. The lattice of Graphene is taken from https://en.wikipedia.org/wiki/Graphene	62
4.12	Bandstructure of Graphene	62
4.13	Linear optical response of Graphene without the cavity. The value of the Lorentzian broadening was $\eta = 150meV$	63
4.14	Opening of the gap in Graphene	64
4.15	Linear optical response of Graphene. The value of the coupling strength was $A_0 = 0.005$, the cavity energy was $\Omega = 272meV$ and the Lorentzian broadening was $\eta = 272meV$	65

List of Tables

3.1	Input variables that define the calculation mode of the utility.	37
3.2	Input variables that define the parameters of the optical cavity.	38
3.3	Input variables that define band of the material used in the calculation. . .	39
3.4	Input variables that define the parameters for the linear optical response and for the DOS.	40
4.1	Rabi splitting (in eV) as a function of the coupling strength	57
4.2	Rabi splitting (in eV) as a function of the coupling strength	61

List of Symbols

Variable	Description	SI unit
eV	Electronvolt	$\frac{J}{C}$
\hbar	Reduced Planck's constant	$J * s$
ϵ_0	Vacuum permittivity	$\frac{C}{V * m}$
A_0	Light-matter coupling	$\frac{\sqrt{J * Kg}}{C}$
ω, Ω	Energy of radiation field $\hbar\omega$	J

Acknowledgements

This thesis work marks the end of a 5 years path through university. Ideally I would like to thank every single person I met in this amazing time-span, as each of them contributed to making me the person I am.

I would like to particularly thank my supervisor Professor Giacomo Claudio Ghiringhelli, who advised both my Bachelor's and Master's degree. I am grateful that you had the intuition that the Theory Department of Max Planck Institute for the Structure and Dynamics of Matter could be the ideal place for me given my interest for computational physics. Jointly with him, I would like to thank Professor Angel Rubio, director of the aforementioned department, for giving me the opportunity of writing my thesis at MPSD. Subsequently, I would like to thank my direct supervisors from MPSD, Simone, Hannes and Umberto for proposing me this amazing project. I cannot wait to give an answer to the open questions we still have! However, a special acknowledgment should go to Simone. Thank you for your patience in explaining me all the concepts I was new to. I am sure that from time to time I asked very stupid questions, but you never said anything and you just found new ways to explain the concepts. I am sure you will be a great professor in your new tenure position at DTU and you will inspire many students. I am really looking forward to keep working with you to bringing QED cavity materials to Quantum Computers!

I would also like to thank all the amazing people I met here in Hamburg, both for the support you gave me in technical aspects and for encouraging me in the down moments. I hope that I also brought something to your lives. I believe that any place is just as good as the people find there, and I was very lucky that you were there (here).

Successivamente, voglio ringraziare i miei amici in Italia. In primo luogo un grazie ai miei compagni di università per aver condiviso questo percorso, sia nei momenti tristi che in quelli felici. Penso che sia fantastico che abbiamo iniziato insieme il corso in Ingegneria Fisica e abbiamo proseguito sempre insieme per tutti gli anni.

Non meno grande è il ringraziamento che voglio dedicare ai miei amici più stretti. Insieme abbiamo vissuto infinite esperienze, riso, scherzato, litigato e riflettuto sui temi più dis-

parati. Indipendentemente da quello che capitasse siete sempre stati presenti e mai per un momento ho dubitato del vostro appoggio. Grazie, perché so che anche se il futuro ci potrà ad essere lontani fisicamente basterà prendere in mano il telefono per sapere che dall'altra parte ci sarà una persona pronta ad ascoltare e dare supporto.

Dulcis in fundo, la mia famiglia. Grazie ai miei zii, anche se siamo sempre stati separati dal fatto che viviamo in città diverse mi avete sempre dato preziosi consigli e avete sempre avuto parole di incoraggiamento. Grazie di cuore ai miei nonni, che occupate un posto gigante nella mia vita da molto prima che io abbia alcun ricordo. Qualsiasi cosa che io possa dire riguardo a quello che significate per me o riguardo a tutto quello che avete fatto per me è riduttiva. Ricordando (o cercando di ricordare) quando da piccolo mi facevate giocare con le prolunghe elettriche o quando mi avete insegnato ad usare il trapano a qualche anno di vita, probabilmente è anche grazie a voi che ho scelto un corso di laurea in ingegneria. Grazie per qualsiasi cosa, spero che possiate essere parte della mia vita ancora per molto tempo.

Infine, il mio più grande ringraziamento va ai miei genitori e a mio fratello. Non ho alcuna idea di dove iniziare a scrivere questo paragrafo, e probabilmente la cosa che più rende l'idea di quello che voglio dirvi è che mentre scrivo queste righe ho le lacrime agli occhi. Grazie per aver sempre creduto in me, per avermi sempre supportato (o talvolta criticato) nelle mie decisioni, per avermi sempre spinto a non fermarmi e a dare di più, sin da quando io abbia ricordo. Alla fine questo ci ha portati fisicamente lontani, e nonostante io sia la persona peggiore del mondo per quanto riguarda il chiamarvi non mi avete mai fatto pesare questa cosa. Anzi vi siete sempre preoccupati di come stessi. Voglio che sappiate che anche quando non ci sentivamo avete sempre occupato il primo posto nel mio cuore. Spero di avervi resi orgogliosi di me, anche se lo siete solo in minima parte rispetto a quanto io sono orgoglioso di voi per me è un successo enorme. Semplicemente, grazie.

Hamburg, September 9th, 2022

Francesco Troisi